STUDIES ON FISSION TIME ANOMALY IN FISSILE AND VERY HEAVY NUCLEI

By

ARINDAM KUMAR SIKDAR

(PHYS04201304002)

VARIABLE ENERGY CYCLOTRON CENTRE

Kolkata-700064, India

A thesis submitted to the

Board of Studies in Physical Sciences

In partial fulfillment of requirements

for the Degree of

DOCTOR OF PHILOSOPHY

of

HOMI BHABHA NATIONAL INSTITUTE

October, 2016

Homi Bhabha National Institute

Recommendations of the Viva Voce Committee

As members of the Viva Voce Committee, we certify that we have read the dissertation prepared by *Arindam Kumar Sikdar* entitled "*Studies on Fission Time Anomaly in Fissile and Very Heavy Nuclei*" and recommend that it may be accepted as fulfilling the thesis requirement for the award of Degree of Doctor of Philosophy.

Alok Chakrabarti — Date: 08/05/2017

Chairman: *Prof. Alok Chakrabarti*

Date:

External Examiner: *Prof. A. K. Jain* — A. K. Jain — Date: 08/05/2017

Guide/Convener: *Prof. Amlan Ray* — Amlan Ray — Date: 08/05/2017

Member: *Prof. Parnika Das* — Parnika Das. — Date: 8/5/2017

Member: *Prof. Satyajit Saha* — Satyajit Saha — Date: 8/5/2017.

Member: *Prof. Gopal Mukherjee* — Date: 08/05/2017

Final approval and acceptance of this dissertation is contingent upon the candidate's submission of the final copies of the thesis to HBNI.

I/We hereby certify that I have read this thesis prepared under my/our direction and recommend that it may be accepted as fulfilling the thesis requirement.

Date: 08/05/2017

Place: VECC, Kolkata

<Signature>
Co-guide (if applicable)

Amlan Ray
<Signature>
Guide

STATEMENT BY AUTHOR

This dissertation has been submitted in partial fulfillment of requirements for an advanced degree at Homi Bhabha National Institute (HBNI) and is deposited in the Library to be made available to borrowers under rules of the HBNI.

Brief quotations from this dissertation are allowable without special permission, provided that accurate acknowledgement of source is made. Requests for permission for extended quotation from or reproduction of this manuscript in whole or in part may be granted by the Competent Authority of HBNI when in his or her judgment the proposed use of the material is in the interests of scholarship. In all other instances, however, permission must be obtained from the author.

Arindam Kumar Sikdar

DECLARATION

I, hereby declare that the investigation presented in the thesis has been carried out by me. The work is original and has not been submitted earlier as a whole or in part for a degree / diploma at this or any other Institution / University.

Arindam Kumar Sikdar

List of Publications

Publications relevant to the thesis

Referred Journals:

1. "*Design of a dynamically orthogonalized Penning trap with higher order anharmonicity compensation*", **A. K. Sikdar**, A. Ray, P. Das, A. Reza, Nuclear Instruments and Methods in Physics Research A 712 (2013) 174.

2. "*Quasifision timescale: Zeptosecond versus attosecond*", A. Ray, **A. K. Sikdar**, A. De , EPJ Web of Conferences 86 (2015) 00038.

3. "*Examination of the fission time of the Z=120 nucleus*", **A. K. Sikdar**, A. Ray and A. Chatterjee, Phys. Rev. C 93 (2016) 041604 .

4. "*Timescale of non-exponential decay for the nuclear* β*-decay process in a decoherence model",* A. Ray and **A. K. Sikdar**, Phys. Rev. C 94 (2016) 055503.

5. "*Direct observation of slow fission of highly excited plutonium nuclei*", **A. K. Sikdar**, A. Ray, Deepak Pandit, B. Dey, Sarmishtha Bhattacharyya, Soumik Bhattacharya, A. Bisoi, A. De, S. Paul, Srijit Bhattacharya, A. Chatterjee**,** Phys. Rev. C (under communication).

Conference Proceedings:

1. "*VECC Cryogenic Penning Ion Trap: A status report*", P. Das, **A. K. Sikdar**, A. Reza, Subrata Saha, A. Dutta Gupta, S. K. Das**,** R. Guin, S. Murali, A. Goswami, H. P. Sharma, A. De, K. Banerjee, B. Dam, DAE Symposium on Nuclear Physics 57 (2012) 876.

2. "*Design of a dynamic orthogonalized Penning trap with higher order anharmonicity compensation*", **A. K. Sikdar**, P. Das, A. Ray**,** DAE Symposium on Nuclear Physics 57 (2012) 884.

3. "*Progress in VECC Cryogenic Penning Ion Trap Development*", P. Das, **A. K. Sikdar**, A. Reza, Subrata Saha, A. Dutta Gupta, M. Ahmed,S. K. Das, R. Guin, S. Murali, K. Banerjee, B. Dam, A.Ray, DAE Symposium on Nuclear Physics 58 (2013) 878.

4. "*Quasi-Bound state formation of an ensemble of dinuclear system at the exit channel in quasifission*", A. Ray, **A. K. Sikdar**, A. Dey, DAE Symposium on Nuclear Physics 58 (2013) 392.

5. "*Indication of long fission lifetime of ^{242}Pu at E_X=55 MeV*", A. Ray, **A. K. Sikdar**, B. Dey, D. Pandit,Sarmishtha Bhattacharyya, Soumik Bhattacharya A. De, Srijit Bhattacharya, A. Bisoi, DAE Symposium on Nuclear Physics 59 (2014) 486.

6. "*Progress in VECC Cryogenic Penning Ion Trap Development*", **A. K. Sikdar**, A. Reza, S. K. Das, K. Banerjee, B. Dam, P. Das, A.Ray, DAE Symposium on Nuclear Physics 59 (2014) 904.

7. "*Progress in VECC Cryogenic Penning Ion Trap Development*", **A. K. Sikdar**, A. Reza, R.Menon, Y.P. Nabhiraj, K. Banerjee, B. Dam, P. Das, A.Ray, DAE Symposium on Nuclear Physics 60 (2015) 926.

Other Publications:

Refereed Journal:

1. "*Trapping of relatively short-lived radioactive ^{146}Eu in a Paul Trap for studying ground state properties of nucleus*", M. K. Joshi, **A. K. Sikdar**, Pushpa M. Rao, T. Bhattacharjee, S. K. Das, P. Das, Physica Scripta 89 (2014) 085404.

Conference Proceedings:

1. "*A proposed method to measure relativistic kinetic energy of electrons in Penning Trap*", **A. K. Sikdar**, A.Ray, P.Das, DAE Symposium on Nuclear Physics 57 (2012) 886.

2. "*Trapping radioactive ^{146}Eu in a Paul Trap for studying ground state properties of nucleus*", M. K. Joshi**,** **A. K. Sikdar**, Pushpa M.Rao, P. Das, T. Bhattacharya, S. K. Das, DAE Symposium on Nuclear Physics 58 (2013) 848.

3. "*Capacitance measurement of Penning trap electrode assembly at cryogenic temperature*", A. Reza**,** **A. K. Sikdar**, P. Das, U. Bhunia, A. Mishra, K. Banerjee, B. Dam, A. Ray, DAE Symposium on Nuclear Physics 58 (2013) 876.

Dedicated to my lovely parents and

my aunt Niva Biswas.....

ACKNOWLEDGEMENTS

This particular page in the thesis gives an opportunity to leave a permanent record to express gratitude to entire bunch of people without whom this work would have not been accomplished. First and foremost, I would like to thank Professor Amlan Ray (my philosopher and guide) for his support, motivation and knowledgeable guidance throughout the process. He always gave his patience ear to my technically impossible ideas and shape my scientific path forward even in his toughest times. I really feel blessed to work with you (Sir).

My sincere thanks go to Dr. Alok Chakrabarti, Dr. Dinesh Srivastava, Dr. Sailajananda Bhattacharya & Dr. Sudhee Ranjan Banerjee (Head, Experimental Physics Group, VECC, Kolkata) for rendering useful guidance and kindest cooperation throughout my work.

I have a great pleasure working with Dr. Parnika Das and my research work would have remained incomplete without her constant support and encouragement. I am grateful to my fellow lab mate Ashif Reza who has been a wonderful co-passenger in this journey. I would like to thank all my collaborators Dr. Deepak Pandit, Soumik Bhattacharya, Dr. Balaram Dey, Sushovan Paul and others for their kindest support and cooperation. I would take this opportunity to thank all my office staffs who directly or indirectly helped us in running Penning Trap facility. I am really thankful to all my VECC folk and fellows (specially Shantonu Sahoo, Santu Manna and entire gang of Table Tennis Team) who kept me motivated all the way.

On personal note, I would like to thank my parents and family to understand my passion and accepting my escape of household duty. Thank you all for your unending support.

Contents

List of Figures

List of Tables

SYNOPSIS

Nuclear fission is one of the most important discoveries of the 20th century and in this context, the fission dynamics of highly excited fissile and superheavy nuclei has a special significance. The timescale of the nuclear fission process is one of the basic characteristics of the fission dynamics. However, the experimental measurements of fission time by the atomic and nuclear techniques give two very different timescales. On the one hand, very long fission times (on the order of 10^{-18} sec) for the highly excited uranium and transuranium nuclei have been measured by the atomic techniques (K x-ray-fission fragment coincidence and crystal blocking techniques) [1,2], whereas much shorter (~10^{-20} sec) fission times had been obtained using nuclear techniques [3,4]. It was argued [5] that the two fission timescales are due to the sensitivity of the nuclear and atomic techniques in short and long timescales and the long fission times could provide information about the viscosity [5] of the nuclear medium and might be used as probes [1,2] for studying the production of long-lived superheavy nuclei. It was recently shown [6] that the observed long fission time for the majority of the fissioning events as obtained by the atomic techniques cannot be reconciled with the short fission time obtained by the nuclear techniques and the observation of long fission time (~10^{-18} sec) for the highly excited fissile nuclei appears to be in disagreement with nuclear calculations [7]. The fission time measurements by the atomic techniques are relatively new and only a few datasets are available. So, it is important to undertake the measurement of fission time of highly excited fissile nuclei by atomic techniques such as by the K x-ray technique. K x-ray-fission fragment coincidence technique clocks the fission time of the compound nucleus by the K vacancy lifetime and determines both the

fission time and the percentage of long fission time component. However, so far only three published measurements [1,8,9] of fission time by K x-ray technique exist and none of them succeeded in observing a narrow K x-ray peak (comparable to the detector resolution) from the atoms containing the fissioning nuclei and could not extract any information from the intrinsic width of K x-ray line. One of the direct evidence of long fission time is the observation of narrow K x-ray peak from the atoms containing fissioning nuclei. According to quantum uncertainty principle, the intrinsic width of K x-ray peak from the atoms containing fissioning nuclei is a direct measure of the fission time given by the formula $\tau_{fission} = \frac{\hbar}{\Gamma_{intrinsic}}$, where $\tau_{fission}$ and $\Gamma_{intrinsic}$ are fission time and intrinsic width of K x-ray line respectively. It would be important to demonstrate long fission time of highly excited fissile nuclei by combining information on both the K x-ray yield and intrinsic width of the x-ray line. So far, long fission times of highly excited uranium-like and transuranium nuclei were measured by producing such nuclei in high energy heavy ion collisions [1]. As a result of production of many compound nuclei with similar Z values and/or due to the electronic configuration mixing in heavy ion reactions, very broad (FWHM ~25 keV) characteristic K x-ray lines from the compound atom/ion (containing fissioning nuclei) were seen in coincidence with the fission fragments in earlier K x-ray-fission fragment coincidence experiments [1]. Alpha and proton induced fusion reactions could produce a single fissioning compound nucleus with little electronic configuration mixing, however they have much smaller probability of creating K-vacancies of the compound atom and so there has been no attempt to see characteristic K x-ray from such reactions in fission reactions. To explore this dimension, ^{242}Pu ($E_X \approx 55$ MeV) has been produced by bombarding a ^{238}U target with a ^{4}He beam at

$E(^4He)_{Lab}$ =60 MeV from the Variable Energy Cyclotron Centre, Kolkata and a K x-ray-fission fragment coincidence experiment has been performed using a very close geometry. A solar cell detector was used to detect the fission fragments and a four-segmented LEPS detector was used to measure the photon spectrum. It has been found that the probability of creating K-vacancy in plutonium is considerably increased by the atomic shake-off process and so it has been possible to see a statistically significant narrow plutonium K x-ray peak in coincidence with the fission fragments. In Fig. 1, the experimental photon spectrum in coincidence with the fission fragments (random coincidence corrected and background subtracted) is shown. Double-humped peaks from the fission fragment γ-rays along with the corresponding GEANT3 simulations have been shown. The fission fragment γ-ray peak is double humped, because the fission fragment emitting the γ-ray could be moving either towards or away from the LEPS detector and the solar cell detector would correspondingly detect either the γ-ray emitting fission fragment or its complementary fragment. Plutonium $K_{\alpha 1}$ x-ray peak has been shown in Fig. 1 and it is a statistically significant peak with >99% confidence level. Plutonium $K_{\alpha 2}$ peak overlaps with the uranium $K_{\alpha 1}$ peak and its presence has been inferred from the observed high yields around 98.4 keV region that cannot be understood from the remnants of the associated uranium $K_{\alpha 2}$ and K_{β} lines. Hence, it is clear that the observed yield around 98.4 keV cannot be all due to the K orbital ionization of uranium atom and more than half of it should be coming from plutonium $K_{\alpha 2}$ line.

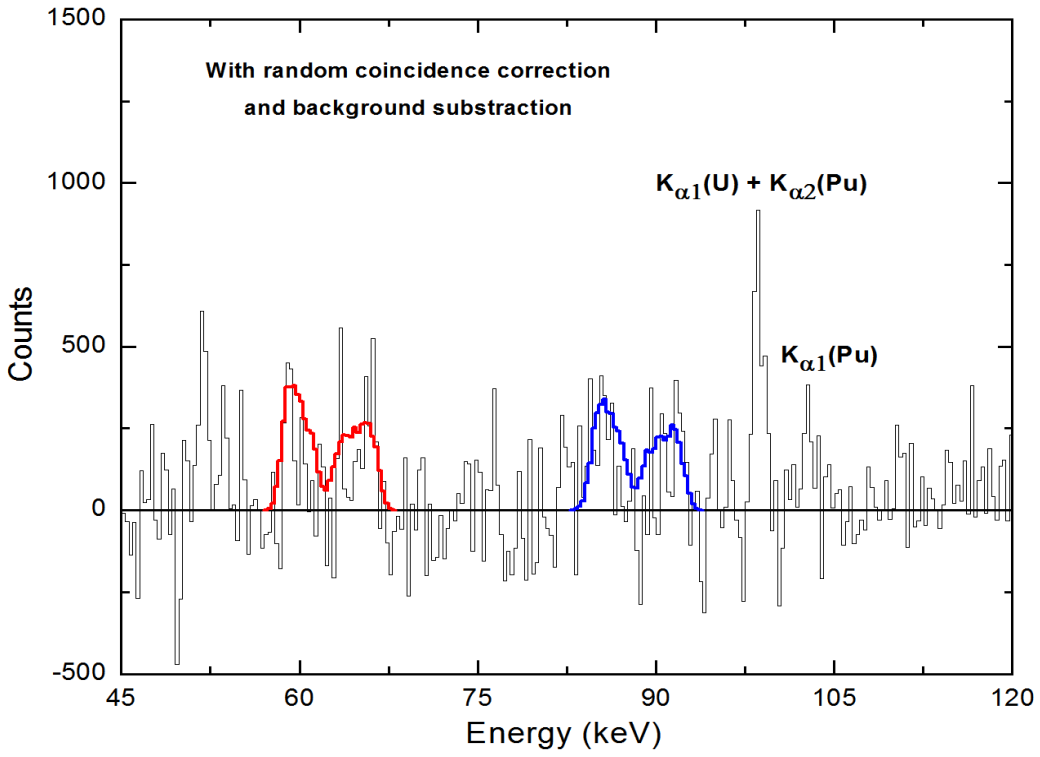

Fig. 1. *Photon spectrum in true coincidence with fission fragments along with superimposed fission gamma lines at 62.3 keV (red curve) and 88.3 keV (blue curve) simulated by GEANT3.*

The observation of a narrow peak (comparable with the detector resolution) demonstrates the presence of a long (~10^{-18} sec) fission time component. We have found from our analysis that for both the plutonium $K_{\alpha 1}$ and $K_{\alpha 2}$ lines, FWHM = (1±0.3) keV. Combining the two results, we obtain that the FWHM of plutonium K x-ray line = (1±0.21) keV compared to the detector resolution of FWHM = (1.00±0.01) keV. Considering detector resolution and the intrinsic width (0.1 keV) of plutonium K x-ray line with a stable plutonium nucleus, we find that the mean fission time of the excited fissioning plutonium nuclei responsible for the atomic K x-ray yield is > 1×10^{-18} sec.

Using the measured K x-ray fluorescence yield and the estimated probability of creation of K-orbital vacancies in the fusion process, we obtain that most of the fission events are slow with a mean fission time ~10^{-18} sec. Saxena *et al.* [10] measured prefission neutron multiplicity of a similarly excited ^{243}Am (Z=95) nucleus and obtained very short fission time (~10^{-20} s) for all the detected fission events. Fission dynamics calculation could obtain a fission time distribution with a long tail, but are unlikely to explain the incompatibility between nuclear and atomic data related to the fission time.

It has been argued that nuclear techniques (prefission neutron multiplicity measurement, fission fragment angular distribution etc.) are sensitive to the short time components of fission time distribution whereas atomic techniques (K x-ray and crystal blocking) are sensitive to long fission time component and so there is no consistency problem [5]. In this context, recent measurement of long fission time (~10^{-18} sec) of Z=120 nucleus by atomic techniques [1] were interpreted as evidence for the formation of superheavy Z=120 nucleus, although nuclear techniques observed [3,4] very short fission time (~10^{-20} sec) for the same nucleus at a similar excitation energy. From a detailed study of all relevant data concerning fission time of Z=120 nucleus, it was found from this work [6] that contrary to the general perception, the nuclear and atomic data related to fission cannot be reconciled by any plausible fission time distribution or the sensitivity of the atomic and nuclear techniques in different time domains. The incompatibility of the nuclear and atomic data arises from the fact that the atomic techniques find most of the fission events very slow (~10^{-18} sec), thus giving prefission neutron multiplicity values close to the saturation limit and almost isotropic mass angle angular distribution, contradicting nuclear results. It was found [6] that all the fission time measurement data

obtained from the nuclear data and calculations are consistent among themselves, whereas the fission time data obtained by the atomic techniques could not be reconciled with the nuclear data. Although the inconsistency among the fission time data obtained by atomic and nuclear techniques was explicitly shown for Z=120 superheavy nucleus, it appears to be a general observation. For example, Andersen *et al.* [11] using crystal blocking technique observed that all the detected fragments (100%) came from slow processes having long fission times (~10^{-18} sec) for a large number of reactions [such as ^{74}Ge+W at E(^{74}Ge)$_{Lab}$=390 MeV, ^{58}Ni+W at E(^{58}Ni)$_{Lab}$=330-375 MeV, ^{48}Ti+W at E(^{48}Ti)$_{Lab}$=240-255 MeV] expected to be dominated by quasifission process. On the other hand, using mass-angle correlation technique, R. du Rietz *et al.* [12] obtained 2D mass-angle correlations plots for very similar systems (^{64}Ni+W, ^{48}Ti+W) at similar center of mass energies and deduced their exponential quasifission lifetime on the order of ~10^{-21} sec to 10^{-20} sec for the detected events. So an important conclusion of this thesis work is that the short fission time obtained by the nuclear techniques and the long fission time obtained by the atomic techniques cannot be due to sensitivity of the two techniques in two time domains and are inconsistent with one another, contrary to general perception [5].

The incompatibility among the measured fission times by the nuclear and atomic techniques could indicate new physics beyond fission dynamics and it was explored in this work. It is possible that quantum decoherence is playing a role here and such a scenario has been considered [13]. Quantum mechanics predicts that the time evolution of an isolated unstable state produces a superposition of initial state and decayed state at any finite time. Then the decay of the initial state will be non-exponential in early time

approximately following a t^2 law. This means that in early time (small value of t), the decay would be very slow. The decaying state would almost remain undecayed in early time as long as quantum coherence would persist [14]. According to a quantum decoherence model [15], the coherence between the initial undecayed state and final decayed state is lost by the interaction of the environment with the decaying state and we can only talk about a decay after the loss of this quantum coherence. Hence, according to quantum decoherence model, the classical exponential decay would start after a time lag i.e. after the loss of quantum coherence. The exponential decay rate depends on the properties of the decaying state. Nuclear techniques obtaining fission time from the measurement of nuclear decay products essentially measure the exponential decay time of the fission process. In a decoherence model, the atom containing the radioactive nucleus could act as a detector making the first observation of the nuclear decay process. So the survival time of the atom containing the fissioning nucleus is expected to be longer than the exponential fission decay time measured by the nuclear techniques. Using such a decoherence model, we have estimated [13] quantum decoherence time of the fission process on the order of 10^{-18} sec. In this model, fission has not taken place as long as the atom containing the fission nucleus could emit characteristic photons corresponding the compound element and the atom is surviving for that long. So in this model, atomic techniques could measure a longer fission time than nuclear techniques would measure.

The mass measurement of superheavy nuclei would provide further insight on this problem of fission time anomaly related to fissile and very heavy nuclei. The fission time depends on the binding energy of the nucleus and microscopic calculations predict high

fission barrier and binding energy around Z=120. One can learn about the nuclear binding energy from high precision nuclear mass measurements and Penning traps are presently being used for the mass measurements of superheavy nuclei to find out the shell stabilization criterion. Although such experiments are beyond the scope of my thesis, I have been deeply involved in the development of a Penning trap to use it in conjunction with the upcoming facilities at VECC, Kolkata where such experiments could be undertaken in the future.

Penning trap is a versatile tool to trap subatomic particles under the combined application of a weak quadrupolar electrostatic potential and strong magnetic field. Magnetic field confines the ions in radial direction and quadrupolar electrostatic potential provides axial confinement. Under this applied field, trapped particles undergo a complicated motion that is a superposition of three eigen-motions. In order to perform high precision measurements using Penning traps, it is essential to create a high quality quadrupolar potential near the center of the Penning trap to avoid any unwanted frequency shift. A five electrode cylindrical Penning Trap has been designed [16] and fabricated to generate a high degree of harmonicity at trap centre including the effect of gaps. The required electronic circuits have been developed and tested. The design and fabrication of the Penning trap as well as the mechanical assemblies and electrical circuitries have been completed and tested as a part of this work. The final commissioning of the Penning trap would be done by putting it in a strong (5T) magnetic field.

In summary, the fission time of highly excited plutonium nuclei produced by $^{4}He+^{238}U$ at $E(^{4}He)_{Lab}$=60 MeV was measured by K x-ray technique combining

information on the intrinsic width of the K x-ray lines and K x-ray fluorescence yield. It was found from the measurement of intrinsic width of K x-ray lines that the fission time is $>1\times10^{-18}$ sec and most of the fission events are slow. A critical analysis of available nuclear and atomic data related to fission time has been performed. It was found that contrary to general perception, nuclear and atomic data cannot be reconciled by the standard sensitivity argument. The apparent incompatibility between the nuclear and atomic data related to fission time could be explained by a quantum decoherence model using the atom containing the fissioning nucleus as a detector. The mass measurement of very heavy nuclei would provide further information on this important topic and in this context a Penning trap facility would be very useful. The developmental works related to a Penning trap including all the mechanical and electrical fabrications and testing have been completed as a part of this work.

Bibliography

[1] M. O. Fregeau *et al*., Phys. Rev. Lett. **108**, 122701 (2012).

[2] M. Morjean *et al.*, Phys. Rev. Lett. **101**, 072701 (2008).

[3] J. Toke *et al.*, Nucl. Phys. A **440**, 327 (1985).

[4] D. J. Hinde *et al*., Phys. Rev. C **45**, 1229 (1992).

[5] D. Jacquet and M. Morjean, Prog. Part. and Nucl. Phys. **63**, 155 (2009).

[6] A. K. Sikdar, A. Ray and A. Chatterjee, Phys. Rev. C **93**, 041604 (2016).

[7] Aurel Bulgac *et al*., Phys. Rev. Lett. **116**, 122504 (2016).

[8] H. W. Wilschut and V. L. Kravchuk, Nucl. Phys. A **734**, 156 (2004).

[9] J. D. Molitoris *et al*., Phys. Rev. Lett.**70**, 537 (1993).

[10] A. Saxena *et al*., Phys. Rev. C **49,** 932 (1994).

[11] J. U. Andersen *et al*., Phys. Rev C **78**, 064609 (2008).

[12] R. du Rietz *et al.*, Phys. Rev Lett. **106**, 052701 (2011).

[13] A. Ray, A. K. Sikdar and A. De, EPJ Web of Conferences **86**, 38(2015).

[14] L. Fonda, G. C. Ghirardi and A. Rimini, Rep. Prog. Phys. **41**, 587 (1978).

[15] W. H. Zurek, Rev. Mod. Phys. **75**, 715 (2003).

[16] A. K. Sikdar *et. al.*, Nuclear Instruments and Methods in Physics Research A **712**, 174 (2013).

Chapter 1

Introduction

1.1 Preface

Nuclear fission is a phenomenon in which a heavy nucleus predominantly splits into two light nuclei of nearly equal masses along with the release of free neutrons, gamma photons and a large amount of energy (~200 MeV per fission) that is manifested mostly as the kinetic energy of the fission fragments. Since its discovery by Otto Han and Fritz Strassmann on December 17, 1938 [Mei39], it managed to engage scientists over decades for its fascinating properties. Its wide spread applications ranging from energy production in nuclear reactor to its application in devastating nuclear warheads mark it as one of the most important discoveries of the last century. In this context, the study of fission dynamics of highly excited fissile and very heavy nuclei (SuperHeavy Element) holds a special significance. The timescale of the nuclear fission process of these highly excited fissile nuclei is a basic characteristic of the underlying fission dynamics. Fission times could be obtained by both nuclear [Rie11, Hin92, Les91] (mass-angle distribution, prefission neutron multiplicity, prefission light charged particles multiplicity, GDR measurement) and atomic techniques [And08, Mor08, Fre12] (crystal blocking and K x ray-fission fragment coincidence). Nuclear techniques infer fission time by measuring fission fragment angular distributions, prefission neutron multiplicities and GDR γ-ray yields that come from the fissioning nucleus, whereas atomic techniques measure the survival time of the atom/ion containing the fissioning nucleus. Normally, one would expect that the survival time of the atom/ion containing the fissioning nucleus would be the same as the fission time inferred by

the nuclear techniques, as the atomic structure of the parent atom cannot survive and emit characteristic K x-ray photons after its nucleus fissions. However, it was found that the atomic techniques directly measuring the survival time of the atom/ion containing the fissioning nucleus gave several orders of magnitude longer lifetime (~10^{-18} sec) compared to the fission time inferred from the nuclear techniques (~10^{-20} sec). It was argued by some authors [Gon02, Jac09] that the atomic clocks (such as x-ray clock) have a longer range of measurement and are sensitive only to the long time component of the fission time distribution, whereas nuclear clocks (neutron clock, GDR clock) have a much shorter range and measure only the short time component. However, this argument still cannot resolve the central issue as to why both the techniques have found dominant fission contributions (>50%) in their respective time range. This implies that the results cannot be understood by the sensitivity argument and indicates a much deeper problem. Moreover, long fission time (~10^{-18} sec) of highly excited Z=120 nucleus produced by ^{238}U+^{64}Ni reaction was measured recently by atomic techniques and claimed [Mor08, Fre12] as a signature for the formation of superheavy Z=120 nucleus, although nuclear techniques [Hin92, Tok85, Hof08] could not find any support for the claim. Hence, it is clear that further measurements of fission times of highly excited fissile nuclei by more direct means are required to clarify the situation.

In earlier K x-ray-fission fragment coincidence experiments[Fre12, Mol93,Wil04], long fission times (~10^{-18} sec) were so far obtained from the measured K x-ray multiplicity per fission and the estimated probability of creation of K orbital vacancies in the element produced by the fusion process. In these experiments, fissioning compound nuclei were produced in high energy heavy ion collisions and very broad (FWHM ~25 keV) characteristic K x-ray lines were seen in

coincidence with the fission fragments because of the contributions from different elements with similar Z values due to the incomplete fusion process and /or electronic configuration mixing. So, it has not been possible so far to obtain direct evidence for long fission time from the intrinsic width of the observed K x-ray peak. However, the intrinsic width of the K x-ray lines from the atom/ion containing the fissioning nucleus is a direct and nuclear model independent measure [Anh85] of the fission time of the corresponding nucleus. Such information could provide a new way of looking at the fissioning nuclei.

Thus, in the present thesis, we have explored this dimension by performing K x-ray-fission fragment coincidence experiments on highly excited ^{242}Pu nucleus formed by bombarding 60 MeV alpha particles on ^{238}U target. Since ^{4}He+^{238}U reaction at $E_{c.m.}$ = 59 MeV should undergo complete fusion, only plutonium should be produced and we expect to see characteristic K x-ray line of plutonium in coincidence with the fission fragments. If the fission time of the highly excited plutonium nucleus is on the order of 10^{-18} sec i.e. comparable to the K vacancy lifetime of plutonium atom, the atom should be long-lived and narrow characteristics K x-ray lines is expected. The fission time could be extracted [Anh85] from the intrinsic width of such K x-ray lines. In this thesis work, we have done such an experiment and compared the fission time obtained by this method with the earlier results obtained by the atomic and nuclear techniques.

Moreover, given the high priority for the search for superheavy elements, we have done a critical analysis of the existing nuclear and atomic data related to the fission time of highly excited Z=120 nuclei and other transuranium nuclei/complexes to investigate whether any plausible fission time distribution could reconcile the apparent discrepancy. We have also studied whether the discrepancy might require a new idea based on quantum decoherence.

Since the nuclear binding energies would play a crucial role to understand the structure of superheavy nuclei, the precision mass measurement of superheavy nuclei in Penning trap would be an important tool in this research. Recently, different groups at various accelerator facilities [Blo10, Ram12] are involved in the mass measurement of SHE (SuperHeavy Elements) with Penning trap mass spectrometers. Although such measurements are beyond the scope of this thesis work, developmental work related to a cryogenic Penning trap facility at VECC has been presented here. In the future, it would be possible to undertake such high precision mass measurements of superheavy elements at VECC using the upcoming radioactive ion beam facility.

1.2 Outline

The thesis has been structured in the following manner. In chapter 2, we have described various fission time measurement techniques. The theoretical idea behind the extraction of fission lifetime from the intrinsic width of the characteristics K x-ray of the compound atom/ion containing the fissioning nucleus has been discussed in this chapter. In chapter 3, the experimental setup to perform K x-ray-fission fragment coincidence experiments on highly excited ^{242}Pu nucleus has been presented. The results of the experiment has been compared with the fission lifetime measured by the pre-scission neutron multiplicity technique and the incompatibility among the measurements has been established. In chapter 4, the fission time anomaly among different measurement techniques has been further surveyed for the case of superheavy Z=120 nuclei and various other highly excited uranium/ transuranium fissioning nuclei/complexes. In chapter 5, we have explored whether quantum decoherence could provide probable answer to this apparent fission time measurement anomaly. In chapter 6, we have elaborated about various developmental progress and initial commissioning results of cryogenic Penning trap at low magnetic field and liquid nitrogen temperature. Finally in chapter 7, conclusion and future perspective of the present thesis has been discussed.

Chapter 2

Overview of fission time measurement techniques

In this chapter, various experimental techniques for measuring fission lifetime would be discussed. These techniques could be broadly classified into nuclear and atomic techniques. We shall discuss about the working principle and sensitivity of various nuclear techniques such as prefission neutron multiplicity technique and mass angle distribution technique as well as various atomic techniques such as crystal blocking technique and K x-ray-fission fragment coincidence technique.

2.1 Nuclear techniques

2.1.1 Prefission neutron multiplicity

When a neutron-rich compound nucleus is formed at a high excitation energy in a nuclear reaction, significant number of neutrons are usually evaporated from the hot nucleus before it undergoes fission. These neutrons are called prefission neutrons. It is possible to deduce fission time of the compound nucleus by measuring prefission neutrons per fission event i.e. prefission multiplicity. So, in prefission neutron multiplicity experiments, the fission fragments are measured in coincidence with all the neutrons evaporated both before fission and from the fission fragments produced after fission [Kra04]. Since the prefission neutrons emitted from the

compound nucleus and postfission neutrons emitted from the fission fragments would have considerably different angular distributions in the laboratory frame, they could be separated out by a multi-source fit of the angular distribution of the detected neutrons. So, both the prefission and postfission neutron multiplicities could be identified in this way. A statistical model code, such as JOANNE2 [Les93] or JULIAN [Ross89], is used to determine the fission time corresponding to the average prefission neutron multiplicity (ν_{pre}). In this code, fission width is totally suppressed for a given time and particle evaporation is allowed from the compound nucleus. The delay time corresponding to the measured prefission neutron multiplicity gives the average fission time of excited nuclei. Thus the average fission time τ is

$$\tau = \sum_{j=1}^{j=\infty} \tau_j W_j \tag{2.1}$$

where τ_j is the neutron emission time at step *j* and W_j is the appropriate weighting factor. These weighting factors are determined from the measured ν_{pre}. The characteristic time τ_j is related to the decay width (Γ_j) of neutron at the corresponding excitation energy.

$$\tau_j = \frac{\hbar}{\Gamma_j} \tag{2.2}$$

The partial decay width (Γ_i) of particle *i* [Ross89] is given as

$$\Gamma_i(E^*, I) = \frac{(2s^i + 1)}{2\pi\rho(E^*, I)} \sum_{l=0}^{\infty} \sum_{J=|I-l|}^{J=|I+l|} \int_0^{E^*-B_i} \rho(E^* - B_i - \varepsilon_i, J) T_l(\varepsilon_i) d\varepsilon_i \tag{2.3}$$

where ε_i, s^i and *l* are the kinetic energy, spin and orbital angular momentum respectively of the particle *i* emitted from the initial compound nucleus with an excitation energy of E^* and angular

momentum I. B_i is the binding energy of the emitted particle. ρ and T_l represent spin dependent level density and transmission coefficient respectively. Both the fission probabilities and neutron emission probabilities are determined at different excitation energies. A Monte Carlo code is used to calculate prefission neutron multiplicity corresponding to a specific fission delay. A typical example of this technique is the work of Hinde *et. al.* [Hin92], where prefission neutron multiplicities for 27 fussion-fission and quassifission reactions were measured in the excitation energy range from 80 to 245 MeV.

The pre-fission neutron multiplicity clock is a non-linear high precision clock with a relatively short range. Pre-fission neutron multiplicity (ν_{pre}) saturates at a value ν_{sat} depending on the excitation energy of the compound nucleus. If ν_{pre} is close to its saturation value (ν_{sat}), the technique loses its precision, because longer fission timescales do not yield significantly higher values of neutron multiplicity. Let us define a fission time $\tau_{\max}$, so that for $\tau \geq \tau_{\max}$, $\nu_{pre} \approx \nu_{sat}$. Hence, the measured prefission neutron multiplicity could be approximately written as [Sik16]:

$$[\bar{\nu}_{pre}]_{\exp} \approx \int_0^{\tau_{\max}} \nu_{pre}(\tau) f(\tau) d\tau + \nu_{sat} \int_{\tau_{\max}}^{\infty} f(\tau) d\tau \qquad (2.4)$$

As a representative example, we have calculated pre-fission neutron multiplicities for the ^{238}U+^{64}Ni reaction at $E_x(^{238}U)_{Lab}$ = 6.6 MeV/A using the code JOANNE2 [Les93] with similar statistical model parameters as used by Hinde *et al.* [Hin92]. The onset of fission was delayed and the amount of delay was an input parameter while running the code. The number of prefission neutrons increases with fission delay. Thus, the measured prefission neutron

multiplicity is a measure of the fission time. In Fig. 2.1, we present our calculations of ν_{pre} using the code JOANNE2 [Les93] for various fission lifetimes of the composite nucleus. Following Hinde *et al.* [Hin92], the effective excitation energy of the saddle to scission emitter has been increased to account for the high mean kinetic energy of the pre-fission neutron spectrum.

Fig. 2.1 shows ν_{pre} as a function of fission time indicating the saturation of ν_{pre} at a value ν_{sat} ≈7.7 for fission time≥ 5×10^{-19} sec. It is clear from Fig. 2.1 that ν_{pre} measurements cannot distinguish among fission lifetimes longer than 5×10^{-19} sec for this system. However, the technique can certainly tell us without any ambiguity whether the fission time is on the order of 10^{-21} sec or greater than 10^{-18} sec.

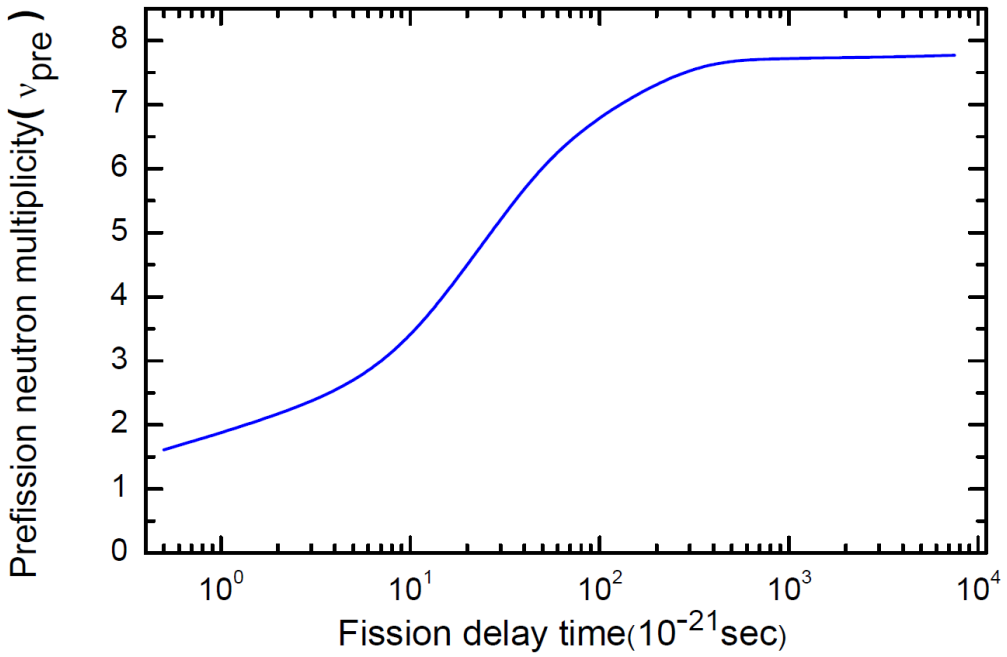

Fig. 2.1: *Fission lifetime versus pre-fission neutron multiplicity (ν_{pre}) for $^{238}U+^{64}Ni$ reaction at $E(^{238}U)_{Lab}$=6.6 MeV/A as obtained from JOANNE2 code calculations* [Sik16].

2.1.2 Mass Angle Distribution (MAD) technique

When the projectile hits the heavy target nucleus, they form a dinuclear system which rotates and exchange masses between themselves. For quasifission events, it is found that on average, mass flow occurs from the heavy to the light partner and mass symmetry being approached asymptotically with an expected [Tok85] time dependence $(1-\exp(-t/\tau))$, where τ is the mass-equilibration time constant. If the scission occurs soon after the initial contact, projectile nucleus is ejected at a backward angle with the corresponding target like nucleus in the forward angle. An increase of lifetime results in larger rotation and more mass exchange. In the case of a very long lifetime, as the system rotates more than one revolution, the correlation between the mass-ratio M_R and the fragment emission angle is lost resulting in almost symmetric mass split [Rie11]. In this technique, the emitted fission fragments are detected in coincidence with each other. The fragment velocities are determined by obtaining the position information of the fission fragments, together with either the measured time-of-flight [Hin96] or the time difference between two coincident fission fragments [Tho08]. Correcting for energy loss in the target, the mass ratio M_R of fragment mass to CN mass is plotted with the center-of-mass scattering angle θ_{cm}, and thus the mass-angle distribution (MAD) is obtained. The relationship between MAD data and the scission lifetime is extracted by performing a Monte-Carlo simulation where quasi-fission sticking time is parameterized by half Gaussian followed by an exponential decay. This exponential decay time gives the scission time of the dinuclear complex. A representative example of this technique is the work of R. du Rietz *et al.* [Rie11] who performed measurements of mass-angle distributions (MAD) for reactions of ^{34}S (149-189 MeV) , ^{48}Ti (220-260 MeV),

and ^{58}Ni (310-341 MeV) with ^{184,186}W target and measured fission lifetime ~ 10^{-21} sec for the dinuclear system.

The lack of reflection symmetry in the angular distribution of fission fragments is observable when the fission time is less than or comparable to the time taken by the composite system to complete one rotation. Since typically the fissioning nucleus takes time (~10^{-20} sec) to complete one rotation, this method is sensitive to the timescale of 10^{-21} sec. If the fission timescale is much longer than 10^{-20} sec, the composite system undergoes many rotations before fission resulting in essentially symmetric angular distribution of the fission fragments, implying fission time > 10^{-20} sec. The differential cross-section ($\frac{d\sigma}{d\theta_{c.m.}}$) versus $\theta_{c.m.}$ plot generally shows a peak-like structure at a small angle θ_p and then drops following a function that could be approximated by a decaying exponential function [Sch84, Rie11]. Let L be the orbital angular momentum, I the moment of inertia of a dinuclear system and $f(\tau)$ is the normalized fission time distribution. Then the differential cross-section at an angle $\theta_{c.m.}$ [Sik16] in the center of mass frame for $\theta_{c.m.} > \theta_p$ could be written as

$$\frac{d\sigma}{d\theta_{c.m.}} = K\int_0^{\infty} f(\tau)\exp(-\frac{\theta_{c.m.}I}{L\tau})d\tau \approx K\int_0^{\tau_{max}} f(\tau)\exp(-\frac{\theta_{c.m.}I}{L\tau})d\tau + K\int_{\tau_{max}}^{\infty} f(\tau)d\tau \qquad (2.5)$$

where K is a normalization constant and for ($\tau \geq \tau_{max}; \tau_{max}$~$10^{-20}$ sec) angular distribution could be considered isotropic.

2.2 Atomic techniques

2.2.1 Crystal blocking technique

In this technique, the projectile ions strike a single crystal serving as a target. Nuclear reaction occurs with one of the nuclei of the atoms of the crystal and fission takes place. In a crystal lattice, the atoms are arranged in a regular pattern. The atom that is struck by the projectile ion starts moving and it undergoes fission while moving. If the fission time is very short, the atom would hardly move from its initial position and the fission fragments would be blocked by the neighboring atoms and would not be able to come out. On the other hand, if the fission is on the order of 10^{-18} sec, the atom of the lattice would move sufficient distance so that fission would occur in the interstitial space and the fission fragments would come out from the lattice site and could be detected by the detectors. So, the angular distribution of the fission fragments coming out from the lattice carry a characteristic signature of the fission time. The angular distribution of fission fragments exhibits dips (blocking) in the direction of crystal axes and planes. Due to the repulsive coulomb potential of atomic planes or rows experienced all along the fission fragment trajectories, these dips are formed and hence these are more pronounced when the scissions occur at small distances (in the interstitial space) from a row or plane of crystal atoms [Gol99]. However, this technique has no sensitivity for the part of fission time distributions corresponding to times longer than the one needed by the fissioning nucleus to reach a neighboring string or plane at a distance of a few Å. It is also insensitive to scissions occurring at times shorter than the one needed by the fissioning nucleus to move away from the thermal

vibration region of the crystal atoms. So, these technique measure average fission time between these two limits and hence sensitive to longer fission time in the range 10^{-18} sec to 10^{-16} sec. Andersen *et al.* [And08] used this technique to study reactions like ^{74}Ge+W at E(^{74}Ge)$_{Lab}$=390 MeV, ^{58}Ni+W at E(^{58}Ni)$_{Lab}$=330-375 MeV, ^{48}Ti+W at E(^{48}Ti)$_{Lab}$=240-255 MeV and observed that all the detected fragments (100%) came from slow processes having long fission times (~10^{-18} sec).

2.2.2 K x-ray fission fragment coincidence technique

In nuclear collisions, highly excited transuranium nuclei and complexes are produced and they have large probabilities of undergoing fission. In these collisions, usually both the projectile and target nuclei have electrons in atomic orbitals. Vacancies in the atomic orbitals are created when a projectile ion collides with a target atom to produce a compound ion with a fused compound nucleus. The characteristic photons are emitted from the orbitals of the compound ions due to filling up of the vacancies. In this technique, the fission time of the compound nucleus is clocked by the vacancy fill up time of K orbital. The fission lifetime could be determined either from the compound element K x-ray multiplicity per fission event or from the width of the corresponding K x-ray lines measured in coincidence with the fission fragments.

The number of K x-ray photons (N_k) obtained depends on

$$\frac{dN_k}{dt} = \lambda N_{CN}(t) e^{-\lambda t} \tag{2.6}$$

where λ is the K shell hole decay rate and $N_{CN}(t)$ is the number of compound nucleus that survives fission at time t. Let $f(\tau)$ be the normalized fission time distribution, then $N_{CN}(t)$ is given as

$$N_{CN}(t) = N_f P_k \int_{\tau=0}^{\infty} f(\tau) e^{-t/\tau} d\tau \tag{2.7}$$

where N_f is the number of compound nuclei produced initially and P_k is the K shell ionization probability [Sik16].. Thus,

$$N_k = \int_0^{\infty} \lambda N_{CN}(t) e^{-\lambda t} dt = \lambda N_f P_k \int_{t=0}^{\infty} \int_{\tau=0}^{\infty} f(\tau) e^{-t/\tau} e^{-\lambda t} d\tau dt \tag{2.8}$$

So, assuming that all the compound nuclei undergo fission with an average fission time (τ), we obtain [Kra04] the following relation

$$\frac{N_k}{P_k N_f} = \frac{\lambda\tau}{1+\lambda\tau} \tag{2.9}$$

In atomic collisions, there are mainly three possible mechanisms for K orbital ionization:

a) **Direct Ionization** - When the projectile ion passes through the heavy target, it knocks off orbital electrons by electromagnetic interactions and creates inner shell vacancies in the target atoms [Kra04]. K shell ionization probability for ion induced reaction has been studied thoroughly both in theory and experiment. There are basically two distinct approximations in theoretical predictions namely United Atom (UA) approximation and Separated Atom (SA) approximation. In UA approximation, it is assumed that when the projectile nucleus penetrates the inner electronic shell, these shells readjust themselves in response to the increased binding energy of the combined target (Z_T) and projectile (Z_P) nuclear charge. Whereas in SA

approximation, it is assumed that projectile moves too fast to effect such change. In order to select the appropriate approximation, the most relevant velocity is the velocity of projectile nucleus relative to the K shell electron velocity. This is characterized by reduced velocity ξ_K given as

$$\xi_K = \frac{2}{\theta}\frac{v_p}{v_K} \tag{2.10}$$

where v_p is the projectile velocity and v_K is the velocity of K-shell orbital electron. $\theta = \frac{E_B}{(Z_{eff} - 0.3)^2 R}$ is the screening parameter taking care of non-hydrogenic character of K-shell ionization energy with E_B is the K shell binding energy, Z_{eff} is the effective atomic number of the target nucleus and R=13.6 eV is the Rydberg constant. In UA approximation, v_K and θ are calculated with $Z_{eff} = Z_T + Z_P$ [Tra80] and in SA approximation, $Z_{eff} = Z_T$ is considered. The plot of various light ion induced reaction data as shown in Fig. 2.2 has been obtained from ref. [Kra01]. Fig. 2.2 shows how (P_k / Z_p^2) varies with the corresponding reduced velocity (ξ_K), where P_K is the probability of creation of K orbital vacancies in the target atom.

b) **Internal Conversion** - When the excited nucleus interacts electromagnetically with one of the orbital electrons, it comes to its lower energy states with the ejection of the electrons. This process results in the creation of inner shell vacancies. However, this process takes relatively long time ~ 10^{-15} sec associated with γ-ray de-excitation time of the residual nucleus in comparison to the long-lived component of fission time (~10^{-18} sec). Thus, internal conversion

processes does not come into consideration of the K orbital ionization probability (P_k) of the compound element required to extract fission lifetime.

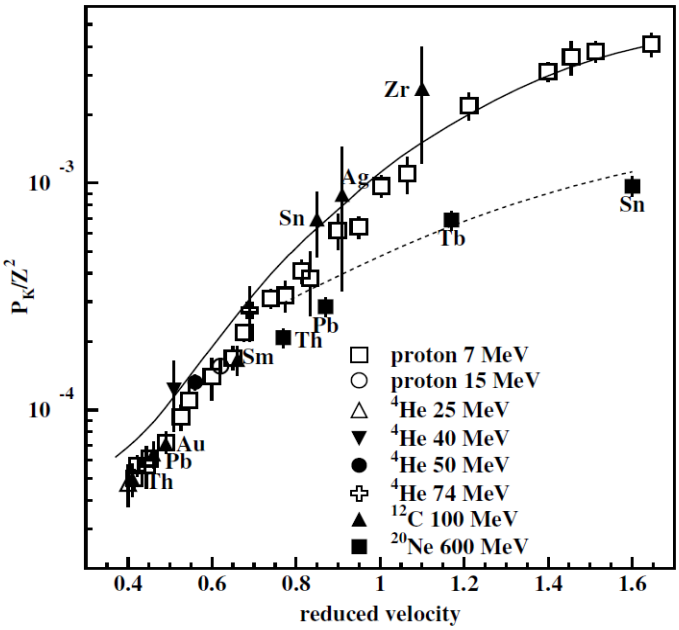

Fig. 2.2: *The K-shell ionization probability normalized to the square of the atomic number of projectile with the reduced velocity for various target-projectile combinations. For details, please see* [Kra01].

c) **Shake-off Ionization** - When the projectile nucleus comes within the nuclear interaction range of target nucleus, it fuses immediately to form compound nucleus. Due to this sudden change in the nuclear charge, electrons from various orbitals are ejected leading to inner shell vacancies. Shake-off ionization is treated in sudden approximation [Tho68] and has been investigated thoroughly for the beta decay process. The shake-off ionization probability is obtained in terms of square of the overlap integrals of initial atomic wavefunction and final wavefunction obtained as a result of sudden change in central potential. The shake-off

probability of an electron coming out of an orbital designated by n, l , j where n and l are the principal and angular momentum quantum number and $j = l \pm \frac{1}{2}$, is given as [Tho68]

$$P = 1 - \left[\left| \int \psi_{nlj}^{*}(z+1)\psi_{nlj}(z)dr \right|^2 \right]^N - P_F \qquad (2.11)$$

where $\psi_{nlj}(z)$ and $\psi_{nlj}(z+1)$ are the single-electron wavefunctions for the initial and final states of a given orbital. P_F are the contributions to filled states (for n' =1 to x) which is

$$P_F = \sum_{n'=1}^{n'=x} N \left| \int \psi_{n'lj}^{*}(z+1)\psi_{nlj}(z)dr \right|^2 \qquad (2.12)$$

where $n' \neq n$ and N is the number of electrons in the n' , l , j shell.

Usually for heavy ion induced reaction, direct ionization is the dominant phenomenon and the contribution of shake-off ionization is negligible. But, in case of light ion induced reaction, the contribution of shake-off ionization to the total K shell ionization probability of the compound element could be important compared to the direct ionization of the target atom.

So, in this technique, the determination of fission time of the compound nucleus from the fluorescence yield of characteristic K x-ray line requires the knowledge of the ionization probability (P_K) of the K orbital of the compound element as expressed in (eqn. 2.9). In this method, the lifetime of K orbital vacancy is used as a clock to determine fission time of the compound nucleus and the method is sensitive for measuring fission time from 10^{-18} sec to 10^{-16} sec.

However, without any information of K orbital ionization probability (P_k), it is still possible to determine the fission lifetime of the compound nucleus from the width of the K x-ray line of the

compound element produced by the fusion process. In his review work [Anh85], Anholt showed from the molecular orbital calculations how the atomic K x-ray line shape would change with the fission time of the corresponding atomic nucleus. In Fig. 2.3, we show the dependence of the width of K x-ray peak on the fission lifetime calculated for Uranium atom which is obtained from ref. [Kra04].

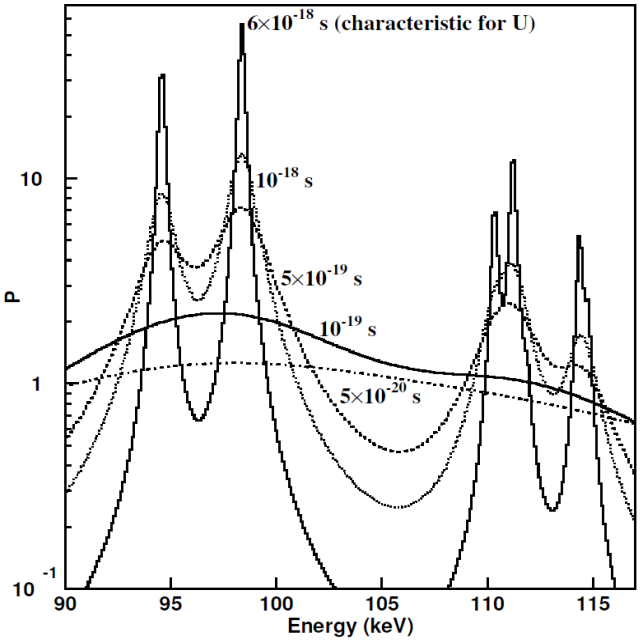

Fig. 2.3: *Variation of the shapes of K x-ray spectra calculated for different compound nucleus (U) lifetime obtained from ref.* [Kra04].

The results of the calculations can be obtained from the quantum energy-time uncertainty principle [Anh85]. If an atom contains a fissioning nucleus and it has a K orbital vacancy, then the survival time of the atom would depend on the fission time of the nucleus. Hence, the lifetime of the K orbital vacancy would also depend on the fission time of the nucleus. Following ref. [Anh85], the width of the K x-ray line ΔE can be related to the fission time τ by the relation

$$\Delta E \cdot \tau \geq \hbar \qquad (2.11)$$

Thus, the fission lifetime can be deduced from the observed width of the characteristic K x-ray lines (provided that it has approximately Gaussian shape) of the atom containing a fissioning nucleus by appropriately subtracting out both the detector resolution and the intrinsic width of the K x-ray line of the corresponding compound element. So in this technique, the intrinsic width of K x-ray line acts as a clock for measuring fission time and it would generally be sensitive to the fission time is $>10^{-18}$ sec. However, the advantage of this method is that one only needs to know the intrinsic width of K x-ray lines for determining fission time and no other input parameter is required.

In summary, the nuclear clocks are more sensitive and measure time with better precision compared to the atomic clocks. However, they have a relatively short range and saturate earlier compared to the atomic clocks. Atomic clocks (x-ray, crystal blocking) are less precise, but can measure longer fission times in the range of 10^{-18} sec to 10^{-16} sec. Short fission times from 10^{-21} sec to 10^{-18} sec do not produce any observable characteristic x-ray peak and blocking ratios remain below the thermal vibration limit. Hence, atomic clocks put fission times from 10^{-21} sec to 10^{-18} sec in a single time bin designated as less than 10^{-18} sec. So, atomic clocks cannot distinguish between fission times on the order of 10^{-21} sec from fission times on the order of 10^{-19} sec, but can certainly distinguish unambiguously between short fission times on the order of 10^{-21} sec and long fission times on the order of 10^{-18} sec. Similarly, nuclear clock cannot differentiate between time on the order of 10^{-19} sec to 10^{-17} sec but can clearly distinguish short fission times ($\sim10^{-21}$ sec) and long fission times ($\sim10^{-18}$ sec).

Chapter 3

Experiment

3.1 Introduction

Atomic techniques used to measure fission lifetimes are relatively new and only three published measurements [Fre12, Mol93, Wil04] of fission time by K x-ray fission fragment coincidence technique exist. All those K x-ray experiments used the measured K x-ray fluorescence yields and the estimated probabilities of production of K vacancy to determine fission time. Although, the intrinsic width of K x-ray line of the atom containing fissioning nucleus is a direct measure of the fission time as explained in section 2.2 [Anh85], none of the previous experiments succeeded in observing a narrow K x-ray peak (comparable to the detector resolution) from the fused element and could not extract any information from the intrinsic width of K x-ray lines. It would be important to demonstrate long fission time of highly excited fissile nuclei by combining information from both the K x-ray yield and intrinsic width of the x-ray line. So far, long fission times of highly excited uranium-like and transuranium nuclei were measured by producing such nuclei in high energy heavy ion collisions [Fre12, Mol93]. As a result of production of many compound nuclei with similar Z values and/or due to the electronic configuration mixing in heavy ion reactions, very broad (FWHM ~25 keV) characteristic K x-ray lines from the compound atom/ion (containing fissioning nuclei) were seen in coincidence with the fission fragments [Fre12, Mol93]. Alpha and proton induced fusion reactions could produce a single fissioning compound nucleus with little electronic configuration mixing, however they have much smaller probability of creating K shell vacancies of the compound atom and so there

has been no attempt to see characteristic K x-ray from such reactions in fission reactions. To explore this dimension, ^{242}Pu (E_X ≈55 MeV) has been produced by bombarding a ^{238}U target with a ^{4}He beam at E(^{4}He)$_{Lab}$ =60 MeV from the Variable Energy Cyclotron Centre, Kolkata and K x-ray fission fragment coincidence experiment has been performed using a very close geometry. Solar cell detectors were used to detect the fission fragments and a four-segmented LEPS detector was used to measure the photon spectrum. In this chapter, we have described about the various detectors used in the experiment, details of the electronic setup and the outcome of the experiment. The results have been compared with the fission lifetime measured by the pre-scission neutron multiplicity technique. It was found that the results obtained from the atomic and nuclear techniques are apparently incompatible.

3.2 Solar cell detector

Two solar cell detectors of dimensions 2.5 cm x 1.25 cm were electrically connected to give a single output and were used to detect fission fragments. A photograph of the solar cell detector mounted on PCB plate as used in the experiment is given in Fig. 3.1.

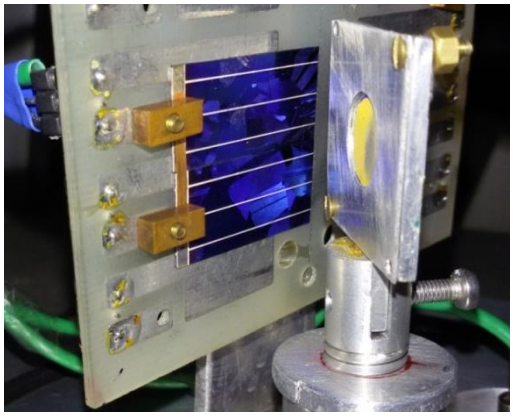

Fig. 3.1: *Photograph of two fission detectors electrically connected placed in front of ^{238}U target.*

In our experimental setup, the solar cell detectors were placed at an average distance of 2 cm from the target. The angular coverage was from 120° to 150° with the beam direction in the horizontal plane. The bare resistances of the solar cells with ambient light were 5.7 kΩ and 1.3 kΩ respectively. In a solar cell detector, alpha particles and fission fragments lose very little energy in the small depletion layer that is on the order of a few micrometers. However, fission fragments produce an almost full energy response due to "funneling" mechanism [Aji91].

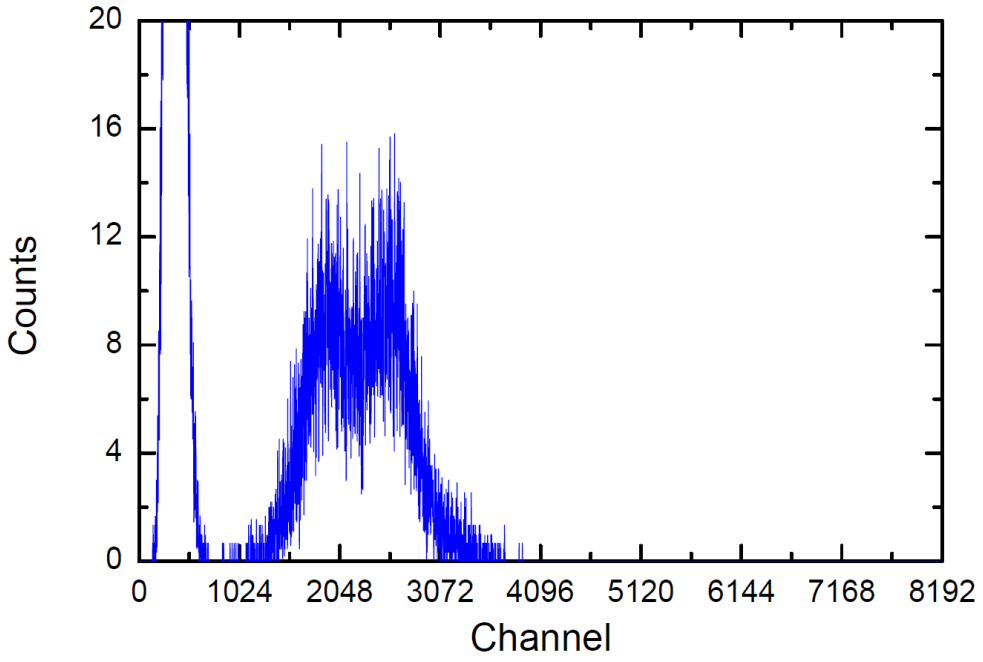

Fig. 3.2: *Pulse height spectrum obtained with solar cell detectors for ^{252}Cf source .*

The high density of ionization produced along the fragment track locally alter the depletion region into a funnel shape enclosing the track which enables the collection of almost the full ionization charge produced by the fragments before the normal shape of depletion depth is restored. The funneling effect depends strongly on the dE/dx profile. So for light particles, this effect is relatively very small which brings down the alpha response into the detector noise level

and gives very efficient pile-up suppression factor in the fission region. The performance of the detectors was tested several times before the experiment. An Ortec 142A charge sensitive preamplifier was used with our solar cell detector. A nice double humped fission spectrum with a standard ^{252}Cf source was obtained as shown in Fig. 3.2.

3.3 LEPS detector

A high purity planar Germinium **L**ow **E**nergy **P**hoton **S**pectrometer (LEPS) detector (Model DSG PGP 4seg80-7 Planar: p-type) was used to detect low energy γ-rays and x-rays. The detector had four segments mounted in a single cryostat and operated at liquid nitrogen temperature. The active area was 4 x 80 mm^2. To maximize the efficiency to detect low energy photons, a thin Be Window (thickness= 0.127 mm) was used which maintained a high vacuum inside the detector required for maintaining crystal purity. Due to high crystal quality of the detector, it required very low reverse bias of only -300 V for operation. This single bias voltage was distributed internally among four segments of the detector [Mou15]. This detector was placed at a distance of 10.7 cm from the target at a polar angle of 90° with the beam direction with each segment subtending a solid angle of about 7 msr. The target vacuum chamber in front of the detector was made up of 2 mm thick aluminium material. This greatly reduced 20 keV uranium L x-rays reaching the LEPS detector. The energy spectra of the four crystals were calibrated individually using various radioactive sources like ^{133}Ba, ^{152}Eu and ^{241}Am. The energies of x-ray and γ-ray from various sources that were used for calibration are listed in Table 3.1.

Table 3.1: *List of photon energies of various radioactive sources used for energy calibration of LEPS detector.*

Source	Energy (keV)	Intensity (%) [NuDat]
^{241}Am	13.9	37
^{133}Ba	30.9	96.1
^{152}Eu	39.9	58.7
^{241}Am	59.54	35.9
^{133}Ba	80.99	32.9
^{152}Eu	121.78	28.53
^{152}Eu	244.69	7.55
^{133}Ba	356	62.05

The gain of each crystal of LEPS detector was adjusted to focus in the region of K x-ray energies of plutonium and uranium atom. The relative efficiency curve for each of the LEPS crystals was obtained by placing various radioactive sources at the target position. Such a curve for one of the crystals is shown in Fig. 3.3. The average absolute efficiency of the detector was obtained as 1.1 x 10^{-4} at 121.78 keV with a calibrated ^{152}Eu source placed at the target position. The energy resolution of LEPS detector as obtained from offline measurement was FWHM = 0.9 keV at 121.78 keV.

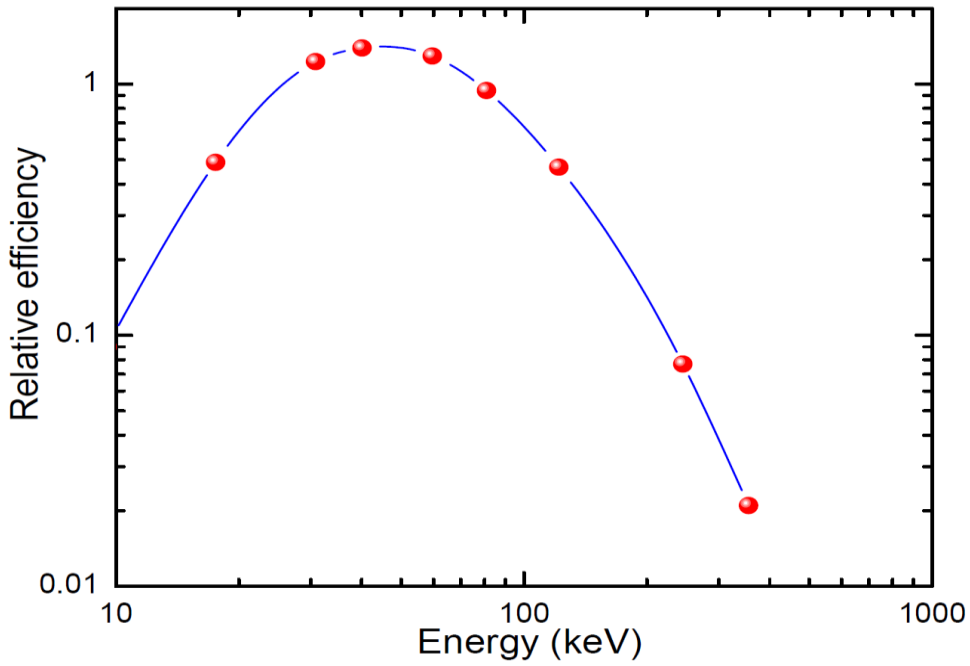

Fig. 3.3: *Relative efficiency curve of one of the crystals with various sources placed at target position.*

3.4 Electronics and data acquisition

The scheme of the complete electronic set-up is shown in Fig. 3.4. The signal from the solar cell detector was first pre-amplified using ORTEC 142A preamplifier. The signal from the output of the preamplifier was split into two parts. One part was sent through a shaping amplifier (ORTEC 572) with a shaping time of 3 μs and then sent to a peak sensing ADC to obtain the energy of the fission fragment. The other part of the signal was passed through a Canberra 2111 Timing Filter Amplifier (TFA) to generate a fast signal (with integration time of 500 ns) and sent to a Canberra 2037A Single Channel Analyzer (SCA) to generate a logic signal with an appropriate delay. This logic signal was sent to the stop channel of ORTEC 567 Time to Amplitude Converter (TAC).

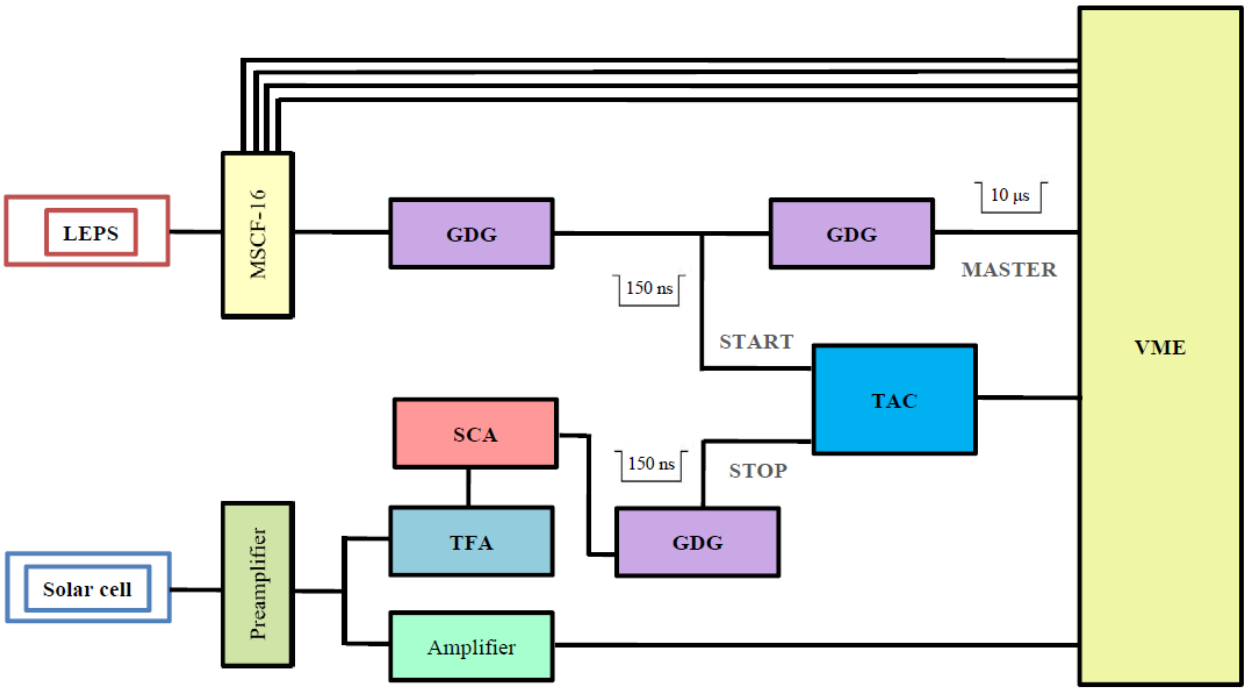

Fig. 3.4: *The complete electronic scheme of the experimental set-up.*

The four signals from DSG LEPS detector were pre-amplified internally and were fed to a Mesytec MSCF-16 unit. This unit served two purposes i) properly shaped the four energy signals of the LEPS output which was further sent to the data acquisition system and ii) gave fast timing output which was OR of the timing output of all the four channels. This output was delayed using LeyCroy 222 Gate and Delay Generator (GDG). The logic signal obtained from the GDG was split into two parts. One part went to trigger the Start channel of the TAC. The output of the TAC was sent to data acquisition system. The other part of the signal was sent to a similar GDG to generate the master gate of 10 µs wide required to trigger the data acquisition system. The delays in the timing signal in both the solar cell side and the LEPS detector side were adjusted properly to obtain the TAC output signal at the centre of the master gate. The data were digitized with a MDC-32 Analog to Digital Converter and acquired using VME 64 crate with CAEN V2718 controller.

3.5 Selection of beam and target

To observe narrow K x-ray peak of the compound element, it is required to produce a single compound nucleus (by complete fusion) with little electronic configuration mixing. Hence, ^{4}He or proton beam should be used. The K-shell ionization probability scales as the square of the atomic number of the projectile (Z_p^2) and linearly with the velocity of the projectile. So, alpha particle is selected over proton. In the case of fusion reaction with alpha particles, complete fusion is expected because of the very high binding energy of the alpha particle. A 60 MeV alpha beam (with average beam current = 2 pnA) from the Variable Energy Cyclotron, Kolkata, India was used to bombard a natural uranium-oxide film (≈ 2.5 mg/cm^2 thick) electrodeposited on a ~1 micron thick aluminum foil. The target thickness was selected judiciously to obtain a high coincident rate and minimize the energy loss of the fragment in the target (average energy loss of the fragments in the target was around 19 MeV). The target was placed at 45° with the beam axis to maximize the number of fission fragments reaching the solar cell detector.

3.6 TAC spectrum

As discussed in section 3.4, the TAC spectrum has been generated by taking start trigger from the LEPS detector and stop signal from the solar cell detector. The different parameters of the electronic setup shown in Fig. 3.4 have been optimized to obtain TAC peak with a minimum width. The minimum FWHM of the TAC peak was obtained as 250 ns in offline testing with ^{252}Cf source for the parameters mentioned in section 3.4. However, the FWHM of the TAC peak deteriorated to 683 ns in online experiment of 60 MeV ^{4}He + ^{238}U. The TAC peak obtained is shown in Fig. 3.5.

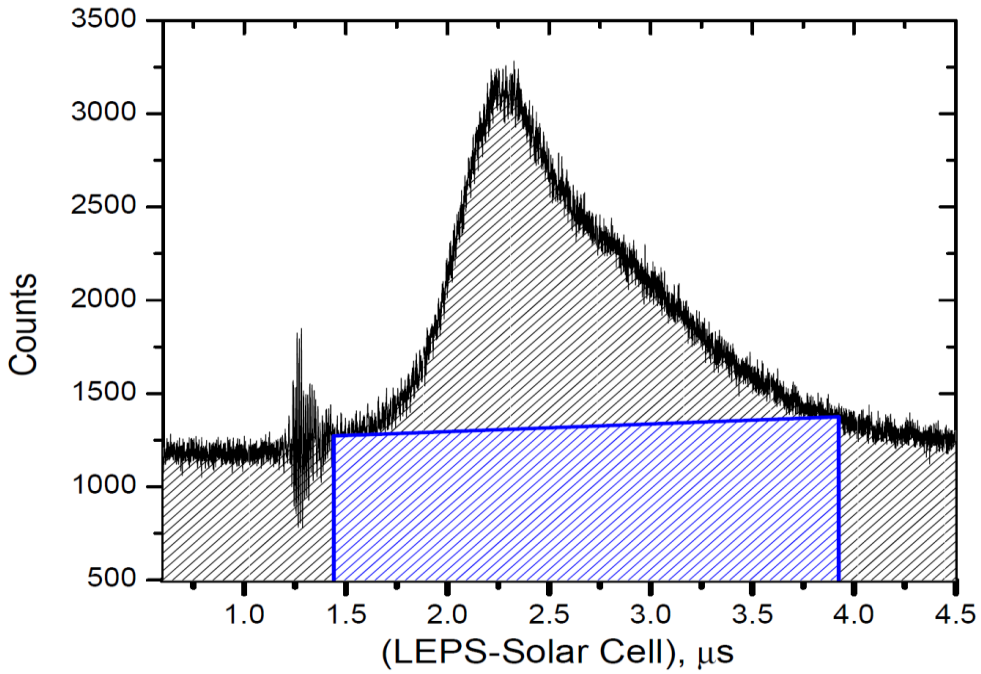

Fig 3.5: *The TAC spectrum between LEPS detector and solar cell detector for the reaction of 60 MeV ^{4}He + ^{238}U. The blue shaded area indicates the random coincident events under the TAC peak.*

In Fig. 3.5, the events within the TAC peak should contain both the true coincident events and random coincident events. The blue shaded region under the TAC peak should contain the randomly coincident events that occur stochastically with the true coincidence events.

The inclusive spectrum of the solar cell detector for the reaction of 60 MeV ^{4}He + ^{238}U reduced by a factor of 500 of its initial value to fit the scale is shown in blue color in Fig. 3.6. The prompt gated fission fragment spectrum shown in red color in Fig. 3.6 is extracted from the inclusive spectrum of solar cell detector by gating on a 2.5 μs time window around the coincidence peak as shown in Fig 3.5. The extracted fission fragment spectrum is symmetric with a slight tailing in

high energy side as expected theoretically [Pal08]. A high noise peak is seen in the inclusive spectrum (blue curve of Fig. 3.6) of solar cell detectors at a very low energy side but its complete absence in prompt gated fission spectra (red curve of Fig. 3.6) clearly shows the efficient performance of the coincidence time window.

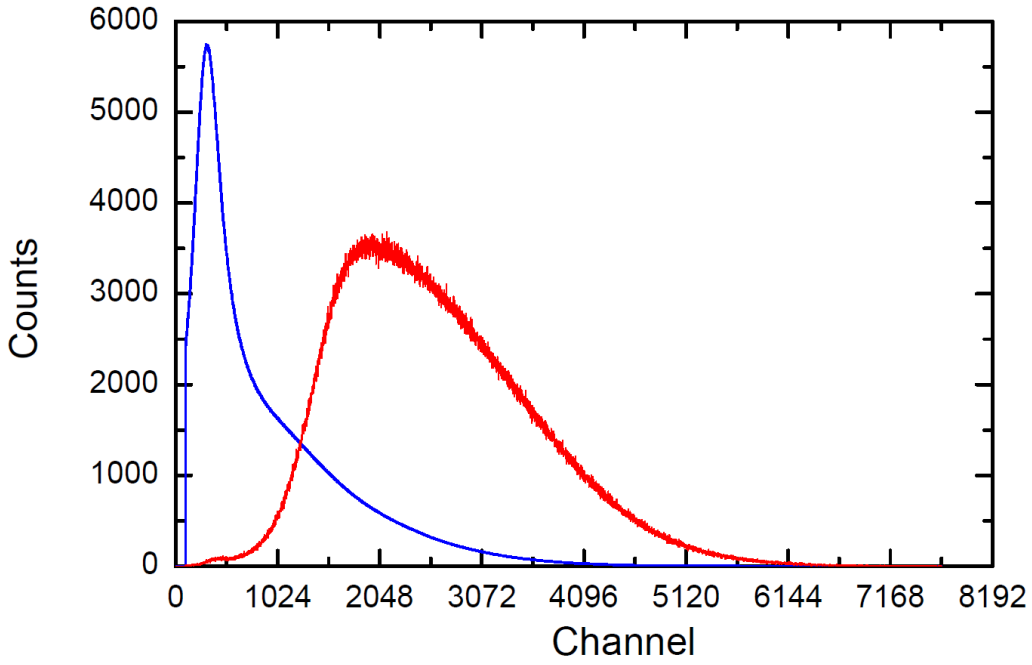

Fig. 3.6: *Inclusive fission spectrum reduced by a factor of 500 to fit the scale is shown in blue color and prompt gated fission spectra is shown in red color for the reaction of 60 MeV* ^{4}He + ^{238}U.

3.7 Analysis of low energy photon spectra

i) **Singles LEPS spectrum**

The inclusive spectrum for the reaction of 60 MeV ^{4}He + ^{238}U as recorded by LEPS detector is shown in Fig. 3.7. This spectrum is the sum of the individual spectrum of the four crystals after

proper gain matching. Uranium $K_{\alpha 1}$ (98.4 keV), $K_{\alpha 2}$ (94.6 keV), $K_{\beta 1}$ (111.2 keV), $K_{\beta 2}$ (114.4 keV) and $K_{\beta 3}$ lines (110.4 keV) coming from the excitation of the uranium atom by the ^{4}He particles are clearly seen in Fig. 3.7.

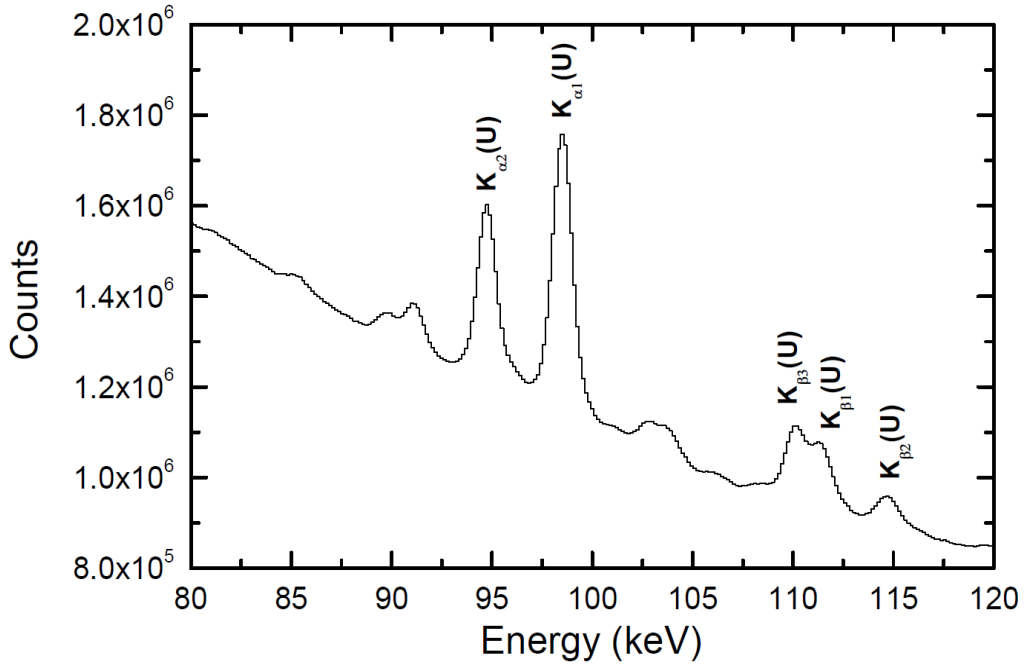

Fig. 3.7: *Singles photon spectrum resulting from the reaction of 60 MeV ^{4}He + ^{238}U.*

We see a broad hump from 100.5 keV to 105.3 keV. This hump could contain Plutonium $K_{\alpha 1}$ x-ray line (103.75 keV), uranium Coulomb excitation line (103.5 keV) [War96], γ-ray lines (102.8 keV) from plutonium isotopes [Ahm83] etc. The highly excited ($E_X \approx 55$ MeV) ^{242}Pu nucleus produced by the fusion of $^{4}He+^{238}U$ at $E_{c.m.} = 59$ MeV undergoes de-excitation by sequential emissions of neutrons followed by a cascade of electromagnetic transitions leading to the production of K orbital vacancies by internal conversion process [Dec73] and subsequent emission of K x-rays (103.75 keV). However, these γ-rays and x-rays should not be present in coincidence with the fission fragments. The plutonium ion produced by the fusion of $^{4}He+^{238}U$

has a small probability of having K orbital vacancies and there should be a small yield of K x-rays from the plutonium ion containing highly excited plutonium nucleus, if the fission time is comparable to the lifetime (6×10^{-18} sec) of the plutonium K vacancy.

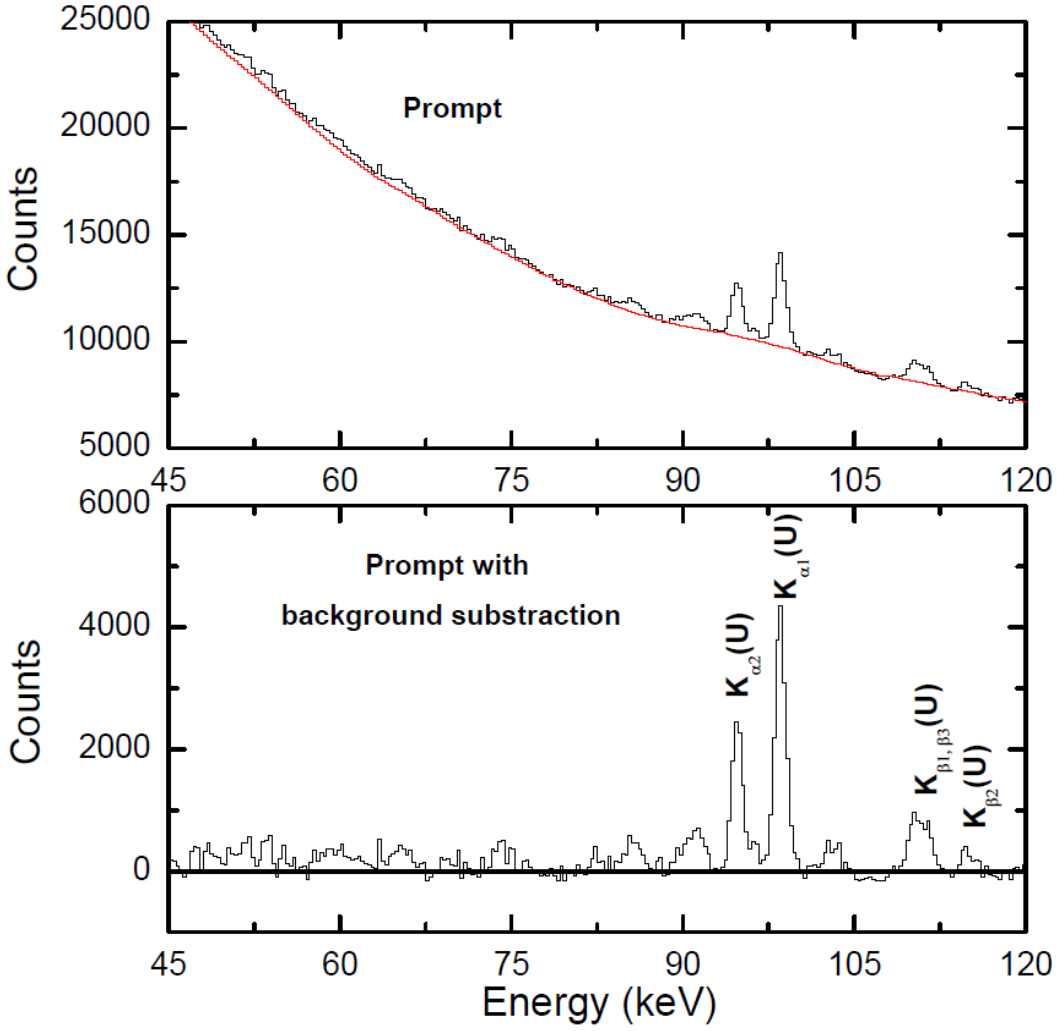

Fig. 3.8: *(Upper panel) Prompt gated photon spectra obtained by gating on a 2.5 μs time window around the coincidence peak seen in the time spectrum between LEPS detector and solar cell (Fig. 3.5). Red curve shows the background. Background subtracted prompt spectrum is shown in the bottom panel.*

Only these K x-rays from the plutonium ion should be seen in the coincidence spectrum. We have obtained the FWHM of 98.4 keV uranium K x-ray line as = (1 ±0.01) keV by the Gaussian fitting of data points from 96.9 keV to 100.5 keV in Fig. 3.7. Since the intrinsic width of uranium K x ray line is about 0.1 keV [Kra79], the resolution of LEPS detector for the online experiment has been obtained as =(1±0.01) keV at 98.4 keV.

ii) LEPS spectrum in coincidence with the fission fragments

We now discuss about the TAC gated LEPS detector spectrum. In Fig. 3.8, we show LEPS spectrum obtained by gating on a 2.5 μs time window around the coincidence peak shown in Fig. 3.5. The red curve shows the background in Fig. 3.8. In the bottom panel of Fig. 3.8, we show the background subtracted prompt spectrum where all the uranium K x-ray lines as observed in singles spectrum (Fig. 3.7) are seen.

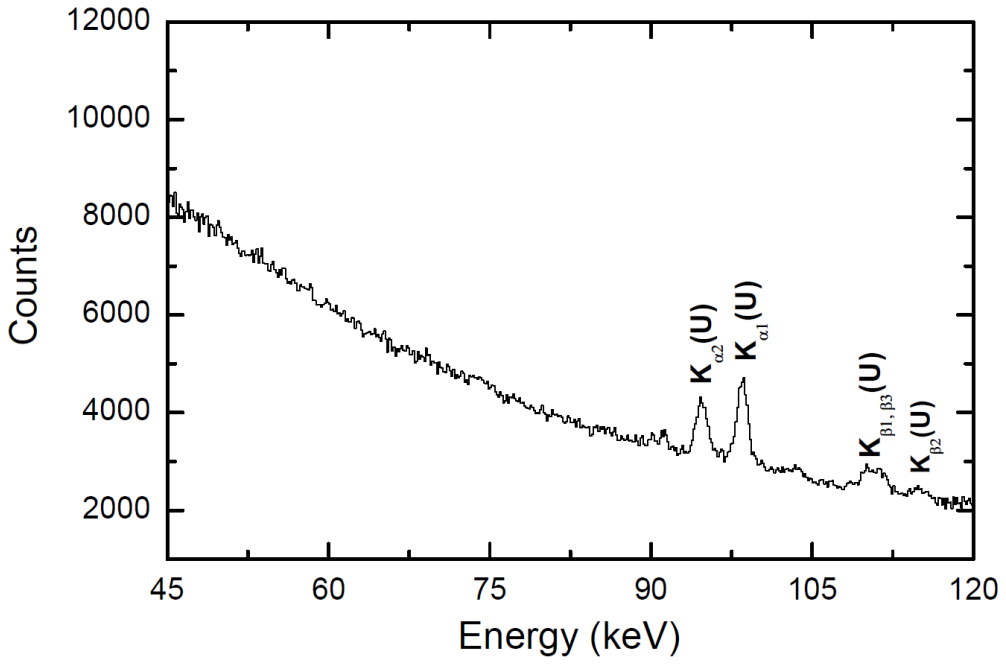

Fig. 3.9: *Random gated photon spectra obtained by gating on flat region on both sides of the TAC spectrum.*

Since the cyclotron beam bursts were 10 ns wide and separated by about 110 ns and our master gate was 10 μs wide, the prompt spectrum includes random coincidence events. The photon spectrum in random coincidence as shown in Fig. 3.9 was extracted from the inclusive spectrum (Fig. 3.7) by gating on both sides of the prompt peak in the time spectrum (after suitable normalization) to make the number of randomly gated events same as the prompt gated events as shown by the blue shaded area under the TAC peak in Fig. 3.5. In the random coincidence spectrum (Fig. 3.9), we see all the uranium K x rays lines as expected.

The random gated spectrum was subtracted out from the prompt spectrum channel by channel and the resulting photon spectrum in true coincidence with the fission fragments along with a red background curve is shown in Fig. 3.10 (upper panel). In the random corrected true coincidence spectrum (Fig. 3.10) small peaks are seen to ride on a large background. We have performed best possible fits of the data points with linear backgrounds and find that the data points around 103 keV and 98.4 keV can be best fitted (typical reduced $\chi^2 \approx 1$) by narrow (FWHM =1 keV) Gaussian peaks (magenta color curves) with linear backgrounds (black lines). The fitting of the data points from 100.5 keV to 105.3 keV with a Gaussian peak (FWHM=1 keV) and a linear background gives a nice fit (reduced $\chi^2=0.9$) and the peak is defined with >99% confidence level (ratio of Gaussian peak area to its statistical error ≈4). On the other hand, if those data points are fitted with a broad Gaussian peak (FWHM = 3 keV), the peak becomes statistically poorly defined (ratio of peak area to its statistical error ≈1.8). Hence, clearly a narrow Gaussian peak centered at 102.6 keV (FWHM=1 keV) is statistically the best description of the data points in the region spanning 100.5 keV to 105.3 keV. So, we have done fittings assuming narrow Gaussian peaks (FWHM= 1keV) at 102.6 keV and 98.4 keV with linear backgrounds shown by

black lines. Broad double-humped peak structures are seen around 63 keV and 88 keV. Considering them as γ-ray lines emitted from fission fragments (more explanation for this assumption can be obtained in the next section), they can be best fitted by GEANT3 [Bru86] simulated curves obtained by using actual experimental geometry and linear backgrounds (black lines). In this way, we have obtained best-fitted linear backgrounds (black lines) under different narrow and broad peaks. A smooth curve (solid red curve) has been drawn by joining these black straight lines and it has been taken as the best background curve (Fig. 3.10). We have studied the effect of drawing different background curves such as dotted blue and dot-dash green background curves obtained by lowering the best-fitted red background curve and it has been elaborated vividly in section 3.13. In Fig. 3.10 (bottom panel), we show random coincidence and background subtracted photon spectrum. We find that all the uranium K x-ray lines have been suppressed by a large factor compared to their intensities in the singles and prompt spectrum as seen in Fig. 3.7 & Fig. 3.8 respectively. A peak around 98.4 keV is a relatively intense line in the true coincidence spectrum. New peaks such as double-humped broad peaks at 62.3 keV and 88.3 keV and a narrow peak near 103 keV are seen in the coincidence spectrum.

3.8 Identification of different peaks

In the final coincidence spectrum [Fig. 3.10 (bottom panel)], we have to first distinguish between the fission fragment γ-rays and K x-rays from the plutonium ion. The fission fragment γ-ray line would be significantly Doppler broadened and double-humped, because the gamma ray emitting fragment could be moving either towards or away from the LEPS detector depending on whether the fission detector would record the gamma emitting fragment or its complementary fragment.

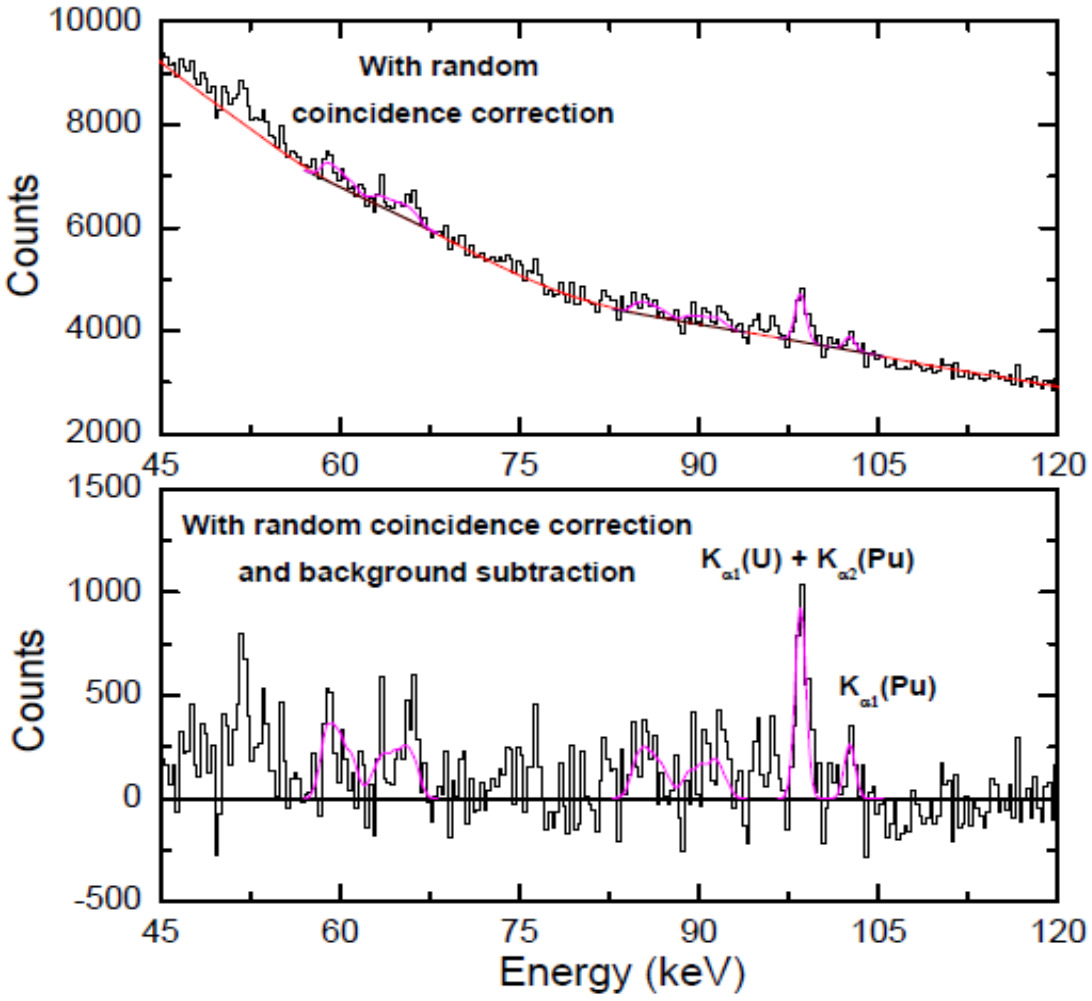

Fig. 3.10: *(Upper panel) Random coincidence corrected photon spectrum with solid red background is shown in the upper panel. Solid red background subtracted spectrum along with GEANT3 simulated fission fragment γ-ray peaks (magenta color curves) at 62.3 keV and 88.3 keV. The peaks at 98.4 keV and around 103 keV are also shown in magenta color.*

Assuming the emissions of 62.3 keV and 88.3 keV γ-rays from the fission fragments, we have performed GEANT3 simulation [Bru86] with the actual experimental geometry and obtained two double humped peaks centered around 62.3 keV and 88.3 keV which resemble the experimental data as shown in Fig. 3.10 (bottom panel) by the superimposed magenta curves. When gated on high energy side of the fission fragment spectrum, 62.3 keV γ-ray went away, implying that the gamma ray was coming from a heavy fission fragment. So, we interpret the double humped broad peaks seen around 62.3 keV and 88.3 keV as fission fragment γ-rays.

The narrow peak seen around 103 keV could be the plutonium $K_{\alpha 1}$ line with its associated $K_{\alpha 2}$ line overlapping with the uranium $K_{\alpha 1}$ line (around 98.4 keV). Alternatively, it could be a fission fragment γ-ray whose lower energy hump is overlapping with the uranium $K_{\alpha 1}$ line. In order to distinguish between these two possibilities, we have first assumed that the peak near 103 keV is the higher energy hump of a fission fragment γ-ray. A GEANT3 simulation [Bru86] of a sharp 100.8 keV γ-ray line from a fission fragment as seen by our detector setup has been done. The simulation produces a high energy hump and a low energy hump that overlap with the plutonium $K_{\alpha 1}$ and uranium $K_{\alpha 1}$ lines respectively. The GEANT3 simulated curve cannot at all fit the data points around 98.4 keV. However, there could be additional uranium $K_{\alpha 1}$ yield due to the imperfect cancellation of the random gated γ-ray photons and long-lived fission component of ^{238}U excited by inelastic ^{4}He collisions. So, additional uranium $K_{\alpha 1}$ yield (assuming a Gaussian peak shape with FWHM = 1 keV) has been added up to the best fitted simulated high energy hump of fission fragment γ-ray spectrum. The overall fit has been obtained by adjusting the areas under the added uranium $K_{\alpha 1}$ line and GEANT3 simulated spectrum simultaneously and the best fit as shown by the dash blue curve in Fig. 3.11 gives a reduced χ^2=1.1. However, this fit

considerably reduces the area under the GEANT3 simulated spectrum and increases the area of the added uranium $K_{\alpha 1}$ line. As a result, GEANT3 simulated high energy hump (100.8 keV to 105.3 keV) of the fission fragment γ-ray becomes poorly defined (ratio of area under the GEANT3 simulated curve to its statistical error bar ≈ 2). So the data points in the 96.6 keV to 105.3 keV region cannot be consistently fitted by GEANT3 simulated spectrum with an added 98.4 keV line with a high statistical significance.

Let us now consider whether the observed peak around 103 keV could be the plutonium $K_{\alpha 1}$ line in true coincidence with the fission fragments. The plutonium $K_{\alpha 1}$ line should be associated with its $K_{\alpha 2}$ line that overlaps with uranium $K_{\alpha 1}$ line. So we fit the data points in the region from 96.6 keV to 105.3 keV by two isolated Gaussian peaks with peak positions at 102.6 keV and 98.4 keV (FWHM= 1keV) as shown by the red curve in Fig. 3.11 and get an excellent fit with reduced χ^2=1.0. Both the peaks at 102.6 keV(FWHM=1 keV) and 98.4 keV (FWHM=1 keV) are statistically significant with > 99% confidence level. Assuming that the yield near 103 keV in the true coincidence spectrum is due to the $K_{\alpha 1}$ line of the plutonium ion, we have subtracted out the expected plutonium $K_{\alpha 2}$ yield from the observed yield at 98.4 keV. The remaining yield at 98.4 keV should be the remnant of uranium $K_{\alpha 1}$ line and tally with the observed remnant of uranium $K_{\alpha 2}$ line at 94.6 keV. We find that the ratio of the relative efficiency corrected yield of the remnants of uranium $K_{\alpha 2}$ to uranium $K_{\alpha 1}$ line is = 0.52 ± 0.17, in good agreement with the known branching ratio of 0.625 [Led78].

So we find that the data points from 96.6 keV to 105.3 could be best described by two isolated narrow Gaussian peaks (FWHM=1 keV) centered at 102.6 keV and 98.4 keV with a high

statistical confidence level (> 99%). The description of those data points with a GEANT3 simulated fission fragment γ-ray and 98.4 keV remnant uranium $K_{\alpha 1}$ line becomes statistically poorly defined. Hence, narrow plutonium K x-ray lines are statistically much better description of the data points than a broad double-humped fission fragment γ-ray peak in this energy region. Moreover, 103 keV narrow peak exists with similar intensity when gated on different parts of the fission fragment kinetic energy spectrum (having equal number of fission fragments), whereas the intensities of the broad humps at 62.3 keV and 88.3 keV depend on the regions of gating over the fission fragment kinetic energy spectrum. This result provides further support to our interpretation that the peak around 103 keV is the plutonium $K_{\alpha 1}$ line.

3.9 Determination of intrinsic width of Plutonium K x-ray peaks and estimation of fission time

The Gaussian fitting of the data points around 103 keV (from 101.7 keV - 103.5 keV) in Fig. 3.11 gives a peak at 102.6 keV (interpreted as plutonium $K_{\alpha 1}$ line) with a FWHM = (1±0.3) keV. A double Gaussian fitting of the peak around 98.4 keV (from 96.9 keV to 100.5 keV) was done considering that the peak comprises yield from plutonium $K_{\alpha 2}$ line (as estimated from the plutonium $K_{\alpha 1}$ line) and remnant of uranium $K_{\alpha 1}$ line. The best fit gives FWHM of the plutonium $K_{\alpha 2}$ line as = (1±0.4) keV. Combining the uncertainties on the FWHM of plutonium $K_{\alpha 1}$ and $K_{\alpha 2}$ lines in quadrature, we obtain the FWHM of plutonium K x-ray line as F_{Pu}= (1±0.24) keV. The detector resolution (F_D) was extracted by Gaussian fitting of the singles 98.4 keV uranium $K_{\alpha 1}$ line and using the intrinsic width of 98.4 keV line as 0.1 keV [Kra79] and we obtained it as

F_D=(1±0.01) keV. Let F_{i_Pu} and F_i be the intrinsic FWHM of plutonium K x-ray line containing a fissioning plutonium nucleus and intrinsic width of plutonium K x-ray line with a stable plutonium nucleus. Let F_{Pu} be the experimentally observed FWHM of the K x-ray line of plutonium in coincidence with the fission fragments. Then $F_{Pu} = \left(F_D^2 + F_i^2 + F_{i\_Pu}^2\right)^{0.5}$ i.e. $F_{i\_Pu} = (F_{Pu}^2 - F_D^2 - F_i^2)^{0.5}$. The quantities F_{Pu}, F_D were obtained from the experimental data and F_i is known from ref. [Kra79]. So, F_{i_Pu} was determined from the above equation. The corresponding error on F_{i_Pu} was obtained by adding up the errors on F_D, F_i and F_{Pu} in quadrature. So, we obtain that the intrinsic width of plutonium K x-ray line in coincidence with the fission fragments F_{i_Pu} =(0±0.24) keV. Since the standard deviation σ=0.24 keV, FWHM= 2.35×0.24 keV= 0.56 keV. Following ref. [Anh85] and using quantum energy-time uncertainty principle, we obtain the corresponding fission time of the excited plutonium nucleus from the measured uncertainty (0.56 keV) on the intrinsic width of the plutonium K x ray line as $\tau_{fission} > \frac{\hbar}{0.56\ keV}$ =1×10^{-18} sec. Of course, fast fission events would produce broader K x-ray lines, but their yield would also be smaller and would be cut out by our background line. So, we could not determine the percentage of fission events responsible for the atomic K x-ray yield from the analysis of the peak width.

The energies of plutonium $K_{\alpha 1}$ and $K_{\alpha 2}$ lines are 103.7 keV and 99.5 keV respectively [Led78]. However, we observed plutonium $K_{\alpha 1}$ line at 102.6 keV from the Gaussian fit. The centroid of the peak as obtained by taking weighted average of the channel counts is = (102.8±0.5) keV, in agreement with the energy of the standard plutonium $K_{\alpha 1}$ line (103.7 keV) [Led78] within two standard deviations. As the plutonium is produced by the fusion of ^{4}He+^{238}U, more than 30% of

the outer orbital electrons of plutonium are expected to be ejected out by the electronic shake-off process [Tho68] and the K x-ray lines of the plutonium ion are expected to come at lower energies. Moreover, K x-ray energies are expected to come at lower energies for a rotating deformed plutonium nucleus.

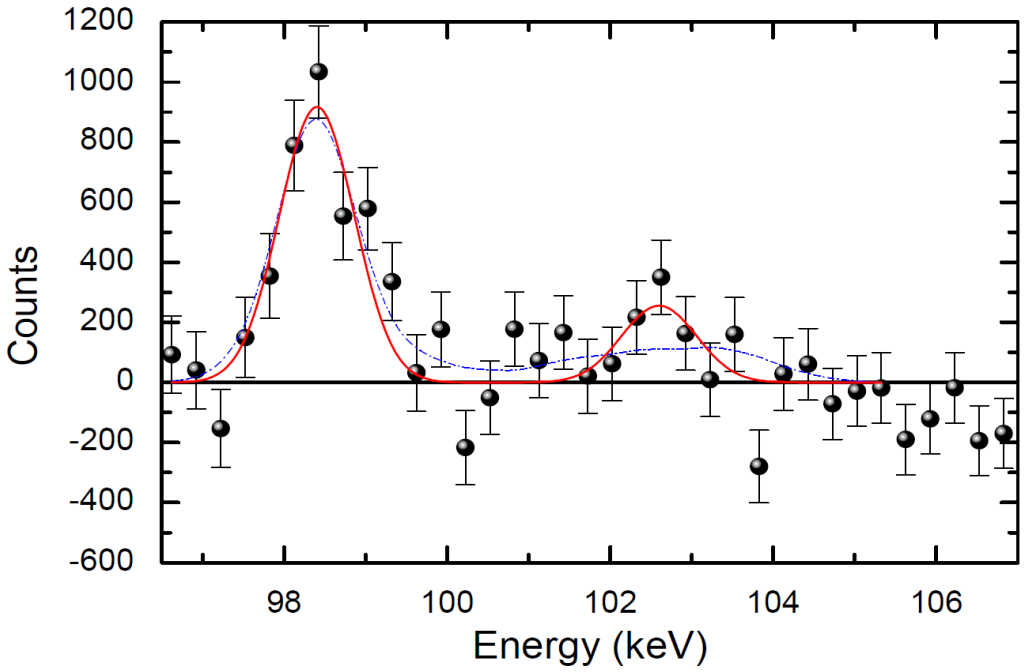

Fig. 3.11: *Data points of Fig. 3.10 (bottom panel) with statistical error bars shown in the energy range between 96.5 keV and 107 keV. Dash blue curve represents GEANT3 simulation of a sharp 100.8 keV γ-ray line from a fission fragment with an additional uranium 98.4 keV line and red curve shows Gaussian fitting of the data points with two isolated peaks. (see text for details)*

3.10 Origin of various γ-rays and x-rays near 103 keV

Apart from the emission of K x-rays from plutonium ion containing fissioning nucleus in coincidence with the fission fragments, there are several other sources of γ-rays and x-rays near 103 keV that do not involve emission of fission fragments and could be present in the true coincidence spectrum (Fig. 3.10) due to the imperfect cancellation of the random gated γ-ray photons. As discussed in the case of singles spectrum, K x-ray and γ-ray yield near 103 keV could also be obtained by the creation of plutonium K vacancy [Dec73] due to the sequential neutron and γ emissions followed by internal K conversion process. Coulomb excitation of ^{238}U would also give a 103.5 keV γ-ray photon. Unfortunately, the Coulomb excitation line of ^{238}U overlaps with the plutonium $K_{\alpha 1}$ line and their relative intensities cannot be determined from the spectrum. So, we took singles LEPS spectrum of ^{4}He+^{232}Th reaction at $E_{Lab}(^{4}He)$=60MeV (Fig. 3.12). The Coulomb excitation line of ^{232}Th is at 112.75 keV [Joh75] well separated from the thorium atomic excitation lines (93.3 keV and 89.9 keV). From the singles spectrum (Fig. 3.12), we find negligible amount of 112.75 keV yield compared to that for atomic excitation lines of thorium. The results for ^{4}He+^{238}U reaction at $E_{Lab}(^{4}He)$=60 MeV must be similar to that for ^{4}He+^{232}Th reaction at the same bombarding energy and so the yield of Coulomb excitation line would be negligible. However, 98 keV K x-ray line of uranium (produced by the sequential neutron emissions followed by electromagnetic transitions and internal conversion process) is seen in Fig. 3.12 and it is much stronger than the Coulomb excitation line of ^{232}Th. Since the reaction mechanism for ^{4}He+^{232}Th and ^{4}He+^{238}U at the same bombarding energy of ^{4}He [$E(^{4}He)_{Lab}$=60 MeV] should be very similar, we expect that the K x-ray yield of plutonium produced by the slow process of internal conversion preceded by sequential neutron emissions and a cascade of electromagnetic transitions would be the dominant background near 103 keV.

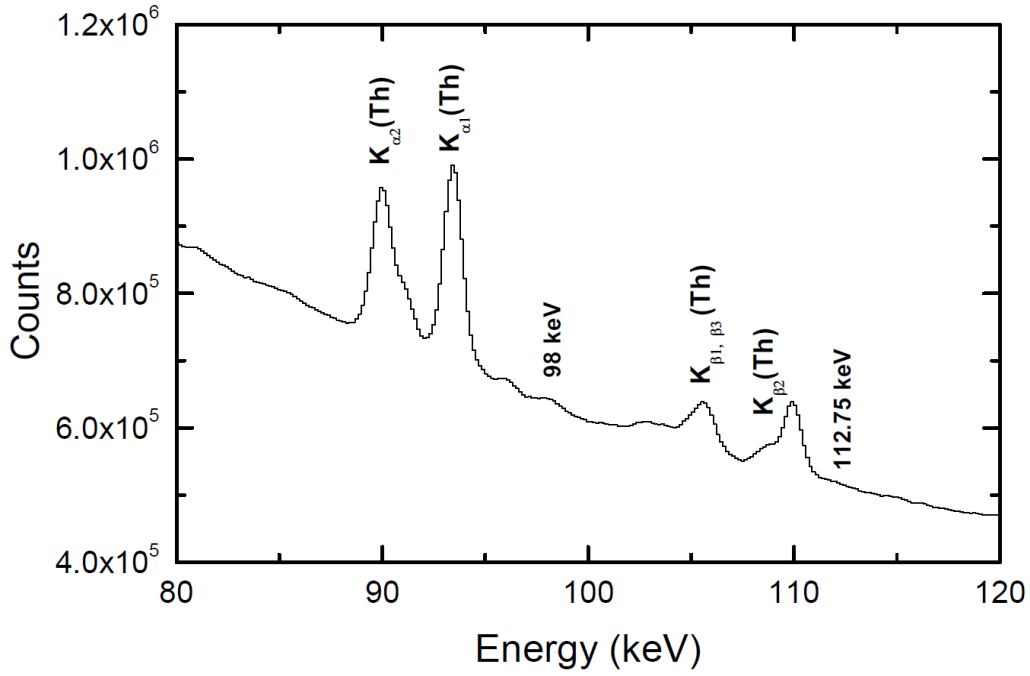

Fig. 3.12: *Singles photon spectrum resulting from the reaction of 60 MeV* $^{4}He + {}^{232}Th$.

We find from the prompt spectrum (Fig 3.8) that the relative efficiency corrected total yield around 103 keV is about 0.13 times that of the uranium $K_{\alpha 1}$ (98.4 keV) line and about 0.22 times that of the uranium $K_{\alpha 2}$ (94.65 keV) line, whereas in the random corrected true coincidence spectrum (Fig 3.10), the relative efficiency corrected yield around 103 keV is about 0.7 times that of the 98.4 keV line and 5 times that of the 94.65 keV line. So, the peak seen around 103 keV in the random corrected true coincidence spectrum [Fig 3.10 (bottom panel)] should not be the remnant of the K x-rays produced by the slow internal conversion process without any fission fragment emission. It should mostly be the K x-ray photons in true coincidence with the fission fragments.

3.11 K x-ray ionization probability and cross-section

K x-ray ionization probability for the fusion of 60 MeV $^{4}He^{2+}$ on ^{238}U target is required for the determination of percentage of long-lived fission components of the highly excited ^{242}Pu nucleus. Kravchuk *et al.* [Kra04] compiled K orbital ionization probabilities (P_K) of different targets (such as Pb, Th etc.] due to the elastic collisions with ^{4}He ion of different energies ranging from 25 MeV to 75 MeV for zero impact parameter (atomic scale). They have plotted the reduced velocity ξ_K (as defined before) versus P_K/Z^2, (where Z is the atomic number of target atom) for various targets and energies and all the data points fell on a single curve as shown in Fig. 2.2. Hence, irrespective of the target used or the bombarding energy of ^{4}He ion, all the data points fall on a specific curve, if plotted in this way [Kra04]. In the case of $^{4}He+^{238}U$ reaction at $E_{Lab}(^{4}He)$=60 MeV, $\xi_K = 0.54$. It is seen from Fig. 2.2 [Kra04] for the elastic collisions with ^{4}He ions, the probability of K orbital ionization is $P_{el} = (5.3\pm0.7) \times 10^{-4}$ for $\xi_K = 0.54$. Since only the incoming part of the trajectory must be taken into account in the case of fusion, the probability of creation of K orbital vacancy in uranium due to elastic interaction with ^{4}He of 60 MeV energy can be approximately taken [Fre12] as $=P_{el}/2 = (2.65\pm0.35) \times 10^{-4}$. As ^{4}He would fuse with ^{238}U to produce ^{242}Pu, all the K orbital vacancies of uranium would be transferred to the plutonium and significantly more K orbital vacancies would be produced by the shake-off process.

As ^{4}He comes within the nuclear interaction region of ^{238}U, we assume that fusion immediately takes place in a timescale much shorter than the electronic rearrangement time causing shake-off ionization as discussed in section 2.2.2. Following Carlson *et al.*'s treatment [Tho68], we use sudden approximation to calculate the probability of K orbital ionization of plutonium due to the

shake-off process. Let $\psi_U(1s)$ and $\psi_{Pu}(1s)$ be the 1s electronic wave functions of uranium and plutonium atoms respectively. Then, in sudden approximation, the probability of creating K orbital vacancy in plutonium due to the sudden transformation from uranium to plutonium is given by $P_k(shakeoff) = 1 - \left| \int_v \psi^*_{Pu}(1s)\psi_U(1s)dV \right|^2$ where the integral is over the entire volume. Carlson *et al.* [Tho68] found that for high Z atoms, wave functions obtained from self consistent field theories (such as Hartree-Fock) gave much better agreement with the beta decay experimental results than the hydrogenic wave functions. It was found [Tho68] that in the case of uranium atom and for beta decays, the square of the overlap integral with self consistent field theory wave functions was about 0.01% smaller than that with hydrogenic wave functions. Using hydrogenic wave functions, we obtain $\left| \int_v \psi^*_{Pu}(1s)\psi_U(1s)dV \right|^2$ =0.9996531. Reducing it by 0.01%, we obtain $P_k(shakeoff) = 0.0045$. In the case of the overlap integral between plutonium and uranium wave functions, the reduction factor could be somewhat larger than 0.01%, but that has not been considered. So, we have taken $P_k(shakeoff) = 0.0045$. Hence, the total probability of creating K orbital vacancy in plutonium due to the fusion of 60 MeV ^{4}He with ^{238}U is $P_K = \frac{P_{el}}{2} + P_k(shakeoff) \geq 7.2 \times 10^{-4}$.

We also need the absolute cross-section of uranium $K_{\alpha 1}$ line produced by the bombardment of 60 MeV ^{4}He on ^{238} U which will be required for normalization and determination of percentage of long lived fission components. It was obtained by scaling [Kra01] the experimentally measured absolute K x-ray cross-sections of Ta, Pb and Th produced by the bombardment of ^{4}He

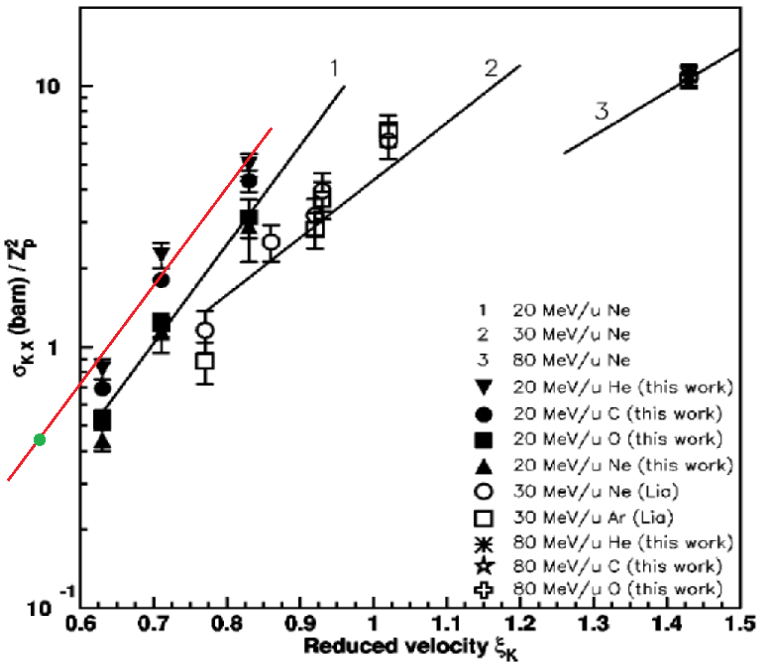

Fig. 3.13: *Experimental reduced K x-ray cross-section is plotted with reduced velocity (ξ_k) taken from ref.* [Kra01]. *The red line shows the extrapolation of data for bombardment of 20 Mev/u ^{4}He particles on various targets and the reduced K x-ray cross-section obtained at reduced velocity (ξ_k=0.54) is pointed in green color.*

particles at E(^{4}He)$_{Lab}$=80 MeV indicated by red line in Fig. 3.13. As indicated in green color in Fig. 3.13, the absolute K X-ray cross-section for reduced velocity (ξ =0.54) is 1.7 barn. The uncertainty on this number should be about 10%, since the uncertainties on all the data points were about 10% and the agreement with KXCROSS calculations were within 10%. Using the known branching ratio of $K_{\alpha 1}$ line for uranium, the absolute cross-section of uranium $K_{\alpha 1}$ line is $\sigma_{UK\alpha 1}$= (0.8 ±0.1) barn.

3.12 Determination of percentage of slow fission component

We have determined the percentage of slow fission component from the K x-ray multiplicity per fission event (σ_K / σ_f) where σ_K is K x-ray cross-section in coincidence with the fission events and σ_f is the fission cross-section. The absolute fission cross-section of plutonium (E_X =55 MeV) has been taken as =(2±0.1) barn [Jai95]. The observed plutonium $K_{\alpha 1}$ yield (as obtained from the Gaussian fitting) in true coincidence with the fission fragments was corrected for contributions from the random events where the correction factor has been obtained by dividing the remnant yield of $K_{\alpha 2}$ (94.65 keV) observed in the coincidence spectrum (Fig. 3.10) with the corresponding yield in the random coincidence spectrum (Fig. 3.7). In order to obtain the absolute cross-section of plutonium $K_{\alpha 1}$ line in coincidence with all the fission events produced in the reaction, the measured coincidence yield was corrected by the coincidence efficiency of the fission fragment detector and relative efficiency of LEPS detectors and normalized with respect to the area of singles uranium $K_{\alpha 1}$ line. The cross-section of plutonium K x-ray was obtained as follows. Let N_{103} be the measured coincidence yield of plutonium $K_{\alpha 1}$ line in coincidence with the fission fragments and N_{98} be the yield of 98.4 keV line in the singles spectrum. Let ϵ_f be the efficiency of the fission detector. Let ϵ_{98} and ϵ_{103} be the absolute efficiencies of the LEPS detector at 98.4 keV and 103 keV. Then normalizing with respect to the yield of 98.4 keV uranium $K_{\alpha 1}$ line measured simultaneously by the same LEPS detector, we obtain the cross-section of plutonium $K_{\alpha 1}$ line as

$$\sigma_{PuK\alpha 1} = \frac{\sigma_{UK\alpha 1} \times N_{103} \times \epsilon_{98}}{N_{98} \times \epsilon_f \times \epsilon_{103}} \quad (3.1)$$

where $\sigma_{PuK\alpha 1}$ and $\sigma_{UK\alpha 1}$ are the cross-sections of uranium and plutonium $K_{\alpha 1}$ lines respectively and $\sigma_{UK\alpha 1}$= (0.8 ±0.08) barn obtained in the previous section. The ratio ($\epsilon_{98}/\epsilon_{103}$) is the relative efficiency of LEPS detector for 98.4 keV line with respect to 103 keV and obtained from our measured relative efficiency curve of the LEPS detector shown in Fig. 3.3. ϵ_f is obtained from the geometry of the fission detector using GEANT3 simulation. Hence, the cross-section $\sigma_{PuK\alpha 1}$ was obtained and it was corrected by the known branching ratio of plutonium K x-rays ($B_{PuK\alpha 1}$= 2.12) to obtain plutonium K x-ray cross-section σ_K . Thus, we obtain $\sigma_K/\sigma_f = 5.3 \times 10^{-4}$ with about 30% uncertainty. The uncertainty mostly comes from the statistical uncertainty on N_{103}.

Although this K x-ray multiplicity per fission is a small number, the probability of creation of a K orbital vacancy (P_K) in the fusion process of ^{4}He+^{238}U is also a small number. The total estimated probability of creation of K vacancy in plutonium produced by ^{4}He+^{238}U at $E(^4He)_{Lab}$=60 has been estimated in the last section as $\geq 7.2\times10^{-4}$. Taking the probability of creation of K-orbital vacancy P_K= 7.2×10^{-4} and fluorescence yield $\omega_K \approx 1$ [Hub94], we obtain $\sigma_K/(P_k\sigma_f) = 0.73$. The result implies that even for a bimodal distribution with a very long fission component ($\tau_f \rightarrow \infty$) and a very short fission component that does not contribute at all to K x-ray yield, a minimum of 73% of all fission events are very slow. Thus, we conclude that most of the fission events are slow with a mean fission time > 1×10^{-18} sec. For any other fission time distribution, the percentage of slow fission components would increase. Considering our uncertainties, we conclude qualitatively that most of the fission events are slow.

3.13 Effect of different background subtractions

In this section, the effects of different background subtractions in Fig. 3.10 (upper panel) on the conclusions drawn from the true coincidence spectrum have been studied in detail. We have drawn three different background curves (solid red, dotted blue and dot-dash green) on the random corrected true coincidence spectrum shown in Fig. 3.14 where solid red curve is the background curve of Fig. 3.10 (upper panel).

Solid red curve background subtraction

Before drawing any background, we have fitted the data points around 103 keV, 98.4 keV regions in the random corrected coincidence spectrum Fig. 3.10 (upper panel) with Gaussian functions plus linear backgrounds shown by black lines. Broad double-humped peak structures seen around 63 keV and 88 keV are best fitted by GEANT3 [Bru86] simulated curves obtained by using actual experimental geometry and linear backgrounds (black lines). We have obtained best-fitted linear backgrounds (black lines) under different narrow and broad peaks. The best fit (χ^2=0.9) for the data points around 103 keV (before drawing any background) gives a narrow Gaussian peak at 102.6 keV with FWHM ≈ 1keV. A smooth curve (solid red curve) has been drawn by joining these best fitted black straight lines and it has been taken as the best background curve (Fig. 3.10). We consider the red background as the most reasonable background and have performed our analysis for the red background. The dotted blue background has been drawn slightly below the red background to study the effect of small changes in drawing background and the dot-dash green background has been drawn far below the red background.

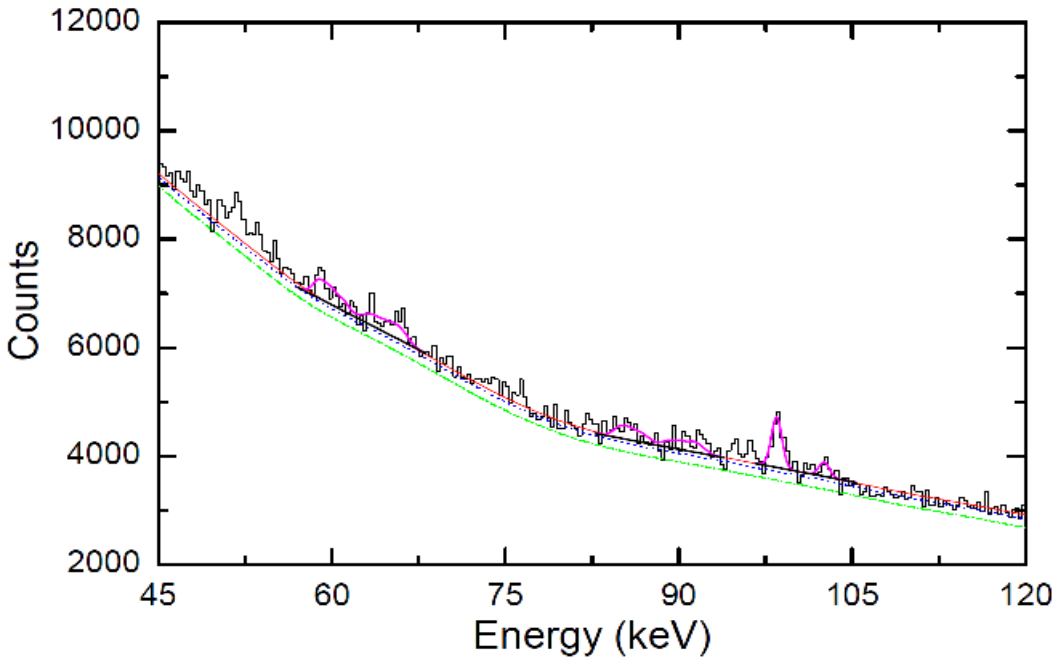

Fig. 3.14: *Random coincidence corrected photon spectra is shown. Plausible backgrounds are shown by solid red, dotted blue and dot-dash green curves where solid red line is the background curve of Fig. 3.10 (upper panel).*

Dotted blue background subtraction

We have repeated the analysis using dotted blue background of Fig. 3.14 which is lower than solid red background by 75 counts at each channel. We show dotted blue background drawn on the random corrected coincidence spectrum in Fig. 3.14 and random corrected coincidence spectrum after subtracting out the dotted blue background in Fig. 3.15 (upper panel). As obtained earlier for solid red background of Fig. 3.10, we find that all the uranium K x-ray lines have been suppressed by a large factor compared to their intensities in the singles spectrum. We see a

relatively intense peak at 98.4 keV, remnant of 94.65 keV peak and broad double-humped peaks at 62.3 keV and 88.3 keV in the coincidence spectrum. The broad double-humped peaks have been interpreted as γ-rays from the fission fragments and the corresponding GEANT3 simulation [Bru86] of the fission fragment γ-rays with the actual experimental geometry has been shown as magenta color curves [Fig. 3.15 (upper panel)]. The peak at 98.4 keV peak and near 103 keV have also been shown in magenta color [Fig. 3.15 (upper panel)]. Considering the suppression factor of the uranium atomic excitation lines in the true coincidence spectrum compared to their yields in the singles spectrum, the contribution of random coincidence events around 103 keV in the true coincidence spectrum [Fig. 3.15 (upper panel)] can account for ~50% of the Gaussian peak (magenta color) area (FWHM = 1keV) centered around 103 keV. So, about half of the peak area seen around 103 keV in the random corrected true coincidence spectrum [Fig. 3.15 (upper panel)] should be the K x-ray photons in true coincidence with the fission fragments.

In Fig. 3.16, we show the random and background subtracted true coincidence spectrum from 96.5 KeV to 107 keV. In order to determine whether the peak around 103 keV is due to fission fragment γ-ray or a plutonium K x-ray line, we have done GEANT3 simulation [Bru86] of a sharp 100.8 keV γ-ray line from a fission fragment as seen by our detector setup. The yield of the GEANT3 simulated curve was adjusted to obtain the best fit of the data points in the region from 96.6 keV to 105.3 keV. In this process, a good fit of the data points around 103 keV (from 100.5 keV to 105.3 keV) was obtained. It is possible to improve the overall fit in the 96.6 keV to 105.3 keV region by adjusting the areas under the added uranium $K_{\alpha 1}$ line and GEANT3 simulated spectrum simultaneously and the best fit shown by the dashed blue curve gives a reduced χ^2=1.1 as shown in Fig. 3.16. However the ratio of the relative efficiency corrected remnants of uranium

$K_{\alpha 2}$ to uranium $K_{\alpha 1}$ yields becomes = 0.95±0.17, in disagreement with the known branching ratio of 0.625 [Led78].

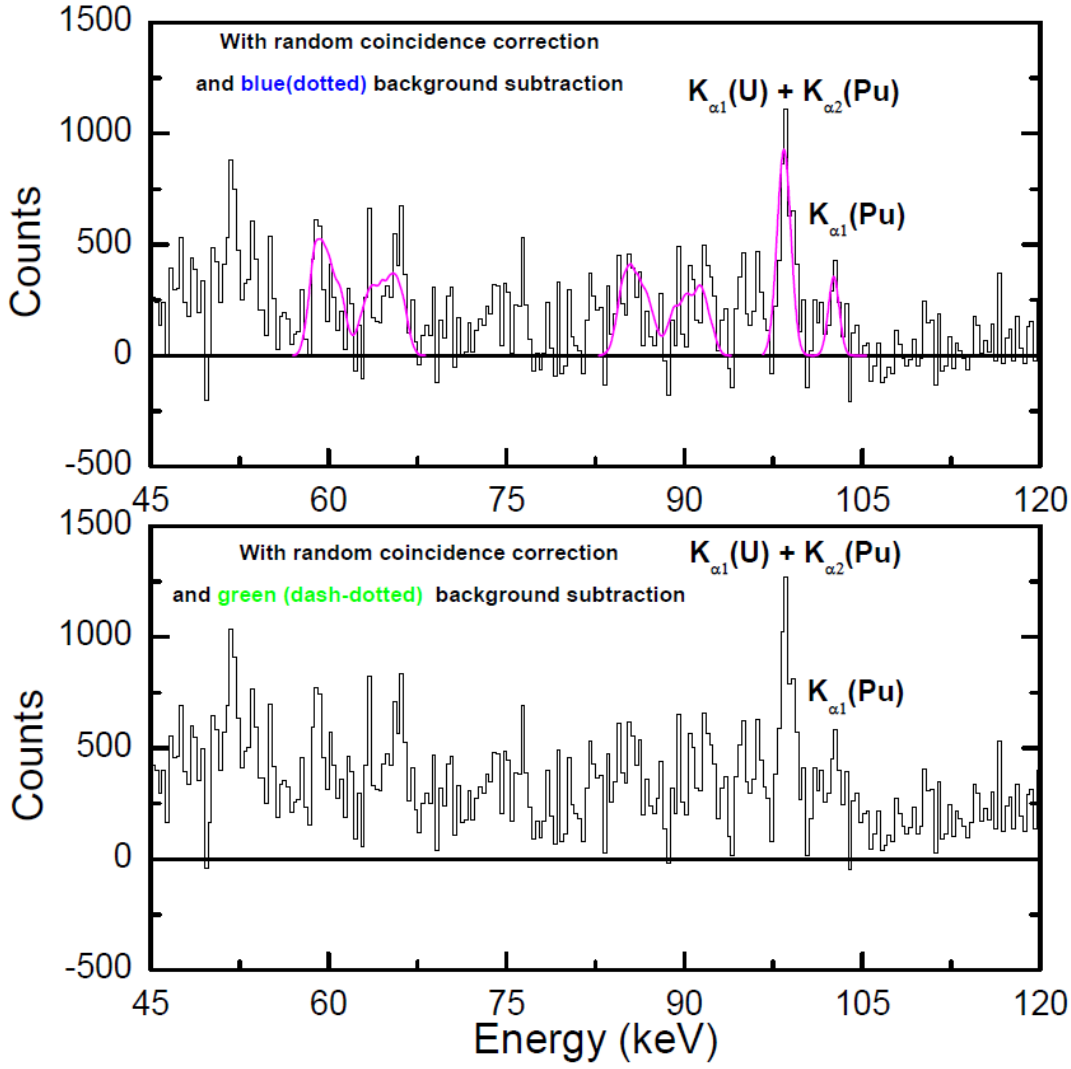

Fig. 3.15: *(Upper panel) Random corrected coincidence spectra for both the dotted blue (upper panel) background subtraction with fission γ-ray and K x-ray line in magenta color and dot-dash green (lower panel) background subtraction. This backgrounds are shown in Fig. 3.14.*

Let us now analyze the spectrum assuming the peak at 103 keV as the plutonium $K_{\alpha 1}$ line and its associated $K_{\alpha 2}$ line is overlapping with 98.4 keV uranium $K_{\alpha 1}$ line. In Fig. 3.16, we show by solid red curve fits with two isolated Gaussian peaks with the peak positions at 98.4 keV and 102.6 keV (FWHM=1 keV) and obtain a very good fit (reduced χ^2=1.1). The estimated plutonium $K_{\alpha 2}$ yield (based on the observed yield at 103 keV) has been subtracted out from the fitted Gaussian peak area at 98.4 keV to obtain the yield of the remnant uranium $K_{\alpha 1}$ line. The ratio of the remnants of uranium $K_{\alpha 2}$ to uranium $K_{\alpha 1}$ yield (after relative efficiency correction) is = 0.64 ± 0.15, in good agreement with the known branching ratio of 0.625 [27]. So we conclude that two isolated Gaussian peaks (FWHM = 1keV) centered at 102.6 keV and 98.4 keV give a consistent description of the observed spectrum, whereas, a broad double humped fission peak plus an additional Gaussian peak at 98.4 keV fail to give a consistent description of the spectrum. Hence, the peak at 103 keV should be the $K_{\alpha 1}$ line from the plutonium ions produced by the fusion process. Using the procedure described earlier, we have obtained plutonium K x-ray multiplicity per fission event(σ_K/σ_f) and finally got $\frac{\sigma_K}{P_K \sigma_f} = 0.92$ implying that a minimum of 92% of all fission events are slow even for a bimodal distribution with a very long fission component ($\tau_f \rightarrow \infty$) and a very short fission component. Hence, the results obtained by using dotted blue and solid red backgrounds of Fig. 3.10 are similar and we conclude that most of the fission events are slow with fission time $>10^{-18}$ s.

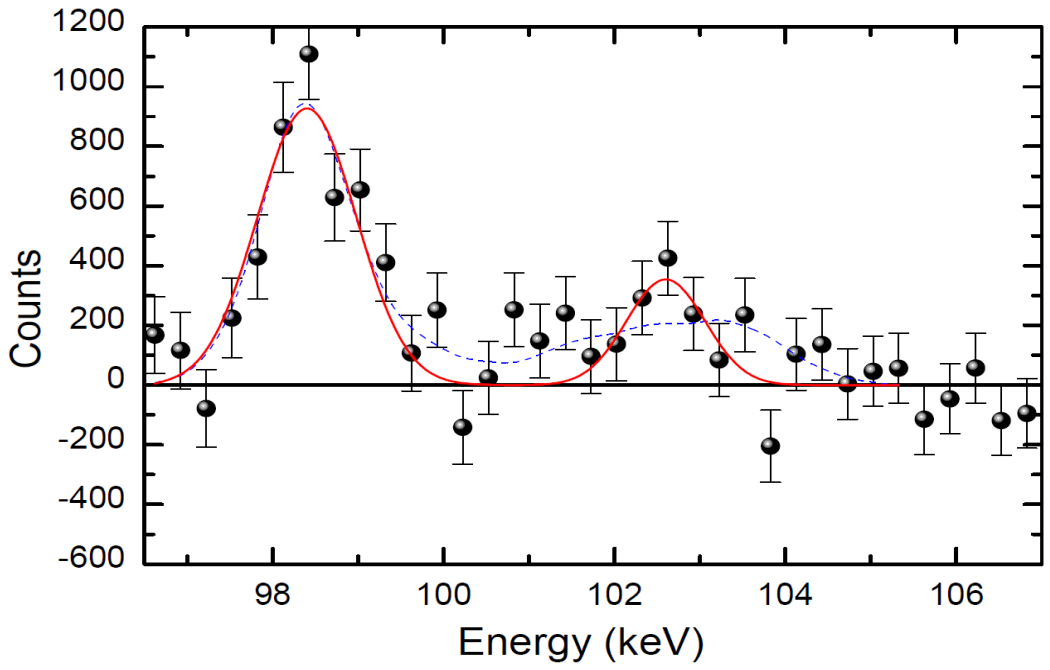

Fig. 3.16: *Random corrected coincidence spectra for the dotted blue subtracted background as shown in Fig. 3.15 (upper pannel) with statistical error bars shown in the energy range between 96.5 keV and 107 keV. Dash blue curve represents GEANT3 simulation of a sharp 100.8 keV γ-ray line from a fission fragment with an additional uranium 98.4 keV line and red curve shows Gaussian fitting of the data points with two isolated peaks.*

Dot-dash green background subtraction

In Fig. 3.15 (lower panel), we show the random corrected coincidence spectrum with the dot-dash green background subtraction. There are hardly any negative counts in this spectrum implying that the background was drawn too low. In Fig. 3.17, we show the dot-dash green background subtracted spectrum in the region from (96.5-107) keV. In this case, a Gaussian fitting of the data points around 103 keV from (101.7 -105.3) keV gives a broad peak with the peak position at 102.6 keV and FWHM = 4.4 keV as shown by the red curve in Fig. 3.17 with a

reduced χ^2=1.4 and a large Gaussian area. However, a linear fit (shown by dot-dash green line in Fig. 3.17) gives a better fit (χ^2 =1.26) for those data points indicating that if there is a peak, it is riding on a high background. Moreover, a large width of plutonium K x-ray would imply a short fission time, whereas a large yield of fluorescence K x-ray would imply a long fission time. The combination of a large width and large yield could be made consistent only for an unrealistically high value (of the order of one) of P_K (probability of creation of K vacancy). This high value of P_K looks implausible for $^4He+^{238}U$ reaction, because such high values of P_K were obtained for U+U [Mol93] and Ni+U [Fre12] reactions. A GEANT3 simulation [Bru86] of a fission fragment γ-ray whose two humps fall on the 103 keV and 98.4 keV regions is shown by dashed blue curve in Fig. 3.17. As before, varying area under GEANT3 simulation and an additional yield from the remnant of uranium 98.4 keV (FWHM = 1 keV), we obtain a best fit of χ^2=1.65. However, the remnant of uranium $K_{\alpha 2}$ (94.65 keV) line is large here and the ratio of uranium $K_{\alpha 2}$ (94.65 keV) to $K_{\alpha 1}$ (98.4 keV) line become 2± 0.5, in disagreement with the known branching ratio of 0.63 by more than three standard deviations. So, clearly the dot-dash green line, background is too low.

Hence, regarding the question whether the extracted width of the plutonium $K_{\alpha 1}$ line depends on the background drawn on Fig. 3.10 (bottom panel), we find similar results for the solid red and dotted blue backgrounds. However, if the background is lowered further to dot-dash green curve, then the width of the plutonium K x-ray could be made very large, but the area under the Gaussian peak also increases making the width and yield inconsistent with each other and the ratio of the relative efficiency corrected remnant of uranium $K_{\alpha 2}$ (94.65 keV) to $K_{\alpha 1}$ (98.4 keV) line becomes very implausible.

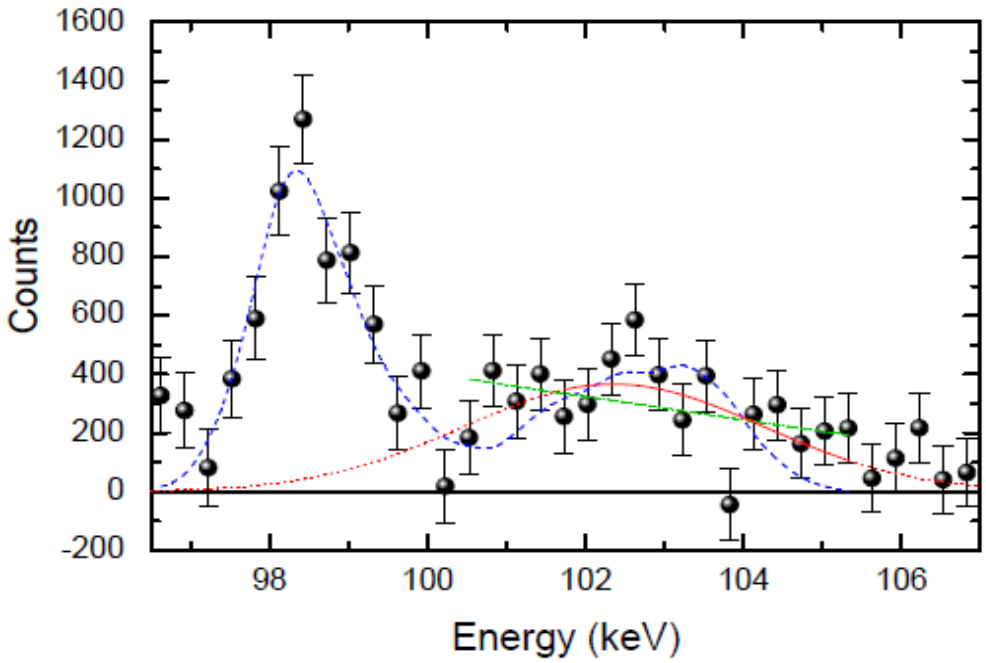

Fig. 3.17: *Random corrected coincidence spectra for the dot-dash green subtracted background as shown in Fig. 3.15 (lower panel) with statistical error bars shown in the energy range between 96.5 keV and 107 keV. Dash blue curve represents GEANT3 simulation of a sharp 100.8 keV γ-ray line from a fission fragment with additional yield at 98.4 keV. The red curve and dot-dash green line shows the Gaussian fitting and the linear fitting of the data points around 102.6 keV. Solid red curve indicates the region over which the data points has been used for Gaussian fitting and dotted red is the extrapolation of the obtained fit.*

3.14 Comparison with previous results

The results obtained from our K x-ray fission fragment coincidence experiment have been compared with previous results obtained by atomic and nuclear techniques for similarly excited fissioning system. Molitoris *et al.* [Mol93] using an K x-ray technique observed a long fission

time (~ 10^{-18} sec) for the majority of the observed fission fragments emitted by the highly excited (E_X = 40–105 MeV) uraniumlike nuclei having low fission barriers [Mol09]. Using the crystal blocking technique, Goldenbaum *et al.* [Gol99] obtained fission time of highly excited ($E_x \approx$ 160 MeV) uraniumlike nucleus (Z = 92 ± 5) on the order of 10^{-18} sec. Wilschut and Kravchuk [Wil04] measured the fission time of highly excited (E_X = 145 MeV) neptunium nuclei on the order of 10^{-18} sec using an K x-ray technique. F. Barrué *et al.* using crystal blocking experiment [Bar02] obtained that the fission time of both uranium and lead nuclei is on the order of 10^{-18} sec for majority of the events at excitation energy (E_x < 250-300 MeV). Thus, our experimental results are in agreement with all the previous fission time measurements of highly excited ^{238}U or similar fissile nucleus by the atomic methods.

On the contrary, Saxena *et al.*[Sax94] measured fission time of ^{243}Am ($E_X \approx$ 60 MeV) produced by ^{11}B+^{232}Th reaction using prefission neutron multiplicity technique and obtained prefission neutron multiplicity = 2.1 ± 0.15 corresponding to fission time ≈ 10^{-20} sec. This result differs from our and other atomic results by at least two orders of magnitude. To understand the problem in more detail, we have done JOANNE2 code [Les93] calculations for ^{4}He+^{238}U reaction at E_{Lab}(^{4}He) = 60 MeV. We have determined prefission neutron multiplicities for different fission delay times. Fig. 3.18 shows a plot of fission delay time versus prefission neutron multiplicity. We find from Fig. 3.18 that for fission delay time > 10^{-18} sec, prefission neutron multiplicity > 4 is obtained. However, statistical model codes (without any fission delay) predict that most of the fission cross-section should be exhausted after first two neutron emissions and the average prefission neutron multiplicity for this reaction should be < 2 corresponding to fission delay time on the order of 10^{-20} sec. Statistical model codes (with

fission delay on the order of 10^{-20} sec) predict that for this reaction, the long-lived fission component (fission time > 10^{-18} sec) corresponding to prefission neutron multiplicity > 4 should be ~5% of the total fission cross-section. The results of the simple statistical model calculations are in agreement with Saxena *et al.*'s results.

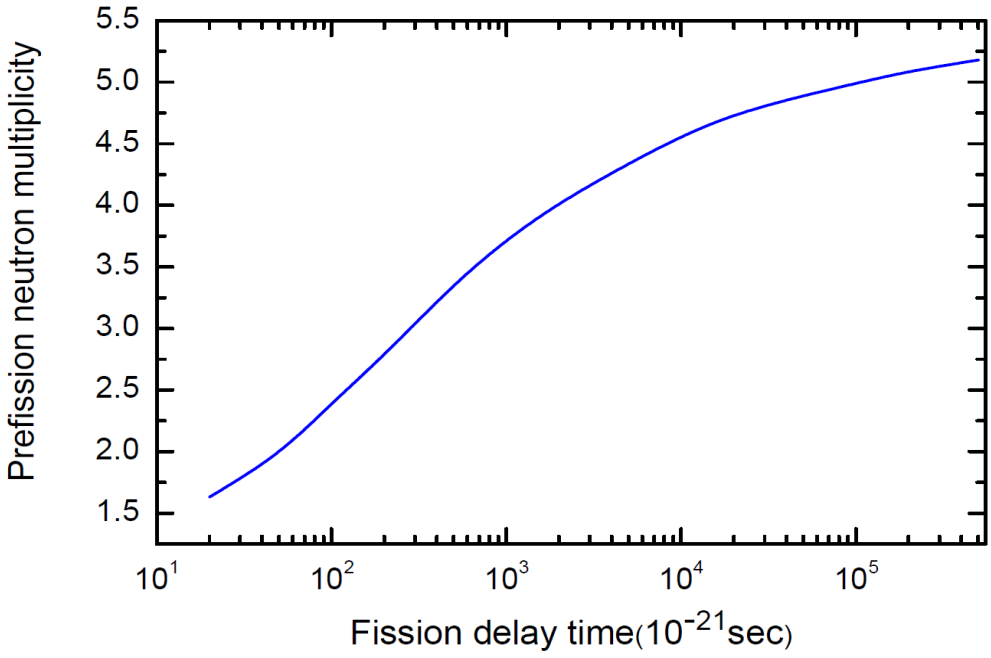

Fig. 3.18: *Fission delay time versus pre-fission neutron multiplicity for $^{4}He+^{238}U$ reaction at $E_{Lab}(^{4}He)$=60 MeV as obtained from JOANNE2 code calculations.*

However, one can increase the average fission time arbitrarily by putting in a fission delay that could be due to the viscosity parameter inhibiting the fission process. In the case of a large fission delay (>10^{-18} sec), the prefission neutron multiplicity would reach close to its saturation value (>4). Jacquet and Morjean [Jac09] showed from Langevin fluctuation-dissipation

dynamical calculations that the long-lived fission component (>10^{-18} sec) could be a very significant fraction of the total fission cross-section, if the viscosity parameter is increased substantially. However, the observation of a low average prefission neutron multiplicity of (2 ± 0.1) [Sax94] is not consistent with the observation of a large percentage (> 50%) of long-lived fission component implying physics beyond standard fission dynamics. To support the nuclear measurements further, the *ab initio* calculation of induced fission of ^{240}Pu at ($E_X \approx 8$ MeV) obtained fission time on the order of 10^{-19} sec [Bul16].

Hence, in conclusion, it is found that both the experiments and calculations determining fission delays from the nuclear decay products or nuclear properties generally give consistent results, but it gives orders of magnitude longer fission time when measured by atomic techniques which actually measure the survival time of the ion containing the fissioning nucleus. Thus, the atomic and nuclear measurements related to the fission time of highly excited plutonium or similar nuclei are incompatible with one another and cannot be understood by fission dynamics calculations.

Chapter 4

Fission time anomaly

4.1 Introduction

In the last chapter, it has been found that the fission times of nuclei measured by the nuclear and atomic techniques differ by several orders of magnitude. The nuclear techniques (prefission neutron multiplicity) typically give fission time on the order of 10^{-21} to 10^{-20} sec for the highly excited transuranium nuclei, whereas atomic techniques (crystal blocking, atomic K x-ray) give the corresponding fission time on the order of 10^{-18} sec. This different measured fission timescales have been attributed to the sensitivity of the nuclear technique to short timescale and that of atomic technique to long timescale and so it appears that there is no inconsistency among them. In this chapter, we shall show that the observed long fission time for the majority of the fissioning events as obtained by the atomic techniques cannot be reconciled with the observed short fission time obtained by the nuclear techniques using sensitivity argument. We shall discuss our point of view in the context of the fission of highly excited Z=120 nucleus, because a lot of data on fission time is available for this nucleus. The fission time of Z=120 nucleus formed by ^{64}Ni+^{238}U reaction at $E_{c.m.}$ ~330 MeV was measured by both the atomic and nuclear techniques. Recently, Morjean *et al.* [Mor08] and Fregue *et al.* [Fre12] measured fission time of Z=120 nucleus produced by ^{64}Ni+^{238}U reaction at $E_{c.m.}$ = 333.9 MeV and $E_{c.m.}$ = 332.9 MeV respectively using atomic techniques and interpreted the measured long fission time on the order of 10^{-18} sec as the evidence for the formation of superheavy Z=120 nucleus. On the other hand, Hinde *et al.* [Hin92] and Toke *et al.* [Tok85] measured fission time of the same nucleus

produced by the same reaction at $E_{c.m.}$ = 328.6 MeV and $E_{c.m.}$ = 302.6 MeV respectively using nuclear techniques and obtained fission time on the order of 10^{-21} sec to 10^{-20} sec. From a detailed study of all the relevant data concerning fission time of Z=120 nucleus, we shall show [Sik16] that contrary to the general perception, the nuclear and atomic data related to fission cannot be reconciled by any plausible fission time distribution or the sensitivity of the atomic and nuclear techniques in different time domains. Although the inconsistency among the fission time data obtained by atomic and nuclear techniques will be explicitly shown for Z=120 superheavy nucleus, similar inconsistencies have been observed for several other fissioning and/or quasifissioning nuclei far away from the island of the predicted superheavy nuclei. All these inconsistencies would be discussed in this chapter.

4.2 Atomic measurement of Z=120 nuclei

Fregeau *et al.* [Fre12] bombarded ^{64}Ni target with a ^{238}U beam at 6.6 MeV/A and detected fission fragments in the angular region $15.9^o < \theta_{lab} < 69^o$ with respect to the beam axis. They detected characteristic K x-ray photons from the compound Z=120 nucleus, in coincidence with fission fragments and found that more than 53% of the mass-asymmetric fission fragments ($70 < Z < 80$) emitted in the angular region $15.9^o < \theta_{lab} < 69^o$ came from a slow process of lifetime greater than that of the atomic K-orbital vacancy ($\tau_x = 2.8 \times 10^{-18}$ sec), in agreement with an earlier crystal blocking experiment [Mor08]. On the basis of these experimental results, it was concluded [Mor08, Fre12] that there is a large component of the long-lived ($>10^{-18}$ sec) asymmetric fission process emitting fragments in the angular region of their study ($15.9^o < \theta_{lab} < 69^o$). The observed

long fission time was thought [Mor08, Fre12] to be due to the high fission barrier of superheavy unbinilium decaying for a long time by neutron emission before undergoing predominantly asymmetric fission.

As discussed in chapter 2, atomic clocks (x-ray, crystal blocking) are less precise, but can measure longer fission times in the range of 10^{-18} sec to 10^{-16} sec. Short fission times from 10^{-21} sec to 10^{-18} sec do not produce any observable characteristic x-ray peak and blocking ratios remain below the thermal vibration limit. Hence, atomic clocks put fission times from 10^{-21} sec to 10^{-18} sec in a single time bin designated as less than 10^{-18} sec. So, atomic clocks cannot distinguish between fission times on the order of 10^{-21} sec from fission times on the order of 10^{-19} sec, but can certainly distinguish unambiguously between short fission times on the order of 10^{-21} sec from the long fission times on the order of 10^{-18} sec. It can be easily seen from (eqn. 2.8) that if $f(\tau)$ is taken as a bimodal distributionas as shown in Fig. 4.1 with a very long time component ($\tau >> \tau_x$, where τ_x =2.8×10^{-18} sec) and a very short time component ($\tau << \tau_x$), one obtains the minimum percentage ($f_{\min}$) of long-lived fission component given by the experimentally obtained ratio $f_{\min} = \frac{N_k}{P_k N_f} \times 100\,\%$.

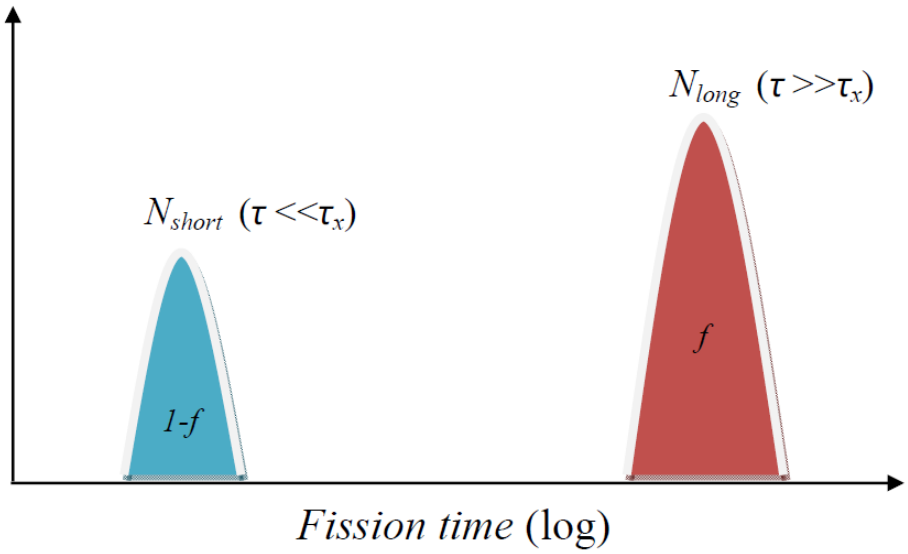

Fig. 4.1: *Bimodal fission time distribution with fraction* f *having very long time component (* $\tau >> \tau_x$*, where* τ_x *=2.8×10*$^{-18}$ *sec) and* $(1-f)$ *fraction with a very short time component (* $\tau << \tau_x$*).*

Any other fission time distribution $f(\tau)$ would produce a larger percentage of long-lived fission component. Fregeau *et al.* [Fre12] found $f_{\min}$=53% for the emission of asymmetric fission fragments 70 < Z < 80, implying that they obtained experimentally $\frac{N_K}{P_K N_f}$ =0.53 for these asymmetric fission fragments. Let us assume a bimodal distribution where only $f_L(\tau)\%$ of total fission events with fission time τ contribute to atomic K x-ray yield and the remaining fission events have short fission times and do not significantly contribute to K x-ray yield. In Fig. 4.2, we have shown [using (eqn. 2.8)] how $f_L(\tau)\%$ would decrease as a function of τ in the context of Fregeau *et al.*'s result [Fre12]. It is seen that for very large values of τ, $f_L(\tau)\% \rightarrow f_{\min}$=53%,

as stated by Fregeau *et al.* [Fre12]. As τ decreases, $f_L(\tau)\%$ must increase to reproduce the observed K x-ray yield.

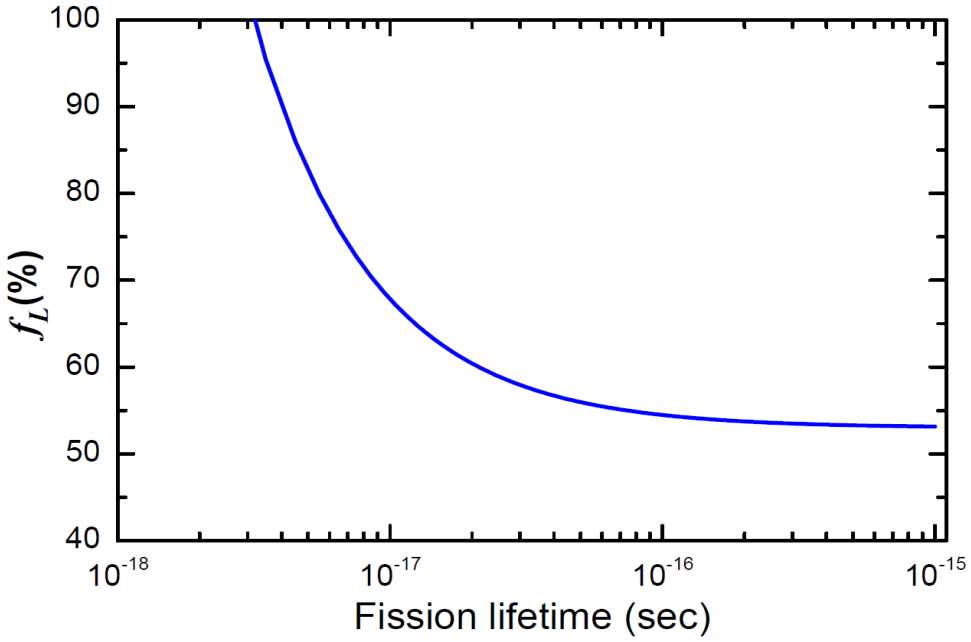

Fig. 4.2: *Percentage of long-lived fission component ($f_L(\tau)\%$) versus fission time (τ) obtained from (eqn. 2.8) using Fregeau et al.'s data* [Fre12].

4.3 Contradiction of atomic data with pre-fission neutron multiplicity data

Hinde *et al.* [Hin92] performed mass and total kinetic energy gated pre-fission neutron multiplicity measurements for this reaction (^{64}Ni+^{238}U) at $E_{c.m.}$ = 328.6 MeV producing the same compound nucleus (Z=120, A=302) at the same excitation energy (T≈1.5 MeV) and

detected fission fragments at similar center of mass angles as studied by Fregeau *et al.* [Fre12]. They obtained [Hin92] pre-fission neutron multiplicity of (4.0±0.8) which translates to an average fission lifetime of $(1.5 \pm 0.5) \times 10^{-20}$ sec, again much shorter than the lifetime obtained in ref. [Mor08, Fre12]. Moreover, Hinde *et al.* [Hin92] stated that their measured prefission neutron multiplicity (4±0.8) for the very fast fission of Z=120 nucleus produced by ^{64}Ni+^{238}U reaction probably contained very significant contributions from the postfission neutrons emitted by the accelerating fragments and the true prefission neutron multiplicity could be significantly lower, consistent with Toke *et al.*'s [Tok85] measured splitting time on the order of 10^{-21} sec. Both Toke *et al.* [Tok85] and Hinde *et al.* [Hin92] concluded that quasifission process having very short lifetime (~10^{-21} sec) is the dominant reaction mechanism for ^{238}U+^{64}Ni reaction in the same angular region studied by Fregeau *et al.* [Fre12] and Morjean *et al.* [Mor08].

The pre-fission neutron multiplicity clock is a non-linear high precision clock with a relatively short range. In Fig 2.2, we have presented our calculations of ν_{pre} using the code JOANNE2 [Les93] for the ^{238}U+^{64}Ni reaction at $E_{c.m.}$ = 328.6 MeV for various fission delay times of the composite nucleus. It is clear from Fig. 2.2 that ν_{pre} saturates at a value $\nu_{sat} \approx 7.7$ for fission time≥ 5×10^{-19} sec. Fig. 2.2 shows that ν_{pre} measurements cannot distinguish among fission lifetimes longer than 5×10^{-19} sec for this system. However, the technique can certainly tell us without any ambiguity whether the fission time is on the order of 10^{-21} sec or greater than 10^{-18} sec. The experimental value, ν_{pre}=4.0 [Hin92] for ^{64}Ni+^{238}U reaction has been reproduced with a fission delay of 2×10^{-20} sec.

Let us now see if Hinde *et al.*'s results [Hin92] could be made consistent with Fregeau *et al.*'s x-ray data [Fre12] assuming that the fission time distribution function $f(\tau)$ for ^{238}U+^{64}Ni is similar to that shown by Cabrera *et al.* [Cab03] for ^{20}Ne+^{159}Tb reaction (E/A= 8 MeV) as shown in Fig. 4.3. Using (eqn. 2.9) and the fission time distribution given in ref. [Cab03], we obtain $\frac{N_K}{P_K N_f} \approx$ 0.3 rather than the experimentally obtained value of 0.53. Using the results from Fig. 2.2, the corresponding prefission neutron multiplicity comes close to 7 rather than the experimentally obtained value of 4. Hence, neither the x-ray data [Fre12] nor the prescission data [Hin92] are consistent with a standard fission time distribution function [Cab03].

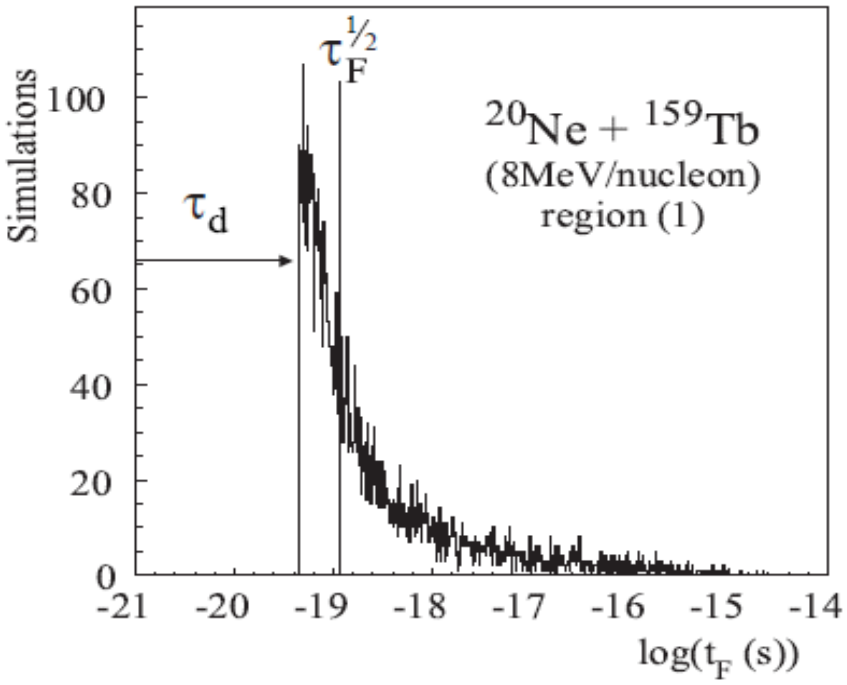

Fig. 4.3: *Fission time distribution predicted by GEMINI simulation for the bombardment of 8 MeV/A ^{20}Ne on ^{159}Tb target taken from ref.* [Cab03].

On the one hand, Fregeau *et al.*'s x-ray data requires $f(\tau)$ must contain a significantly large percentage of long-lived fission component. On the other hand, Hinde *et al.*'s data [Hin92]

requires $f(\tau)$ must contain a significantly lower percentage of long-lived component. Using Fig. 4.2 and Fig. 2.2, we find that the only solution for these two contradictory requirements is an extreme bimodal distribution comprising 53% of very slow fission events with $\tau \geq 10^{-16}$ sec and 47% of very fast fission events with $\tau \leq 10^{-21}$ sec similar to Fig. 4.1. We think such a fission time distribution is very implausible. If we think fast fission events (47% of total fission events) are due to quasifission, then also it is implausible that the time distribution of fusion-fission events would start from $\tau \geq 10^{-16}$ sec. If the time distribution of fusion-fission events would start from an early time before 10^{-16} sec, then its percentage must increase above 53% (and the quasifission percentage must decrease below 47%) to be consistent with x-ray data [Fre12], thus contradicting prefission neutron multiplicity data [Hin92]. Even in the case of such an extreme bimodal distribution (47% fast fission of lifetime $\leq 10^{-21}$ sec and 53% slow fission of lifetime $\geq 10^{-16}$ sec), x-ray data and prefission data are inconsistent, if we consider neutron emission from the accelerating fragments [Hin92]. In the case of very short fission time comparable to the acceleration time of the fission fragments, it becomes very difficult [Hin92] to distinguish between prefission and postfission neutrons from the accelerated fragments and ultimately these postfission neutrons coming from the accelerating fragments determine the minimum fission time that could be measured by the technique. Following Hinde *et al.* [Hin92], we might consider that the minimum fission time that the experiment could measure for ^{64}Ni+^{238}U reaction was 1.5×10^{-20} sec corresponding to $\left[\nu_{pre}\right]_{expt} = 4$. Hence, even for the extreme bimodal distribution, we obtain from (eqn. 2.4), that the expected measured prefission neutron multiplicity should be > $(0.47\times4+0.53\times7.7) = 6$, thus contradicting the experimental result (4±0.8) by more than two standard deviations.

4.4 Contradiction of atomic data with Mass Angle Distribution (MAD) data and other results

As discussed in Chapter 2, in Mass Angle Distribution technique the lack of reflection symmetry in the angular distribution of fission fragments is observable when the fission time is less than or comparable to the time taken by the composite system to complete one rotation. This method is sensitive in the timescale of 10^{-21} sec. If the fission timescale is much longer than 10^{-20} sec, the composite system undergoes many rotations before fission resulting in essentially symmetric angular distribution of the fission fragments, implying fission time > 10^{-20} sec. Considering an extreme bimodal distribution as discussed before, 2nd term of (eqn. 2.5) should dominate for large values of $\theta_{c.m.}$, contradicting the observed 2D mass-angle distribution of ^{238}U+^{64}Ni reaction that shows steep decrease of differential fission fragment cross-section at large angles. Toke *et al.* [Tok85] deduced fission time for a mass split from the corresponding average angle of rotation of the intermediate complex. The average angle of rotation of the intermediate complex was determined by taking weighted average over the entire angular distribution of the relevant fragment. Toke *et al.* [Tok85] measured a rather small average angle of rotation of the ^{238}U+^{64}Ni complex (61°) for the asymmetric splits, thus ruling out the presence of a large percentage of reflection symmetric component in the angular distribution and deduced a short fission time of τ = 3.1×10^{-21} sec. Comparing with the 2D mass angle spectra of ^{238}U+^{27}Al (containing 30% compound nuclear contribution), ^{238}U+^{48}Ti (containing 5% compound nuclear contribution) etc., we conclude that 2D mass angle spectra of ^{238}U+^{64}Ni reaction cannot contain more than 5% reflection symmetric compound nuclear component. The extraction of fission delay from mass-

angle correlation or pre-fission neutron multiplicity experiments [Tok85, Hin92] do not assume a priori that quasifission dominates, as apparently contended in ref. [Fre12]. Even if the transient composite system rapidly splits into two fission-like fragments that cannot be distinguished event-by-event from true fusion-fissions (FFs), the computed fission delays would be the same although it would arise from a different reaction mechanism. Since shorter lifetimes are reported in ref. [Tok85] when the data are gated with asymmetric fission, it is clear that quasifission is indeed distinguishable from fusion-fission. Hence, these nuclear results [Hin92, Tok85] cannot be reconciled with a large saturation term (ν_{pre}) or isotropic term (in mass angle distributions) arising from the presence of a large percentage of long-lived fission component [Fre12].

Toke *et al.* [Tok85] performed measurements at $E_{c.m.}$ = 302.6 MeV, whereas Fregeau *et al.* [Fre12] and Hinde *et al.* [Hin92] performed measurements at $E_{c.m.}$ = 332.9 MeV & $E_{c.m.}$ = 328.6 MeV respectively. Coulomb barrier for ^{64}Ni+^{238}U reaction from Bass model is about 267 MeV [Koz10] in the center of mass frame. Kozulin *et al.* [Koz10] found that the total capture cross-section (sum of quasifission and compound nucleus fission cross-sections) for ^{64}Ni+^{238}U reaction tended to saturate around $E_{c.m.}$ = 300 MeV and the compound nucleus fusion cross-section was negligible compared to the quasifission cross-section. The compound nucleus fusion excitation function generally tends to show saturation at 1.1 to 1.15 times Coulomb barrier energy in the center of mass frame. So, the available evidence suggests that the emitted fission fragments at $E_{c.m.}$ =302.6 MeV and 332.9 MeV or 333.9 MeV should essentially all be from quasifission process. Both Toke *et al.* [Tok85] and Hinde *et al.* [Hin92] determined fission time of strongly damped fission fragments by cutting out the quasielastic regions and gating on strongly damped regions as seen from their 2D total kinetic energy versus fragment mass plots. On the other hand,

Fregeau *et al.* [Fre12] gated on Z-bin (70<Z<80) and fragment energy bin from about 300 MeV to 1100 MeV. Assuming detected fragments in Z-bin (70<Z<80) approximately correspond to a fragment mass bin in the range (160<A<200), the total kinetic energies of the fragments in the center of mass frame were similar to what Toke *et al.* [Tok85] and Hinde *et al.* [Hin92] had observed in this mass region. Hence, the fission lifetime measured by Toke *et al.* [Tok85] in asymmetric mass bin around A=180 should be consistent with the measurements of Fregeau *et al.* [Fre12]. Although Toke *et al.'s* [Tok85] mass-angle distribution measurements cannot rule out the possibility of late-chance fission (fission time ~10^{-18} sec) at some low level [Hin15] consistent with the experimental uncertainty, they certainly contradict presence of a long-lived fission component for a large percentage of the fission fragments as found by Fregeau *et al.* [Fre12].

The conclusion [Mor08, Fre12] that fusion-fission (rather than quasifission) dominates and that the fission barrier is high resulting in rapid cooling by neutron emissions, is also in conflict with the theoretical prediction [Mol09] of a low fission barrier of ~ 6 MeV compared to neutron binding energy ~7.2 MeV. Recent attempts [Uni, Hof08] to detect the Z=120 nucleus as an evaporation residue using the same reaction (^{238}U+^{64}Ni) at an energy near the Coulomb barrier ($E_{c.m.}$≈270 MeV) obtained a null result (upper limit of evaporation residue cross-section < 94 fb), implying the dominance of quasifission and/or low fission barrier of Z=120, contradicting the conclusion of ref. [Mor08, Fre12]. The compound nucleus fusion cross-section of ^{64}Ni+^{238}U (Coulomb barrier = 267 MeV [Koz10]) is expected to saturate before $E_{c.m.}$ = 333 MeV increasing at most by a factor of 10-50 [Koz10] compared to the fusion cross-section near the Coulomb barrier energy. Hence, using Hofmann *et al.*'s results [Hof08], the fusion cross-section for

compound nucleus (Z=120) formation at $E_{c.m.}$ =332.9 MeV should be less than (1-5) pb making it essentially impossible to see compound atom K x-ray yield in a fission fragment K x-ray coincidence experiment. So, an interpretation in terms of seeing asymmetric fission fragments from superheavy Z=120 nucleus and corresponding coincident x-rays would imply many orders of magnitude (compared to pico barn level) higher compound nucleus fusion cross-section contradicting the results of Hofmann *et al.* [Hof08]. On the other hand, both the theoretical calculations [Mol09] of a low fission barrier and the measurement of very short (~10^{-21} sec) fission time by Toke *et al.* [Tok85] and Hinde *et al.* [Hin92] are consistent with the non-observation [Hof08] of Z=120 evaporation residues in ^{64}Ni+^{238}U reaction.

4.5 Fission time anomaly in different systems

The claim [Mor08, Fre12] of observation of superheavy Z=120 element (with a high fission barrier) is based on the observation of long fission lifetime (~10^{-18} sec) for highly excited Z=120 nucleus and shorter fission lifetime (<10^{-18} sec) for similarly excited neutron deficient Z=114, A=280 nucleus. However, the observation of long fission time using atomic techniques is a rather common observation [Gol99, Mor08, Fre12] seen for a large number of quasifission and fission processes unrelated to the formation of superheavy nuclei. For example, Andersen *et al.* [And08] using crystal blocking technique observed that all the detected fragments (100%) came from slow processes having long fission times (~10^{-18} sec) for a large number of reactions [such as ^{74}Ge+W at E(^{74}Ge)$_{Lab}$=390 MeV, ^{58}Ni+W at E(^{58}Ni)$_{Lab}$=330-375 MeV, ^{48}Ti+W at E(^{48}Ti)$_{Lab}$=240-255 MeV] expected to be dominated by quasifission process and producing highly excited transuranium composites (Z=102-106) far away from the predicted landscape of superheavy nuclei. On the other hand, using mass-angle correlation technique, R. du Rietz *et al.*

[Rie11] obtained 2D mass-angle correlations plots for very similar systems (^{64}Ni+W, ^{48}Ti+W) at similar center of mass energies and deduced their exponential quasifission and fission lifetime on the order of ~10^{-21} sec to 10^{-20} sec. Molitoris *et al.* [Mol93] using x-ray technique observed long fission time (~10^{-18} sec) for the majority of the observed fission fragments emitted by the highly excited (E_X= 40 – 105 MeV) ^{235}U having low fission barrier (4.9 MeV) [Mol09]. Using crystal blocking technique, Goldenbaum *et al.* [Gol99] obtained fission time of highly excited (E_X≈ 200 MeV) ^{238}U on the order of 10^{-18} sec. Wilschut and Kravchuk [Wil04] measured fission time of highly excited (E_X=145 MeV) neptunium nuclei on the order of 10^{-18} sec using x-ray technique. Similar kind of discrepancy has been pointed out in our experiment for the reaction of 60 MeV ^{4}He + ^{238}U which has been discussed in the last chapter. Several authors [And08, Gon02, Jac09] attempted to explain such long fission time by introducing a large viscosity parameter of the nuclear medium that produced very broad fission time distribution extending to 10^{-15} sec and shifted the mean value of fission time distribution to ~10^{-18} sec. However, if nuclear medium indeed offers such a high viscous friction, this effect should be present in all quasifissioning /fissioning processes and hence, all the quasifissioning /fissioning systems should have long splitting time (~10^{-18} sec). Hence, one cannot conclude that the observed long fission time [Mor08, Fre12] of Z=120 nucleus measured by atomic techniques implies high fission barrier of the nucleus.

Thus, the observed large percentage of long-lived fission component as measured by atomic techniques and corresponding very short fission time measured by the nuclear techniques (at the lower end of nuclear clock's range) cannot be explained by the sensitivity argument of different techniques in different time domains [Sik16]. The explanation of long fission time in terms of large viscosity parameter of nuclear medium should be applicable to all heavy systems including

Z=120 nucleus. Hence, it is clearly not possible to claim the observation of Z=120 superheavy nucleus with a high fission barrier on the basis of observed long fission time by atomic techniques.

In summary, the long fission lifetime measured by atomic techniques cannot be reconciled with the short fission lifetime measured by nuclear techniques using the sensitivity argument [Sik16]. Fregeau *et al.'s* [Fre12] x-ray data could be made consistent with Hinde et al.'s [Hin92] results only in the context of an extreme bimodal fission time distribution comprising 53% long-lived component ($\tau \geq 10^{-16}$ sec) and 47% short-lived component ($\tau \leq 10^{-21}$ sec), provided the neutron emission from the accelerating fragments could be ignored. Such an extreme bimodal distribution looks implausible. Even in the context of this extreme bimodal distribution, Fregeau *et al.*'s result [Fre12] is inconsistent with Toke *et al.*'s mass-angle distribution data [Tok85]. The non-observation of Z=120 evaporation residue in ^{238}U+^{64}Ni reaction contradicts the conclusions of ref. [Mor08, Fre12] regarding high fission barrier of Z=120. The fission time measurements [Tok08, Hin92] using nuclear techniques agree with each other and consistent with the theoretical calculations [Mol09] as well as with the non-observation of Z=120 evaporation residue [Hof08]. The atomic results [Mor08, Fre12] and the conclusion that fusion-fission reaction mechanism dominates the reaction ^{238}U+^{64}Ni at 6.6 MeV/A leading to the formation of superheavy nucleus Z=120 with a high fission barrier are inconsistent with the nuclear results [Tok85, Hin92, Hof08] and calculations [Mol09]. The incompatibility among the measured fission times by nuclear and atomic techniques might indicate new physics beyond the scope of fission physics and we would provide a quantum mechanical analysis in the next chapter to find out if the concept of quantum decoherence is playing any role in understanding the fission data.

Chapter 5

A quantum mechanical interpretation of fission time anomaly

In the last chapter, we have discussed that the average long fission time (~10^{-18} sec) for most of the fission events as obtained by the atomic techniques cannot be reconciled with the average short fission time (~10^{-21}-10^{-20} sec) obtained by the nuclear techniques for any plausible fission time distribution function. It has been found that the survival time of the atom/ion containing the fissioning nucleus is apparently several orders of magnitude longer than the fission time deduced from the nuclear observables such as fission fragment angular distributions, prefission neutron multiplicity etc. and cannot be explained by fission dynamics calculations. Here, we present a plausible quantum mechanical interpretation of the observed fission time anomaly.

The short time scale (~10^{-21}-10^{-20} sec) deduced from the nuclear observables is actually not a direct observation. In Mass Angle Distribution (MAD) technique, an exponential fission time distribution function was assumed [Rie11] and its time period (fission time) was adjusted to obtain the best fit of the measured mass angle distribution data. In prefission neutron multiplicity technique [Hin92], the average number of prefission neutrons per fission event was measured and the neutron emission time is taken from statistical model calculations assuming exponential decay. So for all these measurements, an exponential decay law is assumed and the fission time is deduced from the nuclear observables. On the other hand, atomic techniques measure the

survival time of the atom/ion containing the fissioning nucleus and could be considered as more direct measurement of the fission time which is independent of any nuclear model.

Although exponential decay law is the hallmark of all radioactive decays, quantum mechanics does not predict exact exponential decay law at all times. In quantum mechanics, the time evolution of an isolated unstable state produces a superposition of initial state and decayed states at any finite time [Fon78, Hom97] and the classical exponential decay does not emerge from such time evolutions. The quantum mechanical time evolution of an isolated state gives a non-exponential decay initially, an approximate exponential decay at a much later time and a power law behavior (non-exponential) after a very long time. However, in practice, we never deal with an isolated quantum state. The environment always interacts with the quantum state. The coupling between the quantum system and its environment leads to a decoherence process [Zur02, Zur03] resulting in the loss of quantum coherence between the initial undecayed state and decayed state very quickly. Before the loss of quantum coherence between the initial state and decayed states, a quantum system should undergo non-exponential decay and the classical exponential decay should occur after the loss of quantum coherence. Decoherence timescale is the timescale of quantum-classical transition when non-exponential decay takes place. In this chapter, we shall estimate decoherence time of the decaying nuclear states produced in a nuclear fission reaction and discuss about the possible impact of decoherence time on the measurements. This could provide a probable solution of the observed fission time anomaly.

5.1 Theory of non-exponential decay

In classical physics, it is assumed that the decay rate (λ) i.e. the number of decays per unit time of a unstable system is constant and does not depend on the past history of decaying nuclei or on the environment surrounding them. If the number of unstable systems at time *t* is *N(t)* (usually a very large number), the number of systems that will decay in the time interval *dt* is

$$dN = -N\lambda dt \text{ or } \frac{dN}{dt} = -\lambda dt\,, \tag{5.1}$$

which gives

$$N(t) = N_o e^{-\lambda t} \tag{5.2}$$

where $N_o = N(0)$. One can define "non-decay" or "survival" probability as

$$P(t) = \frac{N(t)}{N_o} = e^{-\lambda t} \tag{5.3}$$

The positive quantity λ is related to the inverse of "lifetime" τ . It is clear from the above derivation that there is no memory effect between the initial and decayed state. Moreover, it is assumed *a priori* that there is no cooperative effect taking place, which makes λ and $P(t)$ independent of the environment.

Let us now consider the quantum mechanical description of the phenomenon. Let $|\psi\rangle$ be the wave function of a quantum system Q at time $t = 0$. The evolution of Q is governed by the unitary operator $U(t) = \exp(-iHt)$, where H is the Hamiltonian. We define the survival or non-decay probability at time t as the square modulus of the survival amplitude

$$P(t) = |A(t)|^2 \tag{5.4}$$

where

$$A(t) = \langle \psi, \exp(-iHt)\psi \rangle \tag{5.5}$$

When an ensemble of identical systems is considered, the number *N(t)* of systems which are found in the original state at time *t* is given by

$$N(t) = N(0)P(t) \tag{5.6}$$

This equation is classical analogue of equation (5.2). Several authors [Chi77, Fon78, Lev88] has investigated the behavior of $P(t)$ in various context. It has been found that at intermediate times $P(t)$ follows an approximate exponential law, whereas both at large and small times, it deviates significantly from the exponential behavior.

It is possible to comment on some properties of $P(t)$ which is applicable in general that is independent of a particular Hamiltonian H and particular state ψ [Fon78],

$$A(0) = P(0) = 1 \quad \& \quad |A(t)| \leq 1 \tag{5.7}$$

Let us consider a complete set of commutating observable which includes H and denote it as (H,A). The common eigen-states of these operators would be

$$H|\phi_{E,a}\rangle = E|\phi_{E,a}\rangle \tag{5.8}$$

$$A|\phi_{E,a}\rangle = a|\phi_{E,a}\rangle \tag{5.9}$$

Both H and A can have discrete and/or continuous spectrum. The completeness relation can be written as

$$\int dE da |\phi_{E,a}\rangle\langle\phi_{E,a}| = \mathrm{I} \tag{5.10}$$

We now make an assumption, which is based on the physical situation, that H has a spectrum which is bounded from below. Expanding ψ in a series of $|\phi_{E,a}\rangle$, we get

$$A(t) = \int_{E_{\min}}^{\infty} dE\,\omega(E)\exp(-iEt) \tag{5.11}$$

where

$$\omega(E) = \int da \left| \langle \phi_{E,a} | \psi \rangle \right|^2 \tag{5.12}$$

and $E_{\min} \neq -\infty$ is the ground state energy of the spectrum. The expression (5.11) can be written in terms of Fourier transform as

$$A(t) = \int_{-\infty}^{\infty} dE\,\varpi(E)\exp(-iEt) \tag{5.13}$$

where ϖ is given as

$$\varpi = \begin{cases} 0 & E < E_{\min} \\ \omega(E) & E \geq E_{\min} > -\infty \end{cases} \tag{5.14}$$

This is the most general expression true for any quantum system. Considering the hypothesis that the wave-function $|\psi\rangle$ is normalisable and the Hamiltonian H is bounded from below, it can be shown that $P(t)$ exhibits a power law ~ t^{-n} where n is a positive integer in the limit of very long time *t*. If we consider that the mean energy of the system is finite i.e.

$$\int_{E_{\min}}^{\infty} dE\ E\ \omega(E) < \infty \tag{5.15}$$

it can be shown that $P(t)$ varies as t^2 at small times. This temporal behavior of unstable quantum systems at small time is closely related to the so-called quantum Zeno paradox or quantum Zeno effect in the quantum measurement problem. The quantum Zeno paradox (QZP) [Rus46], named after the famous Greek philosopher Zeno, states that an unstable quantum system becomes stable (i.e. never decays) in the limit of infinitely frequent measurements. Of course, in practice, we cannot observe this very limit, but can only investigate the quantum Zeno

effect (QZE) introduced by Misra and Sudarshan [Mis77], i.e. a milder version of the QZP, stating that the probability of finding the initial state is increased by a (finite) number of repetitions of a measurement [Kos05].

Now, if we consider the function $\omega(E)$ to be of Breit-Wigner form as

$$\omega(E) = \frac{\Gamma/2\pi}{(E - E_r)^2 + (\Gamma/2)^2} \tag{5.16}$$

and take ground state energy as $E_{\min} = -\infty$, then putting (5.16) in eqn. (5.13) we get

$$A(t) = \exp(-iE_r t - \frac{1}{2}\Gamma t) \tag{5.17}$$

and $P(t)$ is given as

$$P(t) = |A(t)|^2 = \exp(-\Gamma t) \tag{5.18}$$

and hence, we can get a pure exponential for all times. However, there are two evident problems in assuming a Breit-Wigner spectrum: (i) It does not allow for the existence of a minimum of energy (threshold for the decay), i.e. it corresponds to a Hamiltonian unbounded from below. (ii) The behavior of the Breit-Wigner at large energies is such that, while the normalization can be imposed (and thus unitarity), all the moments of the distribution, including the average energy of the unstable state, diverge [Fon78]. Thus, a Breit-Wigner spectrum cannot explain the real physical scenario.

So, it is clear that for any choice of the quantum state $|\psi\rangle$ at the initial time and of the dynamics of the system, described by Hamiltonian *H*, the non-decay probability *P(t)* cannot be a pure exponential for all times. It follows that the quantum law (eqn. 5.6) cannot be reconciled with the classical one (eqn. 5.2). Hence, there exists no state $|\psi\rangle$ which can give rise to a purely exponential *P(t)* at all times [Fon78] and one has to assert that an unstable system evolves with

time in such a way that the form factor $\omega(E)$ resembles as close as possible to the function (eqn. 5.16), so that the law (eqn. 5.18) will hold true for a time interval very large, compared with $\tau = 1/\Gamma$ and one would get non-exponential decay both at small and very large times.

Moreover, it is possible to see from the quantum mechanical time evolution of a state that, in general, the decay probability cannot be a pure exponential. Let us consider the time evolution of an unstable state $\left(|\psi_{unstable}>\right)$ from the time *t=0* to time *t*. Let $\left(|\psi_{decayed}(t)>\right)$ denotes the decayed state at time *t*. The time evolution should produce the following superposition of undecayed and decayed states at any finite time *t*:

$$e^{-\frac{iHt}{\hbar}}\left|\psi_{unstable}(t=0)>=\alpha(t)|\psi_{decayed}(t)>+\beta(t)\right|\psi_{unstable}(t=0)> \tag{5.19}$$

where H is the Hamiltonian of the system. α(t) and β(t) are time dependent complex coefficients. $\hbar = \frac{h}{2\pi}$,where h is Planck's constant. At any time *t*, $\left(|\psi_{decayed}(t)>\right)$ satisfies $\left\langle\psi_{unstable}(t=0)\middle|\psi_{decayed}(t)\right\rangle = 0$. It can be shown [Fon78, Hom97] that

$$\beta(t+t') = \beta(t)\beta(t') + \alpha(t)\left\langle\psi_{unstable}(t=0)\middle|\exp(-iHt')\middle|\psi_{decayed}(t)\right\rangle \tag{5.20}$$

The second term in (eqn. 5.20) is the so-called memory term or reformation amplitude indicating the possibility of regenerating the initial state $\left(|\psi_{unstable}(t=0)>\right)$ from the decay products, which modifies the classical exponential decay represented solely by the first term. We get $\beta(t) \propto \exp(-\lambda t)$ with $Re(\lambda) > 0$, only when the second term i.e. the reformation amplitude of the unstable state from the decayed state becomes zero. However, it can never be zero from the

solution of the time dependent Schrodinger equation unless the Hamiltonian H is unbounded from below i.e. the lowest eigenvalue would tend to -∞ or the decay does not take place. So, the results imply that in quantum mechanics, a decay process is in general not time irreversible, as expected. Hence, the condition for the start of the exponential decay and the classical description of the process is the loss of the quantum coherence between $\left(|\psi_{unstable}\ (t=0)>\right)$ and $\left(|\psi_{decayed}\ (t)>\right)$ as a result of the interaction of the system with the environment. Thus, in a scattering reaction involving two particles, the time evolution can produce a superposition of a compound unstable state and the decayed states at any finite time. The key characteristic of a compound state is that it consists of fragments localized within a region whose linear dimensions are of the order of the range of forces acting between them [Fon78]. The problem of determining whether at *t=0* instant, an unstable compound state $\left(|\psi_{compound}\ >\right)$ is present reduces to that of extracting from the total wave function |ψ(t=0)> a part $\left(|\psi_{compound}\ >\right)$ that has this localised character. This reduction process from |ψ(t=0)> to $\left(|\psi_{compound}\ >\right)$ is performed in practice by switching on an interaction which is different from that responsible for the decay of the state. So, this reduction process cannot automatically take place by the time evolution of the wave functions of the interacting particles and requires interaction with the external environment [Fon78]. The compound state is projected out from the superposition of states when it is found in the process of measurement that the two fragments composing the unstable state are spatially close to each other i.e. contained within their interaction region. However, a decaying nuclear state would affect the surrounding electronic configuration of the host atom and so it should be considered an open system. Decoherence time of a decaying nuclear state should depend on the surrounding electronic configuration causing the loss of coherence between the initial state and

the decayed state. On the other hand, the exponential decay time would depend only on the properties of the decaying nuclear state.

5.2 Experiments on non-exponential decay

In the previous section, we have shown that a pure exponential decay law is not obtained in quantum mechanics. It is found that deviations from the exponential law are present at small times which is very close to the initial preparation time ($t=0$) and at very late times, while at "intermediate" times the exponential law should hold approximately. R. G. Winter [Win61] and Duane *et al.* [Dua02] found in their numerical simulations that if a sinusoidal wave function is put in a specific type of potential well, the decay of the initial state follows a non-exponential function for about one exponential lifetime of the system, becomes approximately exponential in intermediate times and again becomes non-exponential after about 10-20 exponential lifetimes. In particular, at late times the decay law follows a power-law, which is however very difficult to observe experimentally because it occurs at times for which the survival probability is already vanishingly small. On the other hand, the deviations at small times occur within a very short time scale, for instance 10^{-15} sec for the electromagnetic decays of an excited hydrogen atom [Fac98] and even shorter for hadronic decays [Pag11]. It is thus experimentally very challenging to observe such deviations and to confirm the predictions of the theory.

Several experimental efforts have been carried out to observe non-exponential decay in radioactive decay of nuclei for short and long times. The first testing of the exponential decay law was performed by Lord Rutherford [Rut11] in 1911 by measuring the alpha decay of radon, ^{222}Rn (half life 3.823 days), in the time interval of $27\, t_{1/2}$ (half-lives). Butt and

Wilson [But72] have measured the same radionuclide for 40 $t_{1/2}$. The β^- decay of isotope of manganese, ^{56}Mn (half life 2.5785 hours), was measured by Winter [Win62] up to 34 $t_{1/2}$ and by Norman *et al.* [Nor88] upto 45 $t_{1/2}$. Gopych *et al.* [Gop84] have measured the β^- decay of isotope of Indium (^{116m}In) for 33 $t_{1/2}$. Norman *et al.* [Nor88, Nor95] measured β^- decay of ^{60}Co (half-life ≈5.3 years) down to 10^{-4} $t_{1/2}$ time and for ^{40}K nuclei (half-life≈1.25× 10^9 years) down to 10^{-10} $t_{1/2}$ time to search for short time behavior. Norman *et al.* did not find deviation from exponential behavior within 1.3 % in long time limit and in short time limit, the exponential decay law was found to be valid within 5.6%. Novković *et al.* [Nov06] carried out the experimental investigation of ^{198}Au β^- decay (half life 2.69517 days) in the time interval from 0.02 to 25 half-lives. No deviation from the exponential decay law was found either at early times or long times within the limits of the experimental uncertainties.

The tunneling of ultra-cold sodium atoms from a magneto-optical trap showed [Wil97] evidence for the non-exponential decay in early time. About 10^5 sodium atoms were trapped and cooled in a periodic optical potential created by a standing wave of light. The Gaussian width of the energy distribution of the sodium atoms was about 3×10^{-9} eV [Wil97, Fis01]. An accelerating potential of the form $V = V_0 cos[2k_L x - K_L a t^2]$, where V_0, a, x, t, k_L are well depth, acceleration, position in laboratory frame, time and laser wave number respectively was applied and the tunneling of the sodium atoms from the trapped states to the continuum took place. The survival probability of sodium atoms in the trap was measured as a function of the duration of the acceleration. It was found that the survival probability followed a non-exponential curve for about 5-6 μs and then followed an exponential curve with an exponential lifetime on the order of several tens of μs. The tunneling process took place as a result of exchange of energy between the reservoir and the

trapped atoms. The energy was taken out from the reservoir to accelerate the trapped atoms and the very low energy sodium atoms tunneled out and gave back the energy to the reservoir. The applied acceleration separated out the trapped and tunneled out sodium atoms by their energies and so the trapped and tunneled out sodium atoms could be distinguished. As long as the trapped and tunneled out sodium atoms could not be resolved within a certain time window by their energy difference, even in principle (i.e. by applying the energy-time uncertainty principle), the coupling between the atom and the reservoir remained reversible and the decay was non-exponential within that time window. When an acceleration of 7000 meter/sec^2 is applied for 1 μs, then the energy difference between the tunneled out atoms and trapped atoms would be about 6×10^{-12} eV and from the energy-time uncertainty principle, a minimum time of about 100 μs would be required to distinguish between the trapped atom and tunneled out atom. So, it was necessary to apply the acceleration for 5-6 μs so that the energy difference between the trapped and tunneled out sodium atoms becomes sufficiently large to distinguish them within a time period of 5-6 μs [Ray16]. Kofmann [Kof01] included the effect of external reservoir in the analysis of transition rate between the eigenstates of a Hamiltonian in the framework of time dependent Schrodinger equation and found that the decay process becomes irreversible and classical in a timescale when the decayed and undecayed states could be unambiguously distinguished as a result of interaction with the environment. Fischer *et al.* [Fis01] performed a similar experiment using ultra-cold sodium atoms in a magneto-optical trap, but interrupted the accelerating potential after every 1 μs for a long time (of about 50 μs) and found that the tunneling of the trapped atoms was severely inhibited (quantum Zeno effect). The results implied that the acceleration for 1 μs was not sufficient to distinguish between the trapped atom and tunneled atom within this short time period and because of the long interruption time, a new t=0

time was defined after each interruption followed by a slow non-exponential decay. Hence, the results of the tunneling of ultra-cold sodium atoms from an atom trap could be understood by considering the interaction of the atoms with the environment and they clearly demonstrate the importance of such interactions for the onset of exponential decay [Ray16].

Quantum Zeno effect has also been studied for various systems like in case of Rf transition between two states of a single trapped ion [Ita90], nuclear magnetic resonance (NMR) [Xia06], atomic systems [Str06, Ber08] as well as in rubidium Bose–Einstein condensate [Sch14]. C. Rothe *et al.* [Rot06] observed for the first time, deviation from exponential decay at long lifetimes for luminescence decays of many dissolved organic materials after pulsed laser excitation. So, all this experiments confirm that the dynamics of a quantum system is greatly modified by the interaction with the surrounding external environment.

5.3 Non-exponential decay in nuclear fission process

In nuclear reaction, highly excited transuranium nuclei and complexes are produced and they have large probabilities of undergoing fission. In the case of nuclear collisions, usually both the projectile and target nuclei have electrons in atomic orbitals. Vacancies in the atomic orbitals are created when a projectile ion collides with a target atom to produce a compound ion with a fused compound nucleus and it has been discussed in detail in Chapter 2. The excited combined ion might be represented by the following coherent superposition of all the atomic orbitals: $|A^* >= \sum_{i=1}^{i=n} C_i |A_i^* >$, where $|A_i^* >$ indicates atomic wave function with one vacancy in i^{th} orbital and n is the total number of orbitals. The magnitude of C_i increases rapidly for outer electronic orbitals [Ger78]. The characteristic photon emissions from the orbitals of the compound ions act like

measurement processes inhibiting the time evolution of the unstable dinuclear state and projecting out the unstable dinuclear state from the superposition of states.

The quantum decoherence process for the nuclear fission might be thought as a two step process [Zur02, Zur03]. In the first step, the entire atom or ion whose nucleus is undergoing fission acts as a quantum detector observing the nuclear fission process. As a result, after a certain time, the nuclear system couples with all the atomic orbitals of the atom or ion and produces a fully correlated pure nuclear-ion state. So, the diagonal elements of the corresponding density matrix will be real numbers and the off-diagonal elements will contain complex numbers expressing purely quantum correlations. In the second step, by considering the interaction of the environment with the pure nuclear-ion state, one gets a reduced density matrix by tracing over the environment [Zur02, Zur03] and this reduced density matrix contains only classical correlations, thus indicating complete loss of quantum coherence.

Let us now consider the time evolution of an unstable compound dinuclear state $|\psi_{dinuclear}\ (M_1, M_2, t=0)>$ (comprising two fragments M_1 and M_2) fissioning to M_1 and M_2 fragments from time *t=0* to time *t* [Ray15]. Let $|\psi_{fissioned}\ (M_1, M_2, t)>$ denotes fissioned state at time *t*. We can write

$$e^{-\frac{iHt}{\hbar}}|\psi_{dinuclear}\ (M_1, M_2, t=0)>$$

$$= \alpha(t)|\psi_{fissioned}\ (M_1, M_2, t)> + \beta(t)|\psi_{dinuclear}\ (M_1, M_2, t=0)> \quad (5.21)$$

where H is the Hamiltonian of the system, $\alpha(t)$ and $\beta(t)$ are time-dependent complex coefficients. At any instant *t*, $|\psi_{fissioned}\ (M_1, M_2, t)>$ satisfies the orthogonality condition

$$\langle\psi_{dinuclear}\ (M_1, M_2, t=0)|\psi_{fissioned}\ (M_1, M_2, t)\rangle = 0 \quad (5.22)$$

It is important to note that the time evolution of $|\psi_{dinuclear}\ (M_1, M_2, t = 0) >$ produces a superposition of the dinuclear state at *t=0* and fissioned state at time *t*. So at any time, the superposition will contain dinuclear state at *t=0* time.

Let us now consider the interaction of the nuclear state with the ionic state $|A^* >$, (where $|A^* >= \sum_{i=1}^{i=n} C_i |A_i^* >$) producing coupled states. Here $|A_i^* >$ denotes atomic wave function with a vacancy in i^{th} orbital. Let us denote by $|A_i, X_i >$ a stable ion with no vacancy in i^{th} orbital and X_i denotes the corresponding characteristic photon of the compound ion due to the electronic transition to i^{th} orbital from a higher orbital. Characteristic photon emission due to the transition of an electron to i^{th} orbital should start from time *t=0* (when the unstable dinuclear state was formed) and continue as long as M_1 and M_2 are close to each other compared to the diameter of the i^{th} orbital. At time t_i, when the fragments M_1 and M_2 would be separated by a significant distance compared to the diameter of i^{th} orbital, the electronic configuration becomes so much altered that the overlap of the electronic wave function with the original i^{th} orbital becomes negligible. So for time $t \geq t_i$, i^{th} orbital might be considered destroyed and characteristic photon emission (X_i) from the compound atom due to the transition to the i^{th} orbital cannot take place. We indicate by $|\bar{A}_i, \bar{X}_i >$, the state with destroyed i^{th} orbital and no corresponding photon emission (X_i) due to the transition to the i^{th} orbital. We have the orthogonality conditions $\langle A_i, X_i | \bar{A}_i, \bar{X}_i \rangle = 0$ and $\langle A_i, X_i | A_j, X_j \rangle = 0$ for i≠j. Since $|A_i, X_i >$ and $|\bar{A}_i, \bar{X}_i >$ are time-independent stable states that should remain correlated with the outcome of the measurements in spite of interactions with the environment, they could be considered as pointer states [Zur03]. Pointer state $|A_i, X_i >$ implies the presence of either $|\psi_{dinuclear} >$ or $|\psi_{fissioned}\ (M_1, M_2, t) >$ where M_1 and M_2 are still sufficiently close to each other. Pointer state $|\bar{A}_i, \bar{X}_i >$ implies the presence of

$|\psi_{fissioned}\ (M_1, M_2, t)>$ where M_1 and M_2 are sufficiently separated so that i^{th} orbital of the combined atom could be considered as destroyed. Let us abbreviate $|\psi_{dinuclear}\ (M_1, M_2, t=0)>$ and $|\psi_{fissioned}\ (M_1, M_2, t)>$ as $|\psi_{dinuclear}\ >$ and $|\psi_{fissioned}\ (t)>$ respectively. At any time *t*, we get

$$|\psi_{dinuclear}\ > |A_i^*> \rightarrow \gamma_i(t)|\psi_{dinuclear}\ > |A_i, X_i> \tag{5.23}$$

For $t << t_i$, we get

$$\left|\psi_{fissioned}\ (t)> |A_i^*> \rightarrow \gamma_i(t)\right|\psi_{fissioned}\ (t)> |A_i, X_i> \tag{5.24}$$

where $\gamma_i(t)$ is a time-dependent complex coefficient.

In eqns. (5.23) and (5.24), there should also be amplitudes for the presence of $|A_i^*>$. However, $|A_i^*>$, being an unstable state, cannot be considered as a pointer state [Zur03] because it will not remain correlated with the outcome of the measurement throughout the process. Hence, it has not been considered in our analysis.

For $t \geq t_i$,

$$\left|\psi_{fissioned}\ (t)> |A_i^*> \rightarrow\right|\psi_{fissioned}\ (t)> |\bar{A}_i, \bar{X}_i> \tag{5.25}$$

So for time $t \geq t_n$, (where the total number of atomic orbitals =*n*), the combined dinuclear-ion state evolves [Zur02, Zur03] into a correlated state

$$|\psi_{correlated}\ (t)> = \alpha(t) \sum_{i=1}^{n} C_i |\psi_{fissioned}\ (t)> |\bar{A}_i, \bar{X}_i>$$

$$+\beta(t) \sum_{i=1}^{n} C_i \gamma_i(t) |\psi_{dinuclear}\ > |A_i, X_i> \tag{5.26}$$

where the summation is over all the atomic orbitals. The corresponding density matrix of the pure state $|\psi_{correla\ ted}(t)>$ is $\rho^c(t) = |\psi_{correlated}\ (t)><\psi_{correlated}\ (t)|$ whose diagonal elements

are real numbers. After tracing over the environment [Zur02, Zur03], one gets the reduced density matrix at time $t \geq t_n$ [Ray15]

$$\rho^r(t) = |\alpha(t)|^2 \sum_{i=1}^{n} |C_i|^2 |\psi_{fissioned}\ (t) >< \psi_{fissioned}\ (t)|\ |\bar{A}_i, \bar{X}_i >< \bar{A}_i, \bar{X}_i|$$

$$+|\beta(t)|^2 \sum_{i=1}^{n} |C_i|^2\ |\gamma_i(t)|^2 |\psi_{dinuclear}\ >< \psi_{dinuclear}\ ||A_i, X_i >< A_i, X_i| \qquad (5.27)$$

The reduced density matrix contains only classical correlations implying that the system would be either in the fissioned state or dinuclear state. Since an ion is a relatively large object, we might consider the time required to transform from ρ^c to ρ^r as instantaneous and take the time t_n required to form the coupled state with all the orbitals of the ion (as given in (eqn. 5.27)) as the decoherence time of the fissioning nucleus. It is very important to couple with all the atomic orbitals, because otherwise the reduced density matrix will contain quantum correlations and decoherence will not be achieved. For example, at $t = t_{i'}$ ($t_{i'} < t_n$, n being the total number of atomic orbitals), the nuclear-ion wave function might be approximately written as

$$|\psi_{corr\ e_{partial}}\ (t) >\approx$$

$$\alpha(t) \left[\sum_{i=1}^{i'} C_i |\psi_{fissioned}\ (t) > |\bar{A}_i, \bar{X}_i > + \sum_{i=i'}^{n} C_i \gamma_i(t) |\psi_{fissioned}\ (t) > |A_i, X_i >\right] +$$

$$\beta(t) \sum_{i=1}^{n} C_i \gamma_i(t) |\psi_{dinuclear}\ > |A_i, X_i > \qquad (5.28)$$

The diagonal elements of the corresponding density matrix

$\rho_{corr\ e_{partial}}\ (t) = |\psi_{corr\ e_{partial}}\ (t) >< \psi_{corr\ e_{partial}}\ (t)|$ are complex numbers and after tracing over the environment, the reduced density matrix will contain quantum correlations. However, for $t \geq t_n$, the fully correlated coupled state as given by (eqn. 5.27) would be produced and after tracing over the environment, the reduced density matrix will contain only classical correlations and quantum decoherence would be achieved.

So, the question is what is the estimate for t_n ? The problem of two approaching atoms forming a united atom was reviewed by J. Reinhardt and W. Greiner [Rie84]. In our case, the nucleus of the united atom is breaking apart due to fission. Since the speed (~10^9 cm/sec) of the fission fragments is much smaller than the orbital speed of the electrons, adiabatic approximation could be applied. As the fission fragments start separating out, the electronic wave function is described in terms of molecular orbitals [Anh85] involving two separating charge centers. However, when the distance between the charge centers is very small compared to the diameter of i^{th} atomic orbital of the compound atom, the distortion of the i^{th} orbital should be very small and so its overlap with the original i^{th} orbital would be large. As the distance between the charge centers becomes comparable to the diameter of the i^{th} orbital, electrons of the i^{th} orbital would be so much disturbed that the overlap of its wave function with the original i^{th} orbital becomes negligible and the i^{th} atomic orbital of the compound atom could be considered destroyed and no characteristic photon (X_i) due to the transition to i^{th} orbital could be seen. Hence, when the distance between the charge centers is comparable to the diameter of the atom/ion, all the atomic orbitals could be considered destroyed and no characteristic photon of the compound ion could be emitted. An estimate of the upper limit of the destruction time of all the atomic orbitals might be done by calculating the time taken by the fission fragments to cross the atomic radius i.e. $\frac{10^{-8}cm}{10^{9}cm/sec} = 10^{-17}$ sec. So $t_n < 10^{-17}$ sec i.e. t_n should be of the order of 10^{-18} sec. The classical exponential decay should start after the loss of quantum superposition in attosecond time scale (10^{-18} sec) and very little fission decay would occur before that because of the reformation amplitude of forming the dinuclear state from the decayed states.

A compound dinuclear state can also decay by emitting neutrons, high energy GDR gamma rays etc. [Van73] in addition to undergoing fission. So, the superposition of states produced by the time evolution of $|\psi_{dinuclear} >$ would also include the superposition of neutron-emitted and GDR-emitted states in addition to the fissioned states and undecayed $|\psi_{dinuclear} >$ state, as given below.

$$e^{-\frac{iHt}{\hbar}}|\psi_{dinuclear}\ (M_1, M_2, t=0) >$$

$$= \alpha_f(t)|\psi_{fissioned}\ (M_1, M_2, t) > +\beta(t)|\psi_{dinuclear}\ (M_1, M_2, t=0) > +\alpha_n(t)\big|\psi_{neutro\ n\_emitted}\ (t) >$$

$$+\alpha_\gamma(t)\big|\psi_{GDR\_emitted}\ (t) > \qquad (5.29)$$

Very little neutron, GDR emission or fission decay would take place as long as quantum superposition would persist because of the reformation amplitudes discussed earlier. So, the nuclear techniques such as mass-angle distribution [Tok85, Rie11] and pre-fission neutron multiplicity techniques [Hin92] detect decay products from the decaying nuclear state primarily after the loss of quantum coherence. Hence, the nuclear techniques cannot measure how long the quantum superposition of the decayed and undecayed nuclear states persisted. For example, prefission neutron multiplicity technique measures the ratio $M_n = \frac{\int_0^{\tau_f} |\alpha_n(t)|^2 dt}{\int_0^{\tau_f} |\alpha_f(t)|^2 dt}$ where τ_f is the fission lifetime and it tells us how many neutrons would be emitted, on the average, before fission takes place. Then one determines fission time knowing the exponential decay time of neutron emission from statistical model codes [Hin92]. So, nuclear techniques [Tok85, Rie11, Hin92] measure the exponential fission decay time that would only depend on the properties of the decaying nuclear state and cannot provide any information about the coherence time of undecayed and decayed nuclear states. On the other hand, atomic techniques [Gol99, Mor08, And08, Fre12, Wil04, Mol93] measuring the survival time of the ions hosting fissioning nuclei

should measure the sum of the quantum coherence time between the undecayed and decayed nuclear states and the exponential fission decay time.

In the case of low excitation energy of the fissioning nucleus, the exponential fission decay time becomes much longer than the quantum decoherence time of the fission process (~10^{-18} sec). So, the measured survival time of the concerned ion would be dominated by the exponential fission decay time and could be much longer than 10^{-18} sec. However, for highly excited (E_X > 50 MeV) uranium and transuranium nuclei/complexes, the survival time of the concerned ion could be dominated by the quantum decoherence time. It was found from ref. [Gol99] that as ^{238}U is excited to high excitation energy (above 250 MeV) by scattering from ^{28}Si at a small impact parameter, the fission time of the excited ^{238}U drops below 10^{-18} sec. The quantum decoherence time of such highly excited ^{238}U fission process is expected to be short in this situation, because in the case of small impact parameter collisions (producing high excitation energy) higher ionic states of ^{238}U having smaller ionic radii would be produced, thus reducing destruction time of the ionic orbitals and the quantum decoherence time.

Qualitatively speaking, the interaction of the dinuclear/compound state with the atomic states producing photons is like a measurement process projecting out the unstable dinuclear state from the superposition of states. The measurement process is creating quantum Zeno effect [Hom97] inhibiting the time evolution of the dinuclear state. We consider the timescale of creation of fully correlated nuclear-ion wave function as decoherence time of the quasifission/fission process and this is the timescale of destruction of all the atomic orbitals when no further photon emission due to the transitions of electrons between orbital states is possible.

Comment on TDHF calculations

The time dependent Hartree-Fock calculations (TDHF) [Sek13, Wak14] apparently show that the quasifissioning fragments separate out in zeptosecond (~10^{-21} sec) timescale. However, in TDHF calculations of heavy ion collisions, the relative motion between the nuclei is treated classically while the internal degrees of freedom of nucleons and their couplings to collective excitations are treated quantum mechanically on a mean field level described by a single Slater determinant. TDHF calculations consider time evolution of an initial state wave function that is a product of ground state wave functions of two nuclei boosted with a relative velocity. After collision, single particle wave functions extend spatially and the final stage wave function remains a superposition of states with different particle number distributions. TDHF calculations use classical trajectories and for collisions outside the fusion critical impact parameter, the fragments are assumed to separate out irreversibly. Hence, quantum decoherence time is not included in TDHF calculations and the separation time of the fragments is essentially based on classical considerations.

Comment on Carjan et al.'s calculation

Carjan *et al.* [Car94] considered sub-barrier fission as tunnelling of wave function through a one-dimensional barrier and obtained pre-exponential decay time of the order of 10^{-21} sec. They assumed formation of an unstable compound state comprising two fragments contained within the nuclear dimension at $t=0$ instant and obtained a time-dependent fission decay rate by calculating the fraction of wave function that has tunnelled through the barrier at time t. This time-dependent fission decay rate shows saturation after a time of the order of 10^{-21} sec that depends on an arbitrary parameter. However, the coherence between the parent state and

fissioned state would continue indefinitely even after the fragments would tunnel through the barrier. Carjan *et al.* [Car94] assumed implicitly that the coherence between the parent state and fissioned state would be lost and the decay process would be irreversible as the fragments tunnel through the barrier and their separation becomes larger than a certain distance taken as comparable to the nuclear dimension. However, there is no a priori reason to assume that the coherence between the parent and fissioned state would be lost as the fragments come out of the nuclear potential well, because quantum coherence is not due to the attractive force between the fragments. As long as the initial compound nuclear state and the fissioned state cannot be distinguished, the decay should be reversible and non-exponential decay should be dominant. As discussed before, the time evolution of an isolated state with energy form factor $\omega(E)$ of the form of a Lorentzian multiplied by a threshold factor to take care of the low energy behaviour shows that the square of the amplitude of the undecayed state approximately becomes an exponential function of time at a time t given by $\frac{\lambda t}{\hbar} e^{-\lambda t/\hbar} \gg \left(\frac{\lambda}{E_R}\right)^2$ [Kha58], where λ and E_R are width and resonance energy of the state. However, this result has to be analyzed in proper perspective. Suppose a nuclear reaction is performed to produce a fissioning nucleus at *t=0* instant. However, this instant has no physical significance. A measurement process has to be performed to determine whether a compound fissioning state comprising two fragments very close to each other has been formed and this measurement process would define a new *t=0* instant when the time evolution of the state could be considered. Then another measurement has to be performed to distinguish between the initial state and fissioned state and determine whether a fission has occurred. Suppose the initial compound nuclear state is evolving without any interaction with the environment and the non-exponential timescale is on the order of 10^{-21} sec as obtained by Carjan *et al.* [Car94]. In order to see decay in such a short timescale, a measurement

process to distinguish between the initial compound nuclear state and fissioned state has to be completed in a timescale on the order of 10^{-22} -10^{-21} sec. So the energy uncertainty of the compound nuclear state would be on the order of 1 -10 MeV. In the case of sub-barrier fission, the fission time is very long and so the value of λ is very small. As a result of the large increase in the value of λ because of the measurement process, the onset of the exponential decay would be delayed by many orders of magnitude following Khalfin's criteria [Kha58]. So the non-exponential decay for 10^{-21} sec in the case of subbarrier fission cannot be observed even in principle. Hence, it is not a physically meaningful number.

In practice, the superposition of states is lost due to the interaction with the surrounding environment. So, Carjan *et al*.'s calculation [Car94] did not consider the decoherence process and was based on an ad-hoc assumption that the superposition of nuclear states would be destroyed beyond a certain distance taken as comparable to the dimension of the nuclear potential well.

Thus, we have estimated the quantum decoherence time of the nuclear fission processes by considering the interaction of the superposition of decaying and decayed nuclear states with the atomic electronic orbitals [Ray15]. Quantum decoherence time depends on the environment surrounding the decaying state because the coherence between the undecayed and decayed states is lost as a result of interaction with the environment. On the other hand, the exponential decay time depends only on the properties of the decaying state. Our calculated quantum decoherence time of the fission process is consistent with the fission lifetime measured by the atomic techniques and could provide a probable solution of the fission time anomaly between the atomic and nuclear measurements established in the last chapter.

Chapter 6

Penning Trap

The mass measurement of superheavy nuclei would provide further insight on this problem of fission time anomaly related to fissile and very heavy nuclei. The fission time depends on the binding energy of the nucleus and microscopic calculations predict high fission barrier and binding energy around Z=120 [Moe94, Ben90]. One can learn about the nuclear binding energy from high precision nuclear mass measurements and Penning traps are presently being used for the mass measurements of superheavy nuclei [Blo10, Ram12] to find out the shell stabilization criterion. Although such experiments are beyond the scope of my thesis, I have been deeply involved in the development of a Penning trap to use it in conjunction with the upcoming facilities at VECC, Kolkata where such experiments could be undertaken in the future. This chapter provides the information about the status of Penning Trap development at VECC.

6.1 Theory of Penning trap

According to Earnshaw's theorem, a charged particle cannot be held in stable equilibrium by electrostatic forces alone [Gri99]. For example, when a positive test charge is to be held in a fixed position in three dimensions, one need to make the resultant force acting on test charge to be zero from all directions. So, one should keep the test charge at the centre of a positively charged hollow sphere. But, it is known that there is zero potential inside a hollow sphere. So, the test charge will drift to the surface of the sphere and there will be no confinement. So, one

need to apply either magnetic field or varying electric field in addition with static electric field to confine the charged particle in free space.

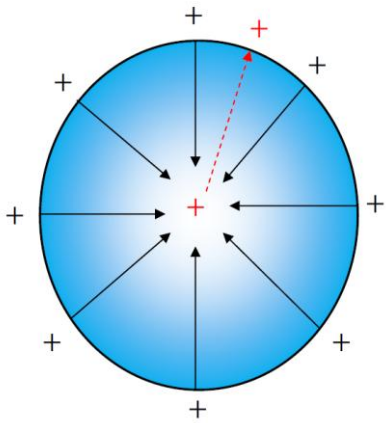

Fig. 6.1: *A positive charge placed at the centre of a positively charged metal sphere will drift to the surface of the sphere and hence, it cannot be confined by electrostatic force alone.*

The configuration in which ions/electrons are trapped under application of strong homogenous magnetic field and weak quadrupolar electrostatic potential is known as Penning Trap [Win73]. In the presence of strong homogenous magnetic field, preferably chosen along z direction, the charged particle is bounded in the plane perpendicular to the field but the motion along the applied field remain unbound. So, a weak quadrupolar potential of suitable polarity is applied which provides axial confinement and result in harmonic motion along z direction. The axial frequency (ν_z) and angular frequency (ω_z) depend solely on the applied electric potential [Bro86] given as

$$\omega_z = 2\pi\nu_z = \sqrt{\frac{qU_{dc}C_2}{md^2}} \tag{6.1}$$

where U_{dc} is the electrostatic trapping potential, d and C_2 are related to trap geometry described in section 6.2. In our work, we have used the axial motion for all detection and monitoring purposes.

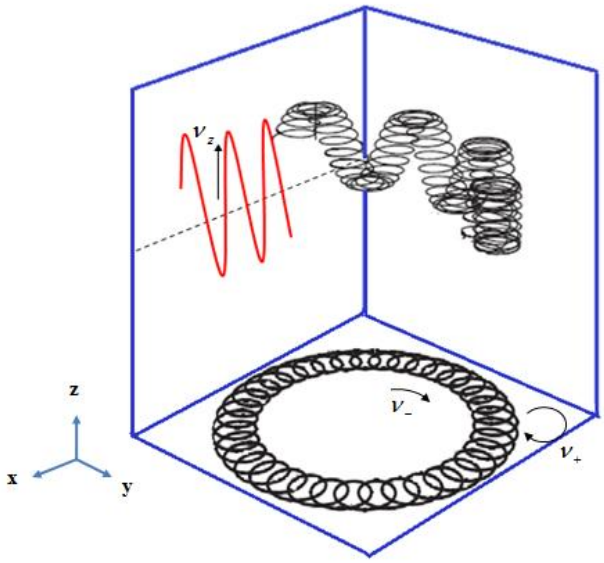

Fig. 6.2: *Trajectory of charged particles in Penning trap with magnetic field along z axis. The projection of the motion on x-y plane is a superposition of two radial motions: modified cyclotron motion with frequency ν_+ and magnetron motion with frequency ν_- and the projection on x-z plane or y-z plane gives the axial motion with frequency ν_z.*

Due to the presence of additional quadrupolar potential that acts opposite to the confining magnetic force, the radial motion becomes a superposition of two independent harmonic motions. The free cyclotron motion ω_c changes slightly [Bro86] and termed as modified cyclotron motion (ω_+).

$$\omega_+ = 2\pi\nu_+ = \frac{\omega_c}{2} + \sqrt{\frac{\omega_c^2}{4} - \frac{\omega_z^2}{2}} \tag{6.2}$$

where $\omega_c = \frac{qB}{m}$ is the free cyclotron frequency. The presence of $\vec{E}\times\vec{B}$ field results in a slow drift motion that is termed as magnetron motion (ω_-).

$$\omega_- = 2\pi\nu_- = \frac{\omega_c}{2} - \sqrt{\frac{\omega_c^2}{4} - \frac{\omega_z^2}{2}} = \frac{\nu_z^2}{2\nu_c} \tag{6.3}$$

The magnetron frequency is independent of both the particle properties *e* and *m*, being determined by the electric and magnetic fields alone. Unlike the other spatial motions, the magnetron motion is only metastable. Any loss of energy in this motion would cause the magnetron orbit to grow until the trapped particle collides with the electrode surface. Typically, the eigen-frequencies obey the following hierarchy [Bro82]

$$\omega_- << \omega_z < \omega_+ < \omega_c \tag{6.4}$$

It is clear from the eqns. (6.2) and (6.3) that to overcome the repulsive radial electrostatic field from making the ion trajectories unstable in the radial direction, the axial frequency has to be chosen sufficiently low and it gives the condition for applied electric and magnetic field to obtain stable confinement of charged particles.

$$\frac{\omega_c^2}{4} - \frac{\omega_z^2}{2} > 0; \quad B > \frac{2m|U_{dc}|C_2}{|q|d^2} \quad for \quad qU_{dc} > 0 \tag{6.5}$$

However, the implementation of those principles for a real Penning trap is much more complicated due to significant deviations from ideal quadrupolar electrostatic potential, misalignments between the electric and magnetic fields and several other factors. The magnetic field inhomogeneities, electric field imperfections, misalignment of the trap axis with respect to the magnetic field axis etc. result in shifts of the measured eigen-frequencies as well as broadenings of the observed resonances. In spite of various shifts in eigen-frequencies, Brown and Gabrielse [Bro86, Gab09] showed that the free cyclotron frequency is given by

$$\omega_c^2 = \bar{\omega}_+^2 + \bar{\omega}_-^2 + \bar{\omega}_z^2 \tag{6.6}$$

where the barred quantities represent the measured frequencies that shift due to various imperfections, while the cyclotron frequency (ω_c) is the ideal free cyclotron frequency in the absence of the electrostatic field. This is known as the Brown- Gabrielse invariance theorem [Bro86]. This theorem opens up the possibility of measuring the free cyclotron frequency with a very high accuracy in the presence of a imperfect magnetic field and realistic electrostatic field and makes trap useful for high precision mass measurement.

6.2 Design of cylindrical Penning trap electrodes

In order to perform high precision measurements using Penning traps, it is essential to create a high quality quadrupolar potential near the center of the Penning trap. Traditionally this was achieved by using hyperbolic electrodes. However, it is generally quite difficult to machine such hyperbolic electrodes with sufficient precision. The quadrupolar potential near the centre of the trap could be created by an open-ended cylindrical trap geometry with the help of suitable cylindrical compensation electrodes [Gab84] and usually that is sufficient for most of the purposes. This important result led to the use of cylindrical traps which are much easier to

fabricate and provide much better accessibility to the trapped particles [Gab89, Win93] and the use of external probes such as laser beam and microwaves [Bol03,Vin98] etc.

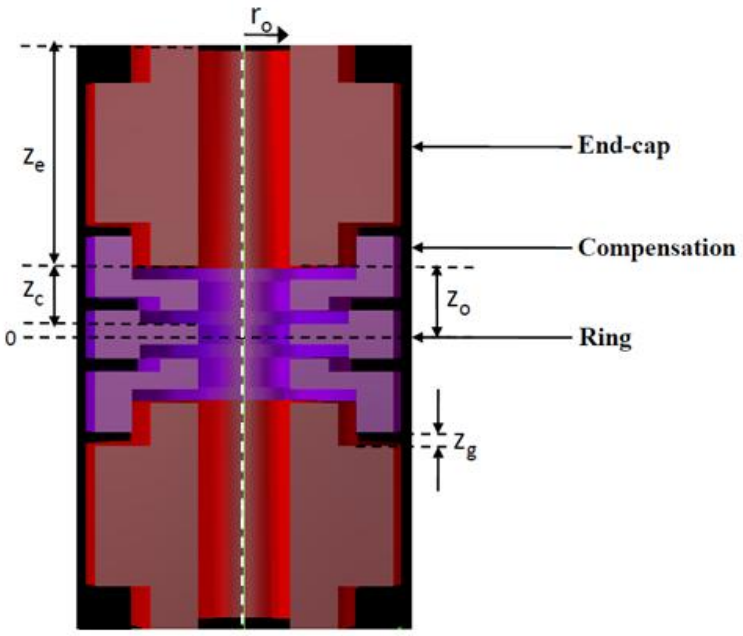

Fig. 6.3: *Open ended, cylindrical Penning trap with five electrodes and one pair of compensation electrodes, with the center of ring electrode at the origin. Special cuts are applied to the electrodes so that the insulators cannot see the trapped particles and charge built-up in the insulator is avoided.*

Assuming that the applied voltage between the end-caps and the ring is V_0 and taking the origin at the center of the ring electrode where the azimuthal symmetry axis i.e. the Z = 0 plane bisects the ring electrode, the electrostatic potential inside the cylindrical trap can be written [Jac75, Bro86] in spherical polar coordinates (r, θ and ϕ) as

$$V(r,\theta) = \frac{1}{2} V_0 \sum_{\substack{k=0 \\ \text{even}}}^{\infty} C_k \left(\frac{r}{d}\right)^k P_k(\cos\theta) \qquad (6.7)$$

where $d = \sqrt{1/2(z_o^2 + r_o^2/2)}$, where z_o is the axial distance from the centre to the beginning of the end-cap electrode and r_o is the radius of the trap shown in Fig. 6.3.

Writing the result in cylindrical coordinates (r, ϕ and z) and keeping only the first two terms, the above equation becomes

$$V(r,z) = \frac{1}{2}V_0\ C_0 + V_0\ (\frac{z^2 - r^2/2}{2d^2})\ C_2 \qquad (6.8)$$

The first term is a constant determined by the choice of a reference point for the potential and has no effect on the electric field. If all higher order coefficients (C_k , $k > 2$) would vanish, then the potential $V(r,\theta)$ would present an ideal quadrupolar potential.

The electrostatic potential in a cylindrical trap comprising a ring electrode and two end-caps departs from the quadrupolar potential as one moves away from the center of the trap. The cylindrical geometry introduces non-linearity in the equation of motion, resulting in amplitude-dependent frequency shifts and instabilities [Bla06]. The use of compensation electrodes [Gab89] that can tune out anharmonicity to first order with the application of proper voltage has mostly overcome this problem. By adjusting the compensation potentials, the leading anharmonic C_4 term can be tuned out. However, the adjustment of the compensation potential complicates the study of particle motion since it changes the axial-oscillation frequency of the trapped particles. If C_2 is independent of the adjustment of compensation potentials, then the trap with this feature is called an orthogonalized trap. So, the concept of orthogonalized Penning trap was introduced [Gab83] implying that the trapping well depth and the axial oscillation frequency of the trapped particle are independent of the anharmonicity compensation. Special configurations were required to achieve such orthogonalized traps.

Let V_0 be the voltage applied between the end-caps and the ring electrode and V_1 be the voltage applied on the compensation electrodes relative to the same reference ground used for V_0. Then following ref. [Fei99], the electrostatic potential inside the trap is

$$V = V_0 \Phi_0 + V_1 \Phi_1 \tag{6.9}$$

where

$$\Phi_0 = \frac{1}{2} \sum_{\substack{k=0 \\ \text{even}}}^{\infty} C_k^{(0)} \left(\frac{r}{d}\right)^k P_k(\cos\theta) \tag{6.10}$$

$$\Phi_1 = \frac{1}{2} \sum_{\substack{k=0 \\ \text{even}}}^{\infty} D_k \left(\frac{r}{d}\right)^k P_k(\cos\theta) \tag{6.11}$$

Here $C_k^{(0)}$ and D_k are yet to be determined coefficients and these coefficients depend on the trap geometry. Since the potential has cylindrical symmetry around Z-axis and reflection symmetry across the Z=0 plane, following ref [Fei99]

$$C_k = C_k^{(0)} + \frac{V_1}{V_0} D_k \tag{6.12}$$

Using the method described in ref [Gab84], it can be shown that

$$C_k^{(0)} = \frac{(-1)^{\frac{k}{2}}}{k!} \frac{\pi^k}{2^{k-1}} \left(\frac{d}{L}\right)^k \sum_{n=1}^{\infty} (2n)^k \frac{S_n^{(0)}}{L\, J_0(i k_n r_0)} \tag{6.13}$$

$$D_k = \frac{(-1)^{\frac{k}{2}}}{k!} \frac{\pi^k}{2^{k-1}} \left(\frac{d}{L}\right)^k \sum_{n=1}^{\infty} (2n)^k \frac{S_n^{(1)}}{L\, J_0(i k_n r_0)} \tag{6.14}$$

where $k_n = \frac{n\pi}{L}$, where L is the length of the trap from centre of ring to the end of end-cap electrodes and where

$$S_n^{(0)} = 2 \int_0^L \Phi_0(r_o, z) \cos\left(\frac{n \pi z}{L}\right) dz \tag{6.15}$$

$$S_n^{(1)} = 2 \int_0^L \Phi_1(r_o, z) \cos\left(\frac{n \pi z}{L}\right) dz \tag{6.16}$$

In order to evaluate the integrals given by eqn. (6.15) & (6.16), the values of $\Phi_0(r_o, z)$ and $\Phi_1(r_o, z)$ representing electrostatic potentials on the surface of the trap electrodes for different

values of z are required. The potentials on the electrodes are known from the boundary conditions. Following ref. [Far02], the potentials in the gaps have been approximated considering semi – infinite gap case which is applicable only when Z_g is much smaller than the electrode thickness and $r_o >> Z_g$.

The boundary conditions for $\Phi_0(r_o, z)$ are:

$$\Phi_0(r_o, z) = \begin{cases} \frac{1}{2} & \text{for } Z_o < z < L \text{ (end-cap)}, \\ \sum_{i=0}^{5} a_i^{(0)} u^i & \text{for } Z_o - Z_g < z < Z_o \text{ (gap)}, \\ 0 & \text{for } Z_o - Z_c + Z_g < z < Z_o - Z_g \text{ (compensation)}, \\ \sum_{i=0}^{5} b_i^{(0)} w^i & \text{for } Z_o - Z_c < z < Z_o - Z_c + Z_g \text{ (gap)}. \\ -\frac{1}{2} & \text{for } 0 < z < Z_o - Z_c \text{ (ring)}. \end{cases} \quad (6.17)$$

The boundary conditions for $\Phi_1(r_o, z)$ are:

$$\Phi_1(r_o, z) = \begin{cases} 0 & \text{for } Z_o < z < L \text{ (end-cap)}, \\ \sum_{i=0}^{5} a_i^{(1)} u^i & \text{for } Z_o - Z_g < z < Z_o \text{ (gap)}, \\ 1 & \text{for } Z_o - Z_c + Z_g < z < Z_o - Z_g \text{ (compensation)}, \\ \sum_{i=0}^{5} b_i^{(1)} w^i & \text{for } Z_o - Z_c < z < Z_o - Z_c + Z_g \text{ (gap)}. \\ 0 & \text{for } 0 < z < Z_o - Z_c \text{ (ring)}. \end{cases} \quad (6.18)$$

where $u = \frac{Z}{Z_g} - \frac{Z_o}{Z_g} + 1$ and $v = \frac{Z}{Z_g} - \frac{(Z_o - Z_c)}{Z_g}$

The coefficients $a_i^{(0)}$, $b_i^{(0)}$, $a_i^{(1)}$ and $b_i^{(1)}$ have been determined by fitting the gap potentials with a fifth order polynomial [Far02] and the values of the coefficients are given in Table 6.1.

Table 6.1: *Values of various coefficients used in (eqn. 6.17 & 6.18) to estimate the gap potential.*

Coefficients	Values	Coefficients	Values
$a_0^{(0)}$	0.00427	$a_0^{(1)}$	0.99146
$b_0^{(0)}$	-0.49573	$b_0^{(1)}$	0.00854
$a_1^{(0)} = b_1^{(0)}$	0.79975	$a_1^{(1)} = -b_1^{(1)}$	-1.5995
$a_2^{(0)} = b_2^{(0)}$	-1.65852	$a_2^{(1)} = -b_2^{(1)}$	3.31704
$a_3^{(0)} = b_3^{(0)}$	3.55116	$a_3^{(1)} = -b_3^{(1)}$	-7.10232
$a_4^{(0)} = b_4^{(0)}$	-3.66822	$a_4^{(1)} = -b_4^{(1)}$	7.33644
$a_5^{(0)} = b_5^{(0)}$	1.46729	$a_5^{(1)} = -b_5^{(1)}$	-2.93458

Finally, the coefficients $C_k^{(0)}$ and D_k have been evaluated and the electrostatic potential profiles in the trap are given by (eqn. 6.7) have been determined. Detailed expressions of coefficients $C_k^{(0)}$and D_k are given in ref. [Far02].

Table 6.2: *Trap parameters: Geometric and electrostatic properties.*

Dimension (mm)		Potential parameter	
r_0	3.29	V_0	10 V
Z_0	3.04	V_c	4.9874 V
d	2.7068	C_0	0.57463
Z_c	2.58	C_2	0.65202
Z_e	10.0	C_4	1.17×10^{-4}
Z_g	0.6	C_6	0.0668
D_2	7.7×10^{-4}	C_8	-0.00934

In a compensated Penning trap, it is possible to achieve orthogonalization i.e. $D_2 = 0$ and tune out C_4 term by varying the potential at compensation electrode. The optimum dimensions have been achieved for a five electrode, open-ended cylindrical Penning trap which has been used for fabrication. The dimensions and different electrostatic coefficients for our trap are listed in Table 6.2.

Moreover, we have found that by introducing another pair of compensation electrodes, it is possible to tune out up to C_8 terms and achieve dynamic orthogonalization [Sik13].

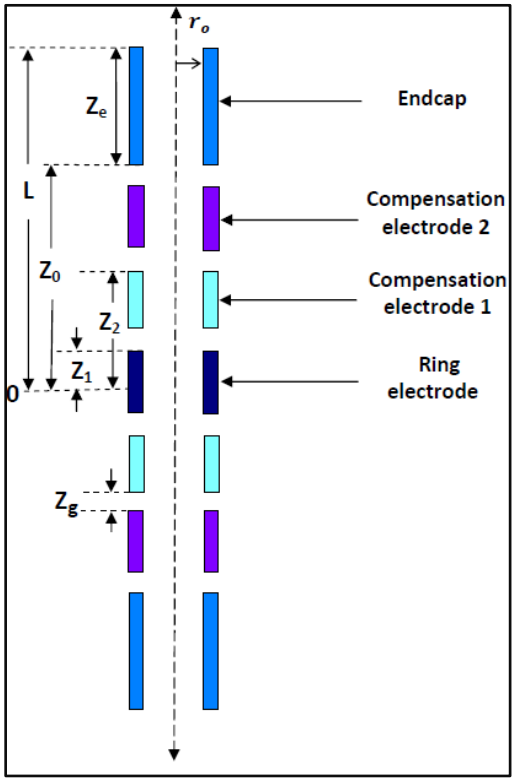

Fig. 6.4: *Open ended, cylindrical Penning trap with seven electrodes and two pairs of compensation electrodes, with the center of ring electrode at the origin.*

Let V_2 be the voltage applied on the outer compensation electrodes relative to the same reference ground used for V_0. Then (eqn. 6.9) becomes,

$$V = V_0\Phi_0 + V_1\,\Phi_1 + V_2\,\Phi_2 \tag{6.19}$$

where

$$\Phi_2 = \frac{1}{2}\sum_{\substack{k=0\\ \text{even}}}^{\infty} D_{2k}\left(\frac{r}{d}\right)^k P_k(\cos\theta) \tag{6.20}$$

Thus, (eqn. 6.12) becomes

$$C_k = C_k^{(0)} + \frac{V_1}{V_0}D_{1k} + \frac{V_2}{V_0}D_{2k} \tag{6.21}$$

Finally, the coefficients $C_k^{(0)}$, D_{1k} and D_{2k} have been evaluated in the similar fashion as mentioned above and one can see [Sik13]. It is possible to make the trap dynamically orthogonalized i.e. $C_2 = C_2^{(0)}$ (so that the axial oscillation frequency is independent of compensation potentials V_1 and V_2) and make $C_4 = 0$ by adjusting the compensation potentials V_1 and V_2 satisfying the following equations

$$\frac{V_1}{V_0}D_{12} + \frac{V_2}{V_0}D_{22} = D_2 = 0, \tag{6.22}$$

and

$$C_4^{(0)} + \frac{V_1}{V_0}D_{14} + \frac{V_2}{V_0}D_{24} = 0. \tag{6.23}$$

Keeping the total length (L) of the Penning trap fixed, we have varied the ratios of the lengths Z_1/Z_o versus Z_2/Z_o for a given gap size to make the trap dynamically orthogonalized with the anharmonicity parameters $C_4 = C_6 = 0$. In Fig. 6.5(a) the variations of the ratios of the lengths Z_1/Z_o versus Z_2/Z_o are shown for a given gap size Z_g/Z_o=0.1(fixed arbitrarily) and four different values of r_o/Z_o [Sik13]. Fig. 6.5(b) shows plots of C_8 versus Z_2/Z_o for different values of r_o/Z_o. We find that the condition $C_8 = 0$ is achieved at a specific value of Z_2/Z_o for a

particular value of r_o/Z_o. This value of Z_2/Z_o moves towards smaller values as we increase the radius of the trap.

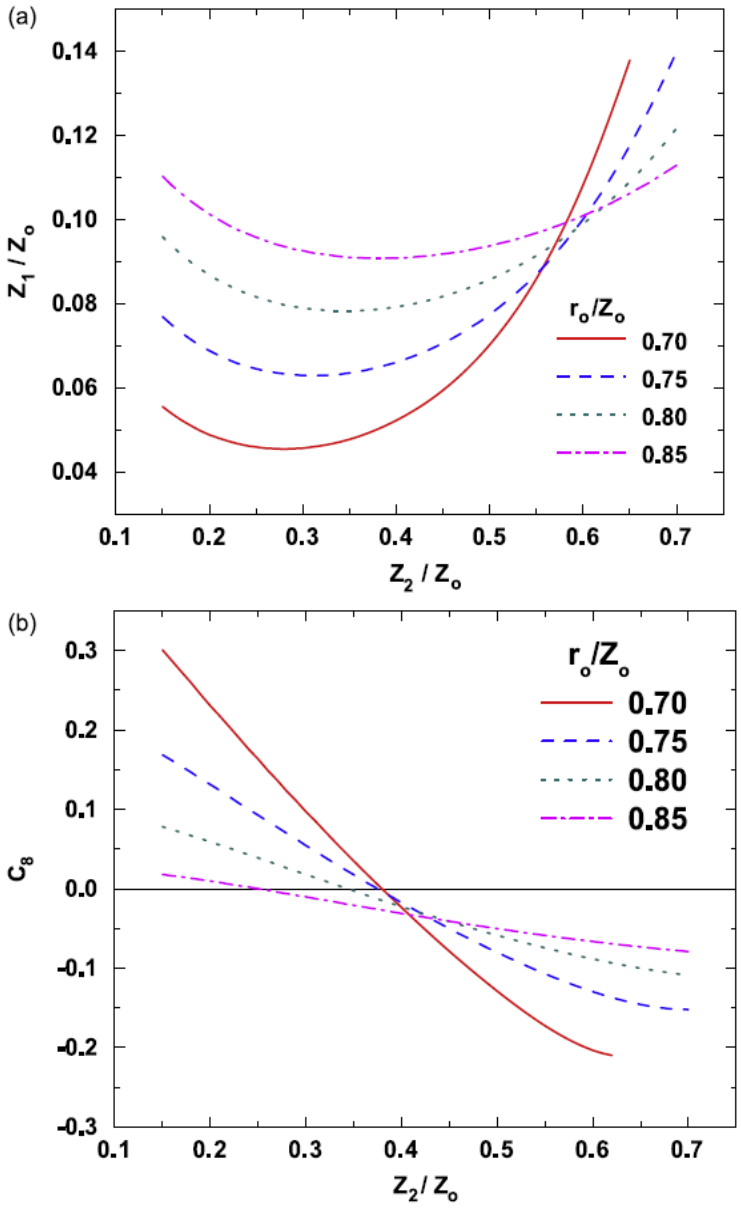

Fig. 6.5: *(a) Variation of Z_1/Z_o with Z_2/Z_o for fixed gap Z_g/Z_o = 0.1 and $Z_e/Z_o = 4.327$ which satisfies $C_2 = C_2^{(0)}$, $C_4 = 0$ and $C_6 = 0$ for an orthogonalized trap with four different r_o/Z_o and (b) respective variation of coefficients C_8.*

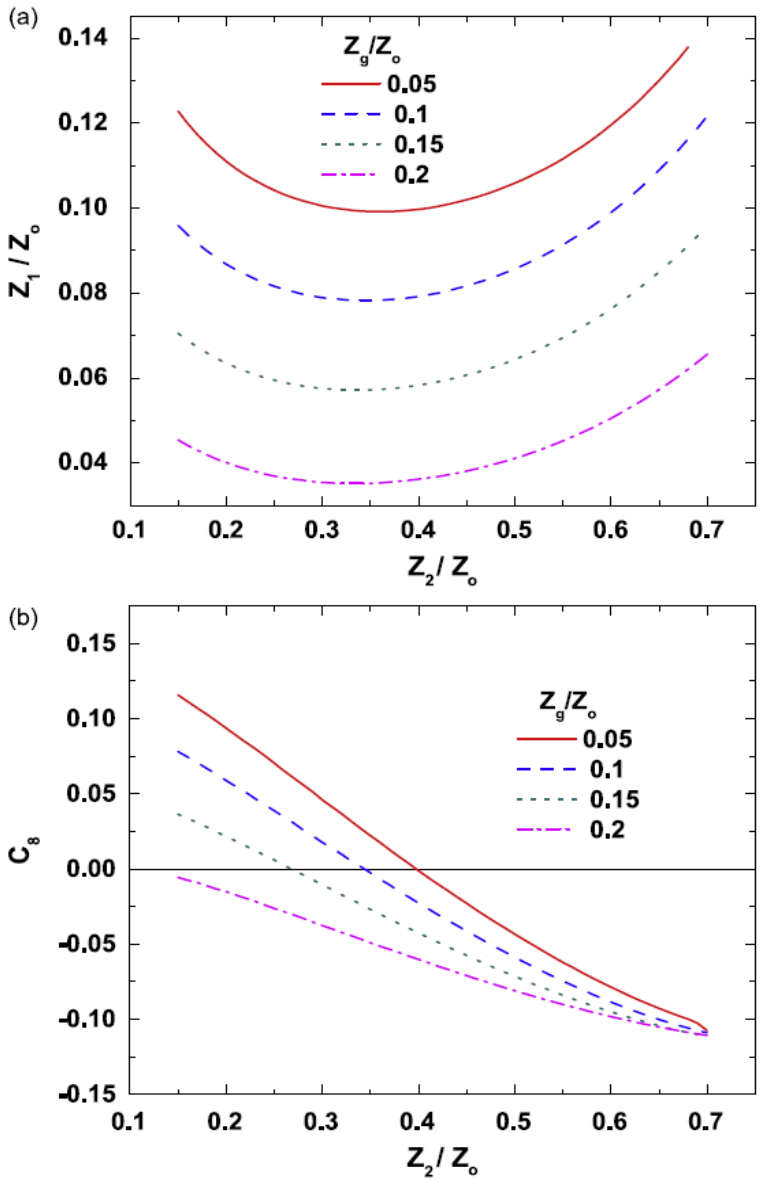

Fig. 6.6 : *(a) Variation of* Z_1/Z_o *with* Z_2/Z_o *for fixed radius* r_o/Z_o *= 0.8 and* $Z_e/Z_o = 4.327$ *which satisfies the conditions* $C_2 = C_2^{(0)}$, $C_4 = 0$ *and* $C_6 = 0$ *for an orthogonalized trap with four different* Z_g/Z_o *and (b) respective variation of coefficients* C_8.

In Fig. 6.6(a) we have plotted the ratio Z_1/Z_o versus Z_2/Z_o for a given radius r_o/Z_o =0.8 (fixed arbitrarily) and for four different values of Z_g/Z_o, creating dynamically orthogonalized trap with

the anharmonicity parameters $C_4 = C_6 = 0$ in each case. Fig. 6.6(b) shows the corresponding variation of C_8 with Z_2/Z_o for different gap lengths. We find from Fig. 6.6(b) that as the gap length between adjacent electrodes increases, C_8 becomes zero for progressively smaller values of Z_2/Z_o. This limits the range of the possible gap lengths to attain very small C_8 values as it makes the Z_2/Z_o rather unrealistic to fabricate [Sik13].

Table 6.3: *Dimensions and* $C_2^{(0)}$ *coefficients for a doubly compensated and dynamically orthogonalized Penning trap with* $C_4 = C_6 = C_8 = 0$ *for different gap lengths.*

Z_g/Z_o	0.05	0.1	0.15
r_o/Z_o	0.8	0.8	0.8
Z_1/Z_o	0.0995	0.0783	0.0585
Z_2/Z_o	0.3953	0.343	0.2695
Z_e/Z_o	4.327	4.327	4.327
V_1/V_o	-0.4716	-0.4801	-0.5056
V_2/V_o	-0.3293	-0.3419	-0.3629
$C_2^{(0)}$	0.6101	0.6336	0.6594

Some of the best configurations for a dynamically orthogonalized Penning trap with $C_4 = C_6 = C_8 = 0$ have been listed in Table 6.3 for different gap lengths [Sik13]. The values of coefficients obtained through analytical calculations have been compared with the results obtained from SIMION8 [Sim8.0] for a typical case with Z_g/Z_o =0.1, r_o/Z_o = 0.8 , Z_1/Z_o =0.0783, Z_2/Z_o =0.343 and Z_e/Z_o=4.327. The values of various coefficients obtained by SIMION8 (using mesh size =0.01 mm) and our analytical method are listed in Table 6.4 showing reasonable agreement between the two methods. The values of C_2 parameter agree within 0.5% for the analytical and SIMION8 calculations. The values of V_1/V_0 and V_2/V_0 agree within 1% for the two calculations. Both the analytical and SIMION8 calculations predict very small values of C_6 and C_8. However, the calculated values from the analytical method are about an order of magnitude lower than the

values calculated from the SIMION8 code. We have done SIMION8 calculations with 0.01 mm and 0.02 mm mesh sizes. It has been found that C_2 coefficient changes very little (only by 0.14%) and approaches the analytical value as the mesh size is reduced to 0.01mm from 0.02 mm. C_6 and C_8 coefficients that are only 0.49% and 0.94% of C_2 respectively differ from their analytical values by 20% and 33% respectively as the mesh size is reduced to 0.01 mm from 0.02 mm.

Table 6.4: *Comparison of the coefficients obtained through analytical calculations and SIMION8 (with mesh size = 0.01 mm) for a typical case* $Z_g/Z_o = 0.1$, $r_o/Z_o = 0.8$, $Z_1/Z_o = 0.0783$, $Z_2/Z_o = 0.343$ *that satisfies dynamic orthogonalization and tunes out* C_4, C_6 *and* C_8 *coefficients.*

Coefficients and Voltage ratios	Analytical results	SIMION8 results
C_2	0.6336	0.6302
C_4	0	0
C_6	-0.0001	0.0031
C_8	0.0004	-0.0059
D_2	0	0
V_1/V_0	-0.4801	-0.4765
V_2/V_0	-0.3419	-0.3410

Numerical fitting errors for C_2 coefficient are negligible and are ~0.2% and ~8% respectively for C_6 and C_8 for both the mesh sizes. SIMION8 calculates the potential in the gap using finite-element method and hence its results are more accurate compared to our analytical expressions which consider the gaps as semi-infinite. However, our analytical method is much faster and in some cases can be more useful for designing traps.

In practice the limitations of mechanical fabrication and the stability of the applied voltage result in additional anharmonicities. Since we have two compensation electrodes we can always satisfy the conditions to make the trap orthogonal and tune out C_4 term. Even if the mechanical tolerance [Sik13] for the fabrication of a symmetric Penning trap is 100 micron, we can still achieve orthogonalization condition with $C_4 = 0$ and $C_6 < 0.1$.

6.3 Cryogenic Penning trap setup

In this section, we shall discuss about various salient features of Cryogenic Penning trap. Since this trap will be used for high-precision mass measurement in the future, long storage times will be needed for which a good vacuum is mandatory. To obtain minimum background pressure, the Penning trap assembly would be placed in an indium sealed vacuum chamber and dipped in the liquid helium filled bore of a superconducting magnet. Due to efficient cryo-pumping at liquid helium temperature, one would achieve very long storage times [Gab90]. Moreover, cryogenic temperature leads to an increase in the quality factor Q as well as a lower noise level of the electronic detection circuits. The mechanical setup has been designed to ensure that the trap would be located at the center of the superconducting solenoid magnet and would endure repeated thermal cycling from room temperature to cryogenic temperature.

The development of the Cryogenic Penning Ion trap poses several challenges for its high precision fabrication and its operation at cryogenic temperature. It has been categorized in following sub-sections describing

1) Detail of the superconducting magnet.

2) Mechanical fabrications of all the components of the trap setup and its testing in liquid nitrogen temperature.
3) Development of a cryogenic multipin as well as coaxial vacuum feedthrough.
4) Detail about cryogenic electronic circuits used for detecting the axial motion of the trapped particles.
5) Finally, the initial commissioning run of the entire setup at liquid nitrogen temperature and low magnetic field.

6.3.1 Superconducting magnet

The magnetic field will be generated by a superconducting solenoid which could provide a maximum magnetic field of 5 Tesla at the centre of the solenoid. It is a cold bore, persistent mode magnet with a bore diameter of 10 cm and it has been procured from Cryomagnetics Inc. The magnetic field can be precisely controlled by a CS4-10V power supply and superconducting switch. The power supply generates current [Lap98] which is given by

$$I(t) = \frac{V}{R} + J(t) \tag{6.24}$$

where V is the voltage supplied by the power supply, R is the shunt resistance in the power supply provided by the superconducting switch and protection resistor and $J(t)$ is the current flowing in the solenoid. Since the voltage drop across the inductor is given as,

$$V = L\frac{dI}{dt} \tag{6.25}$$

So, for a solenoid with inductance L, the solenoid current is given as

$$J(t) = J(0) + \frac{V}{L}t \tag{6.26}$$

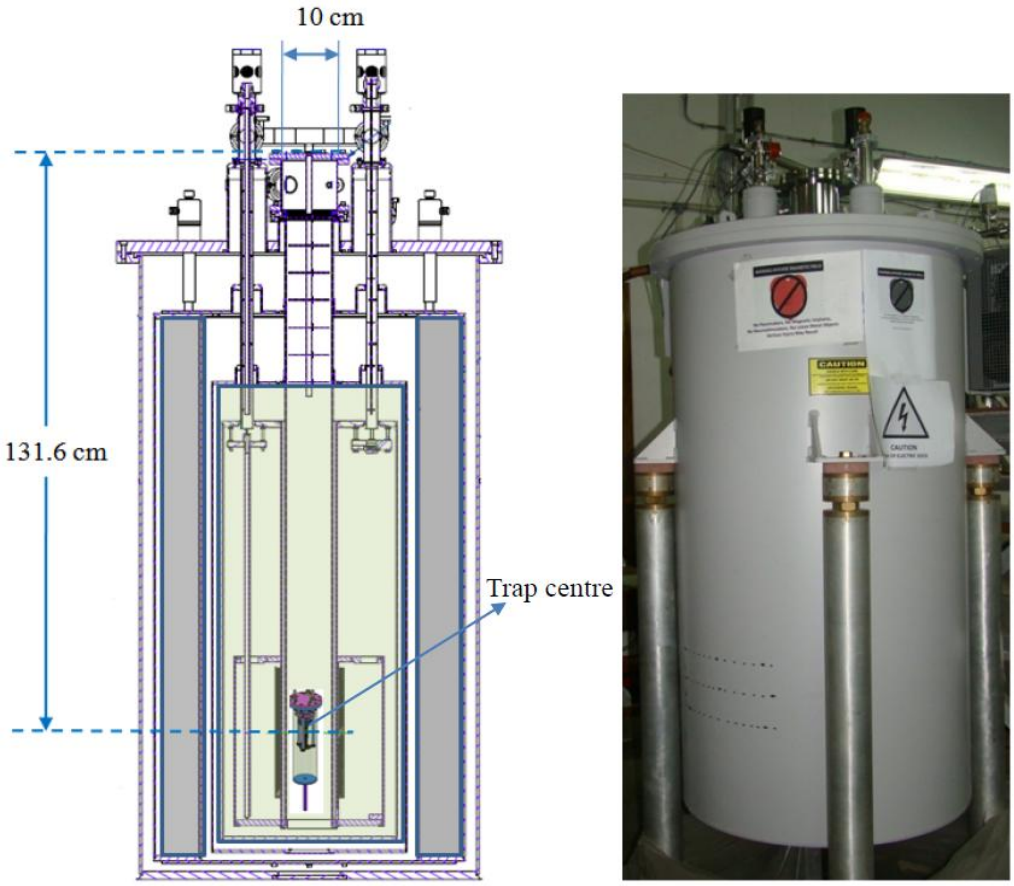

Fig. 6.7: *Sectional view of superconducting magnet with Penning trap vacuum chamber placed inside the bore. Gray color represents the liquid nitrogen filled cryostat and liquid helium filled area is indicated by light green color. Photograph of superconducting magnet installed on vibrationally damped feet is shown in the right side.*

and the magnetic field is given as

$$B(t) = g\left[J(0) + \frac{V}{L}t \right] \tag{6.27}$$

where g is a geometry dependent parameter of the solenoid. This magnet has a spatial homogeneity of better than 1 ppm level over 1 cm DSV and temporal stability of better than

0.01 ppm/hr at the centre of solenoid and it can be achieved by sending current through its ten different shim coils. This magnet has been commissioned by energizing its main superconducting coil to its maximum current of 96.9 Amperes which corresponds to a maximum field of 5T at the centre of the solenoid.

6.3.2 Mechanical detail of Penning trap assembly

The Ultra High Vacuum (UHV) chamber housing the Penning trap assembly has been made of Oxygen Free High Conductivity (OFHC) Copper. The OFHC copper has been selected because of its very high heat conductivity that provides efficient cooling of the trap electrodes and electronics reducing the thermal noise. Moreover, OFHC copper is non-magnetic and does not disturb the highly homogeneous magnetic field produced by the superconducting magnet. The top flange of UHV chamber housing the feedthrough is sealed with indium wire and the other end of the chamber is connected to a thin OFHC copper pinch-off tube. In the future, the vacuum chamber would be baked and pumped down to a pressure of ~10^{-7} mbar and then the thin OFHC copper tube would be pinched off forming a cold welded vacuum seal. It would be dipped in the liquid Helium filled bore of a superconducting magnet. At 4 K temperature, the gas inside the chamber would be adsorbed by the walls of the vacuum chamber that would bring down the pressure to $< 10^{-17}$ mbar [Gab90] which is lower than the pressure in the space. This will basically eliminate any perturbing interaction between the trapped particle and the remaining gas molecules and allows the storage of the trapped particles for virtually infinite time.

Inside the vacuum chamber, the Penning trap stack is hanging from the top flange with three copper rods as shown in Fig. 6.11. The Penning trap stack comprises of an electron gun, electrodes and a Faraday cup as shown in Fig. 6.8.

Electron Gun

The electron gun is made of a sharpened tungsten wire of tip diameter of ~1μm [called field emission point (FEP)] fixed to a holding plate and an acceleration electrode (C1) separated by insulators made up of Macor. The acceleration electrode has a central hole of diameter 1 mm. The tip is carefully installed under microscope to ensure that it is placed at the centre of the hole of acceleration electrode. When an electric potential of a few kV is applied between the holding plate and the acceleration electrode, electrons are emitted from the field emission point [Kre09] with an emission current $\propto E^2.e^{-1/E}$, E being the electric field at the tip.

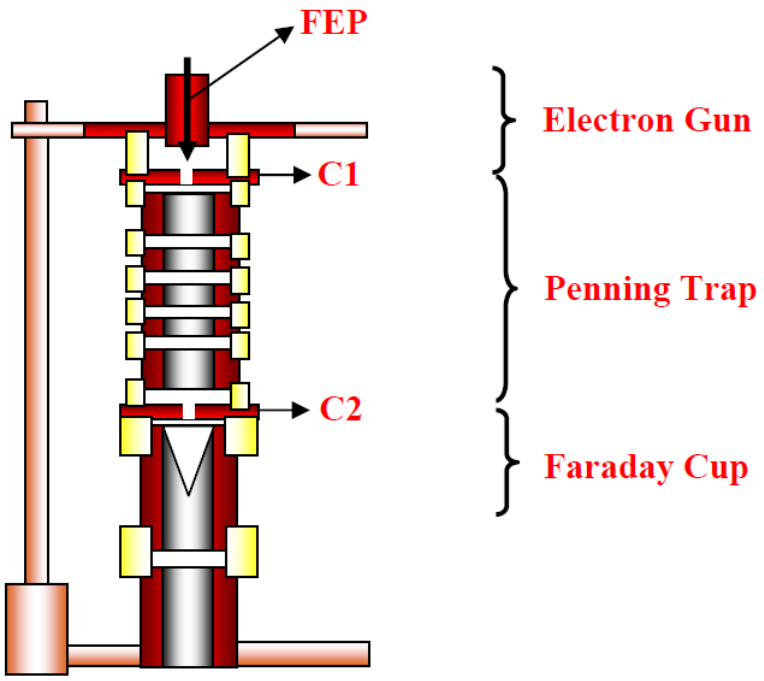

Fig. 6.8: *Schematic drawing of Penning trap setup placed inside the UHV chamber.*

Typically, an electric field of 1keV/mm is applied. If the trap assembly is dipped in liquid nitrogen instead of liquid helium, a pressure on the order of 10^{-9} mbar could be reached in the Penning trap. In that case, the keV energy electrons coming from the field emission tip would interact with the residual gas and produce a large number of low energy secondary electrons that could be trapped. The FEP tip has been tested at a pressure of $8x10^{-7}$ mbar at both 300 K and 77 K. The FEP tips were always dipped in 50% concentrated Hydrofluoric acid for 2 minutes before each installation to remove any unwanted oxide on the tip. Initial emission of electrons from tip requires around 4 kV but once the emission begins, voltages around 2.5 kV is generally sufficient to provide few μA current at the acceleration electrode.

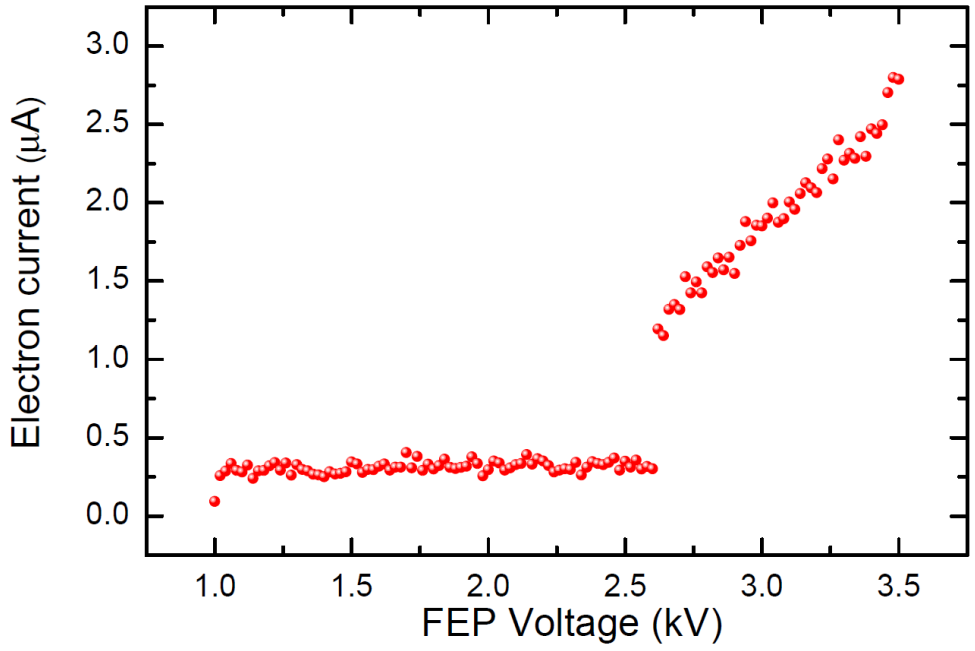

Fig. 6.9: *Measured current-voltage characteristics of Field Emission Point (FEP).*

The emission properties of the tip do not vary at liquid nitrogen temperature provided one ensures that the tip does not slip under mechanical contraction in the cooling down process. A typical I-V characteristic curve of field emission current measured in our setup is shown in Fig. 6.9.

Penning Trap electrodes

Two sets of Penning trap electrodes with dimesions and electrostatic properties mentioned in Table 6.2 and Macor spacers were fabricated. One set was fabricated at VECC workshop and another one at MPIK, Germany with an average tolerance of 20 microns. Precision measurements of the fabricated electrodes had been done using Coordinate Measuring Machine (CMM) and a set of five electrodes was chosen based on our simulation studies to minimize the anharmonic coefficients of the quadrupolar electrostatic potential created by the trap electrodes.

Fig. 6.10: *Fabricated trap electrodes and Macor spacers on the left and Penning Trap assembly with laser welded pins for electrical connections on the right.*

Our simulation studies using SIMION8 show that the assembled electrodes should produce a nearly perfect orthogonally compensated quadupolar potential over a 2 mm region around the center of the trap. Inside the chamber, the Penning trap has been placed in such a manner so that the trap centre coincides with the centre of the solenoid where the magnetic field strength would be maximum and most homogeneous. To provide electrical connections, OFHC copper pins were laser welded to the Penning trap electrodes using a Nd:YAG laser beams of diameter 2 mm at RRCAT, Indore.

Faraday Cup

The Faraday cup electrode is made of OFHC copper and is used to monitor the current flowing through the trap. The special V shaped design prevents the secondary electrons produced in the process of collision to escape from the cup. A OFHC copper electrode (C2) with a hole of diameter 2 mm is placed in front of the Faraday cup. This electrode along with the acceleration electrode (C1) would help to align the trap axis with the magnetic field.

The UHV chamber has been placed in position from the top of the magnet with three G10 rods as shown in Fig. 6.11. Six radiation baffles are held on to the G10 rods by a special arrangement in order to reduce the radiation heat load. Special bellows have been provided to the flange sitting on the top of the magnet for placing the trap electrode assembly at a proper position within 1cm DSV inside the magnet bore. By monitoring the current in the C1, C2 electrodes and Faraday Cup, it would be possible to align the trap axis precisely with the magnetic field by adjusting this special bellows. The entire assembly has been thermal cycled several times from room temperature to 77 K but it never showed any sign of mechanical abrasion.

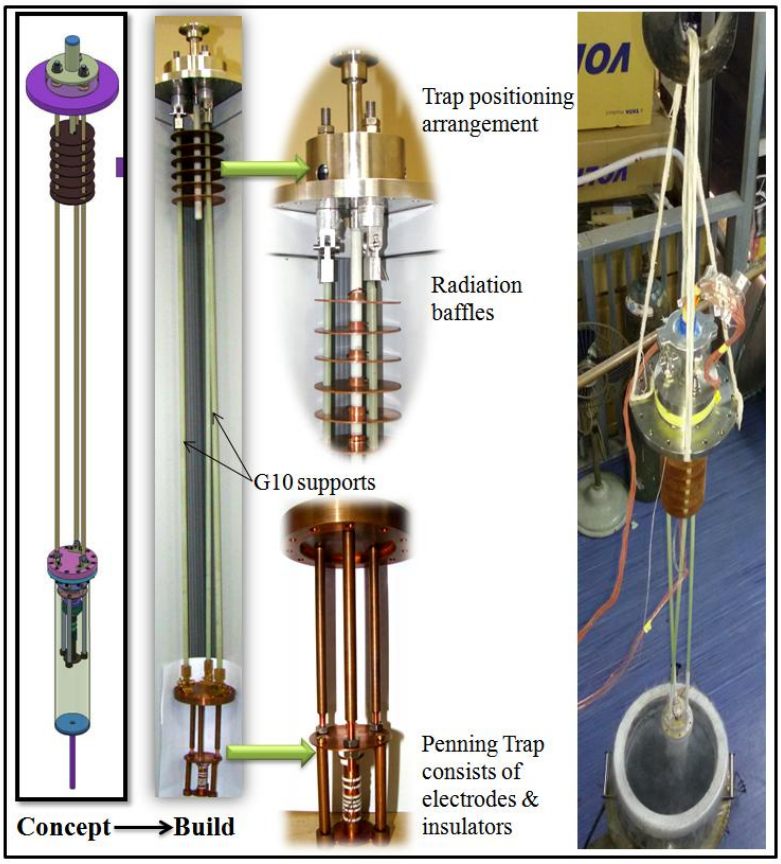

Fig. 6.11: *Conceptual and fabricated design of mechanical assembly of Penning Trap. The testing of mechanical assembly at liquid nitrogen temperature is shown in the right side.*

6.3.3 Cryogenic vacuum feedthrough

A special cryogenic, non-magnetic, multi-pin, vacuum feedthrough is required for applying voltages to Penning trap electrodes that would be placed on the top flange of an ultra high vacuum (UHV) chamber. The feedthrough system must be made of non-magnetic materials so that the high level of spatial uniformity of the magnetic field is not compromised in any way. The development and installation of such special feedthroughs has always been a challenge. We

have developed such a cryogenic feedthrough system (19 pin feedthrough) and tested it successfully down to 4 K. The pins were made of copper wires of diameter 1 mm. An aluminum flange and Stycast 2850 Ft (blue) were used as sealant. Many designs of the flanges and placements of the copper wires were tried. Finally, an optimum design using a wedged-shaped cylindrical aluminum flange filled with Stycast 2850 (blue) was developed [Bas08] and it remained leak-tight down to 4 K under many thermal cycling from room temperature to liquid nitrogen temperature.

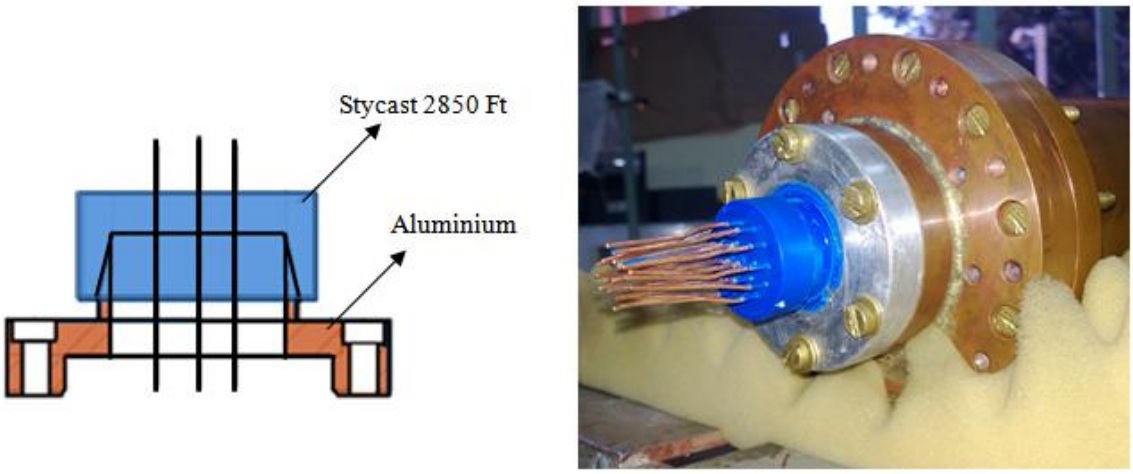

Fig. 6.12: *Conceptual design and fabricated 19 pin, cryogenic, vacuum feedthrough.*

We have also fabricated coaxial feedthrough line with characteristic impedance of 50 Ω and 75 Ω. The characteristics impedance of a coaxial line is given by

$$ohm = \frac{138}{\sqrt{\varepsilon_r}} \log_{10}\left(\frac{D}{d}\right) \tag{6.28}$$

where ε_r is the relative dielectric constant (5.36 for *Stycast 2850 Ft Blue*), *D* is the outer diameter of the wire mesh and *d* is the diameter of the central wire. This coaxial feedthrough line

would help to reduce unwanted noise pickup and prevent mixing of large amplitude excitation signal with the weak signal of the trapped particles.

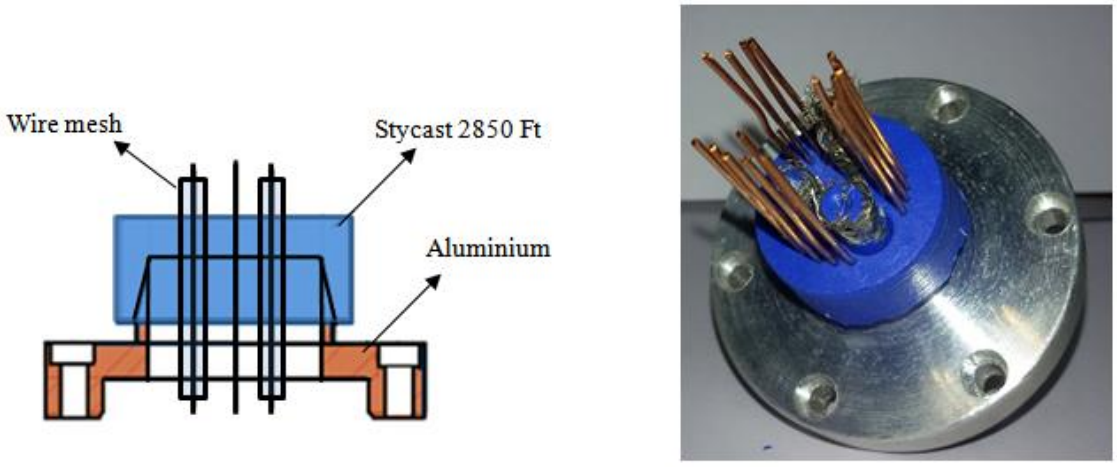

Fig. 6.13: *Conceptual design and fabricated muti-pin cryogenic, coaxial, vacuum feedthrough with one 50 Ω line and two 75Ω line.*

6.3.4 Detection electronics

The initial commissioning of the Penning trap setup would be performed by trapping a cloud of electrons. The image charge induced by these trapped electrons on the electrode wall would be picked up for detection. This non-destructive signal detection system consists of two important parts: [Deh68] a resonance tank circuit (parallel LCR circuit) for selecting out the signal of required frequency and an ultra low-noise cryogenic solid state amplifier that amplifies the voltage drop across the tank circuit so that it could be transported outside the vacuum chamber for further analysis. The final amplified signal contains all the information regarding the motion of the trapped particles. Fig. 6.14 shows a simplified equivalent circuit diagram of the detection system:

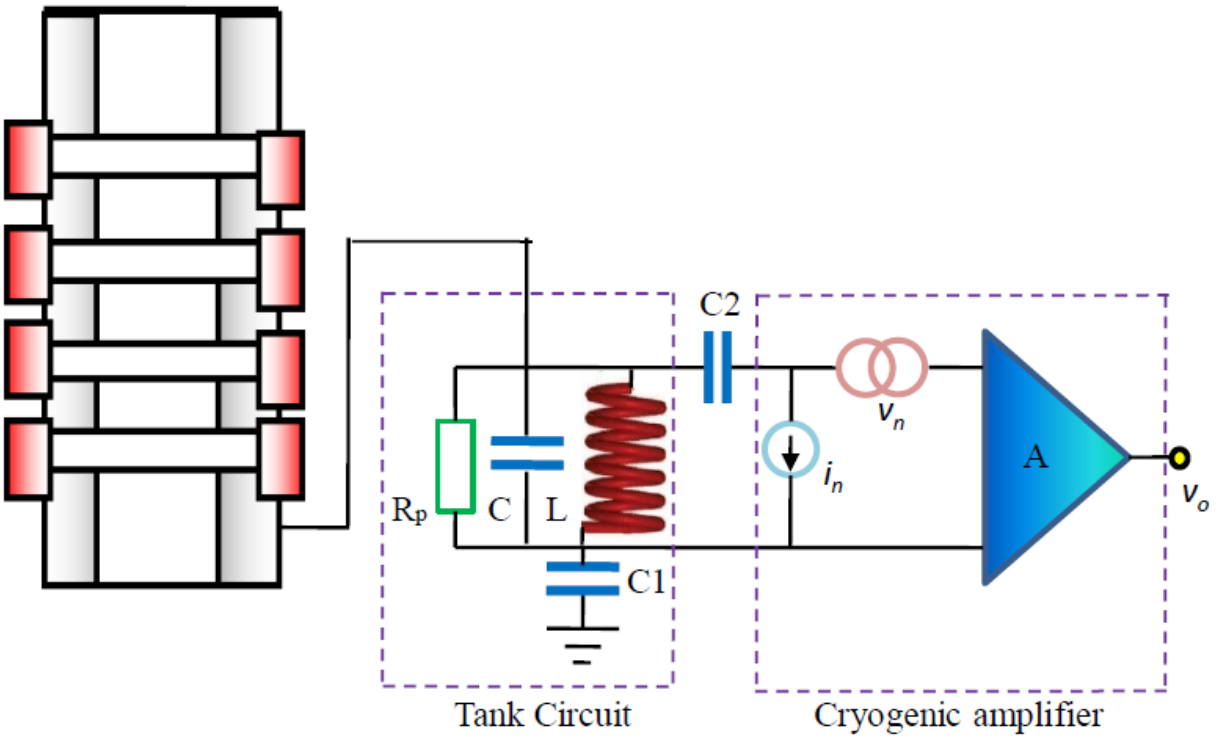

Fig. 6.14: *Equivalent circuit diagram of the detection system where C is the equivalent capacitance of trap, connecting wire and amplifier, L is the inductance, R_p is the effective parallel resistance. C_1 = 100 nF is used for ac grounding and C_2 = 4.7 pF is used as coupling capacitor. The amplifier can be modeled in first approximation as ideal amplifier with input voltage noise density v_n and current noise density i_n.*

Since the tiny induced current need to be transformed to a measurable voltage signal for detection, a large impedance is required at the resonance frequency of the electrons. A large resistance connected at the output is of little help as the impedance at this frequency (~ MHz) is dominated by the parasitic capacitances of the trap electrodes and connecting wires. However,

this could be achieved by connecting an inductor which compensates the parasitic capacitance and provides a large impedance at the resonance frequency. The inductor with inductance L along with the overall capacitance C which includes the capacitance of the trap electrodes, connecting wires and the other parasitic capacitances forms a parallel resonance circuit or tank circuit. For a tank circuit, the resonance frequency (ν_R) is given as

$$\nu_R = \frac{1}{2\pi\sqrt{LC}} \tag{6.29}$$

Table 6.5: *Design parameters of helical resonator* [Rez15].

Outer shield diameter	50 mm
Helix diameter	27.52 mm
Helix length	41.28 mm
Outer shield height	66.3 mm
Number of turns	6
Helix wire diameter	3 mm
Thickness of Teflon core	2.5 mm
Unloaded Q factor	1231 @ 155.11 MHz

Ideally, a tank circuit offers infinite parallel impedance at the resonance frequency. But, in reality, due to ohmic losses in the conductors and dielectric losses in the isolation of the conductors and surrounding material, one obtains a finite value of parallel resistance (R_p). The parallel resistance of a tank circuit with quality factor Q is given as

$$R_p = 2\pi\nu_R QL \tag{6.30}$$

where Q is defined as

$$Q = \frac{\nu_R}{\nu_2 - \nu_1} \tag{6.31}$$

where ν_1 and ν_2 are the frequencies where the power is decreased by 3 dB from its maximum value at ν_R.

The high Q tank circuit has been realized by a helical resonator which consists of thick copper coil wound over PTFE (Teflon) base placed inside closed copper cylinder acting as a High Frequency (HF) shield as shown in Fig. 6.15 (a). It has been designed following the work of Macalpine λ/4 resonator design [Mac59]. The design parameters and performance report of the tank circuit is listed in Table 6.5. With the resonator coupled to the amplifier and end-cap electrodes of Penning trap, a loaded Q factor ~ 115 is obtained at the resonant frequency of 60.97 MHz.

The second important element of the detection system is the low noise cryogenic amplifier. To reduce the capacitive load on the tank circuit due to the connecting wires, it is very important to place the amplifier very close to trap electrode inside the vacuum chamber. This imposes severe restrictions on the design of the cryogenic amplifier that it should be capable of working at liquid helium temperature and made of non-magnetic and vacuum compatible elements. In comparison with other semiconductors which suffer from carrier freeze-out at 4 K [Cam98], Gallium

Arsenide (GaAs) under doping with group III / V elements can generate carrier states with activation energy as low as 6 meV [Stu11] and hence, it can operate at 4K temperature.

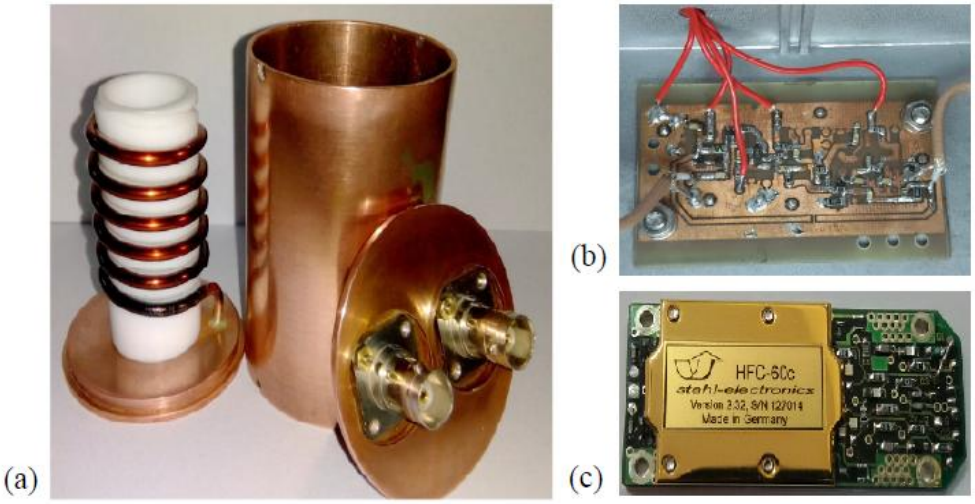

Fig. 6.15: *(a) Photograph of helical resonator built at VECC, (b) Photograph of cryogenic low noise amplifier developed at VECC and (c) Photograph of commercial, cryogenic low noise amplifier from Stahl Electronics.*

Thus, the broadband low-noise amplifier design has been implemented, incorporating high impedance input stages with GaAs (gallium-arsenide) field effect transistors and a subsequent buffer output stage has been used for impedance matching with a 75 Ω transmission line. Since the image current represents a high impedance signal source, a field effect transistor input stage with a low capacitance, low voltage noise density and low current noise density at the axial frequency of the trapped electrons is required. These criteria have been achieved by the commercially available amplifier HFC-60 C from Stahl Electronics shown in Fig. 6.15 (c). Our group is also involved in the indigenous development of such an amplifier whose performance is

comparable with the commercial one and its photograph is shown in Fig. 6.15 (b). The description and performance of our indigenously developed amplifier are given in [Rez16]. The main characteristics of HFC-60 C from Stahl Electronics that has been used for commissioning trials are listed in Table 6.6.

Table 6.6: *The main characteristics of each channel of dual channel HFC-60 amplifier from Stahl Electronics.*

Sl. No.	Specifications	
1	Frequency Range (-3 dB)	160 kHz to 65 MHz
2	Input voltage noise density (v_n)	typ. 0.8 nV/$\sqrt{Hz}$ @ 5 MHz at 4K
3	Input current noise density(i_n)	typ. 30 fA/$\sqrt{Hz}$ @ 1 MHz at 4K
4	Voltage amplification (w/o termination)	typ. x 19.3 @ 1 MHz at 4K
5	Power consumption	typ. 13 mW @ 4K
6	Input Impedance	10 MΩ // 5.1 pF
7	Output Impedance	75Ω

6.3.5 Initial commissioning in low magnetic field and at liquid nitrogen temperature

The Penning trap has been tested with electrons generated from a field emission (FEP tip) source at liquid nitrogen temperature using a low magnetic field (~0.2 T). The trap has been installed inside a four way cross hanging from the top flange and evacuated using a turbo molecular pump

and an ion pump. To keep the conductance maximum, both the pumps were coupled directly to the four way cross. The pressure inside the setup is measured using a combo gauge comprising of a Pirani gauge and a Penning gauge. A schematic picture of the trap setup is shown in Fig. 6.16.

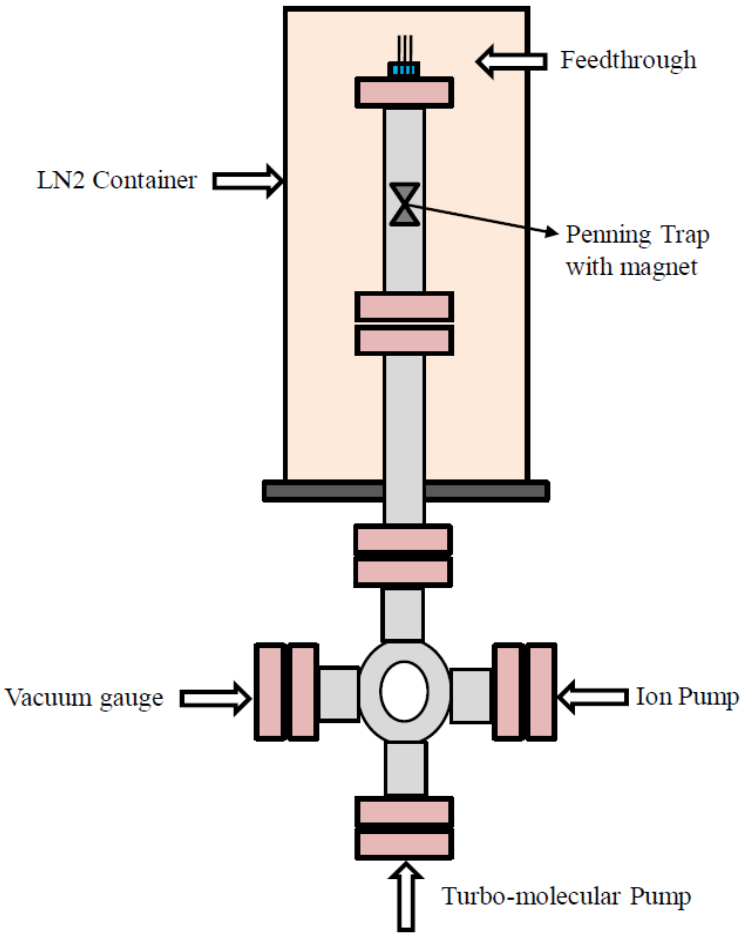

Fig. 6.16: *Schematic drawing of the vacuum setup.*

Initially, the turbo molecular pump is made to run till the pressure inside the chamber drops to $1x10^{-6}$ mbar and then the ion pump is switched on. Both the pumps together could create a vacuum of the order 10^{-7} mbar after being run continuously for two days. As our home-made

cryogenic feedthrough cannot be baked, we use liquid nitrogen to attain ultra high vacuum. At background pressure of 10^{-7} mbar, water vapour give the highest partial vapour pressure and thus on liquid nitrogen cooling, water molecules get adsorbed on the walls of the chamber and hence, we could attain vacuum of the order of $5x10^{-9}$ mbar or better.

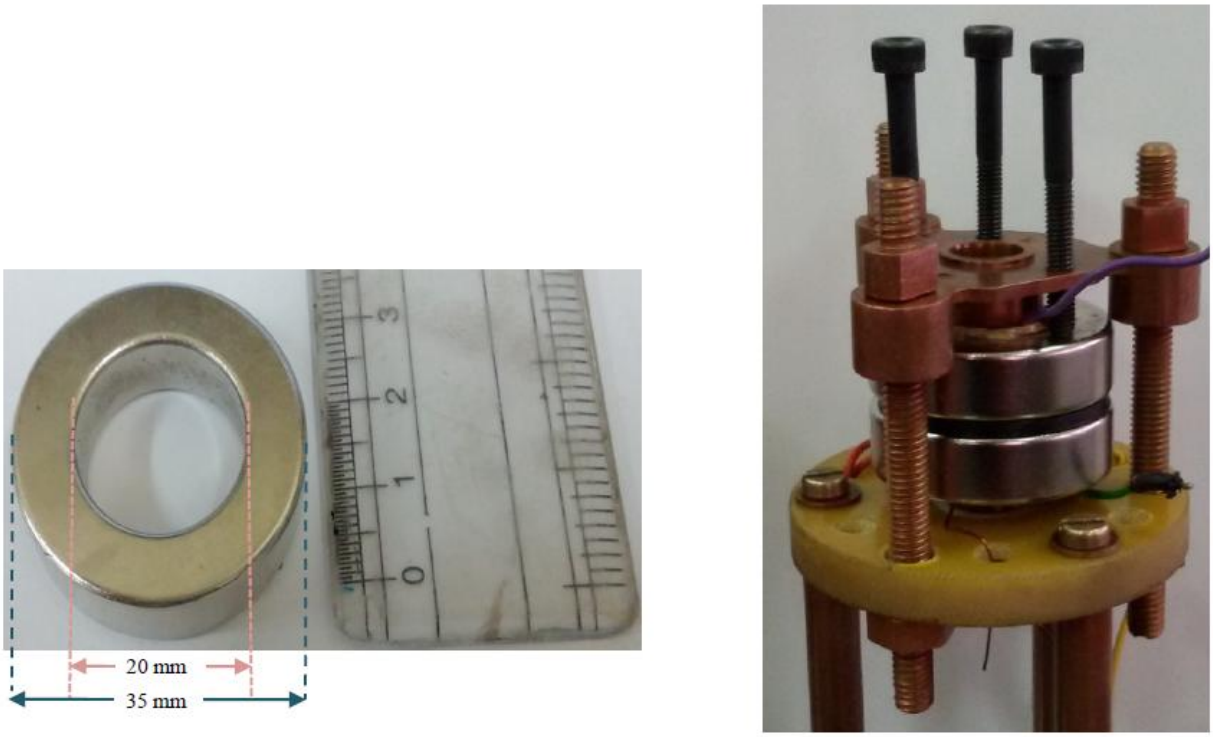

Fig. 6.17: *(Left side) Annular NdFeB (Grade 52) permanent magnet used in experiment & (right side) The Penning trap setup with two annular magnet separated by plastic spacer.*

Since our liquid helium cooled superconducting magnet is not immediately available because of non-availablity of liquid helium at this time, a low magnet field is generated using small annular permanent magnets. We have used two NdFeB (Grade N52) annular magnets whose inner diameters are 20 mm, outer diameters are 35 mm and thickness are 10 mm as shown in the left side of Fig. 6.17. The two magnets were kept separated by a distance of 2 mm with plastic spacer

as shown in the right of Fig. 6.17. The small size of the magnet allows a compact design of Penning trap. The position of the magnet with respect to Penning trap electrodes could be adjusted with three mild steel screws as shown in Fig. 6.17. The region of homogenous magnetic field was midway between the two annular magnets and the screw position was so adjusted that the magnet centre matched with the trap centre. The measured magnetic field at the trap centre was ~ 0.2 T.

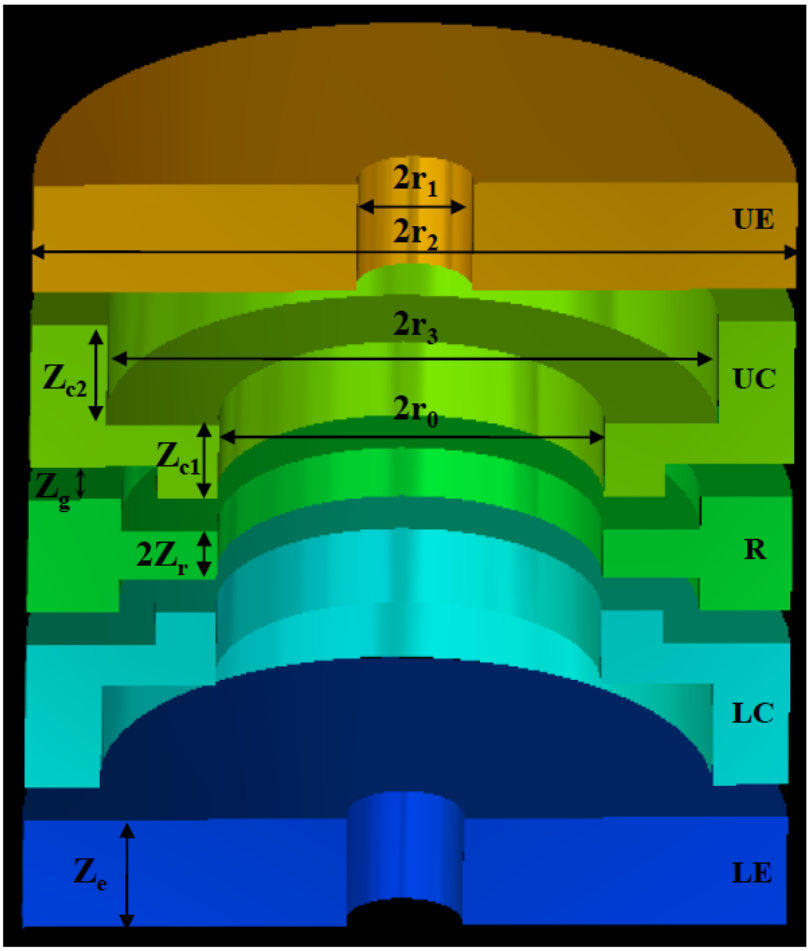

Fig. 6.18: *Closed ended, cylindrical Penning trap with five electrodes with one pair of compensation electrodes where the center of ring electrode is taken as the origin or trap centre. The electrodes are abbreviated as follow, UE: Upper End-cap, UC: Upper compensation R: Ring , LC: Lower Compensation and LE: Lower End-cap.*

Since cylindrical electrodes with closed endcaps offer a larger harmonic region in comparison with the open ended cylindrical geometry, the former arrangement has been used for initial commissioning trials. A larger harmonic region can trap electrons of different energies and make them oscillate with similar frequencies. As a result, the strength of the signal increases. A basic schematic diagram of the Penning trap comprising five cylindrical electrodes with close ended geometry is shown in Fig. 6.18 and the corresponding dimensions are listed in Table 6.7. The adjacent electrodes are kept separated by the cylindrical Macor spacers of thickness 0.6 mm.

Table 6.7: *Dimensions of flat ended, five cylindrical Penning trap electrodes where each parameters has been marked in Fig. 6.18.*

Dimension (mm)			
r_0	3.29	Z_{c1}	1.38
r_1	1.00	Z_{c2}	1.89
r_2	6.50	Z_e	2.00
r_3	5.20	Z_g	0.60
Z_r	0.46		

The schematic diagram of the electronic circuit used for detection has been shown in Fig. 6.19. All the electrodes were AC grounded through 100 nF capacitors and 1 MΩ resistors. Both the compensation electrodes and the ring electrodes were connected together to the signal generator which provided the required ramp voltage ($U_{C\text{-}R}$). The lower end-cap of the trap was connected to the upper end cap with a 1 MΩ resistor which ensured that both the end-cap electrodes would receive the same DC voltage (U_E) but keep the lower end-cap electrode AC floated, thus

allowing pickup of the detection signal. Another line from the lower end-cap was connected directly to the tank circuit and then to the amplifier through a 4.7 pF coupling capacitor. The tank circuit was AC grounded with a 100 nF capacitor isolating the end-cap electrodes from ground. As the lower end cap of our trap was connected to an inductance L, it formed a tank circuit together with the trap electrodes and the connecting wire acting as a capacitance. The third line from the lower end-cap was air coupled to a different signal generator that weakly excited the tank circuit at its resonance frequency [Sat10].

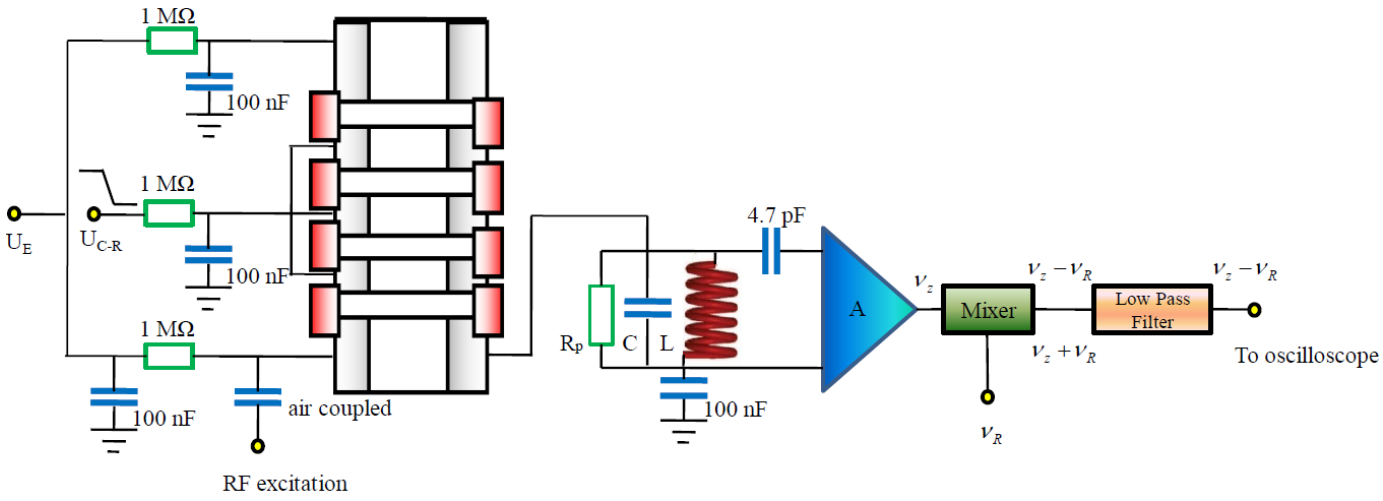

Fig. 6.19: *Electronic Circuit diagram*

The electrons were generated inside the trap by applying high voltage (~2 KV) to the FEP tip and the emitted electrons typically have energies ~ 2 keV. Theses high energy electrons collided with the residual gas inside the trap to produce low energy secondary electrons that could be trapped in the trapping potential.

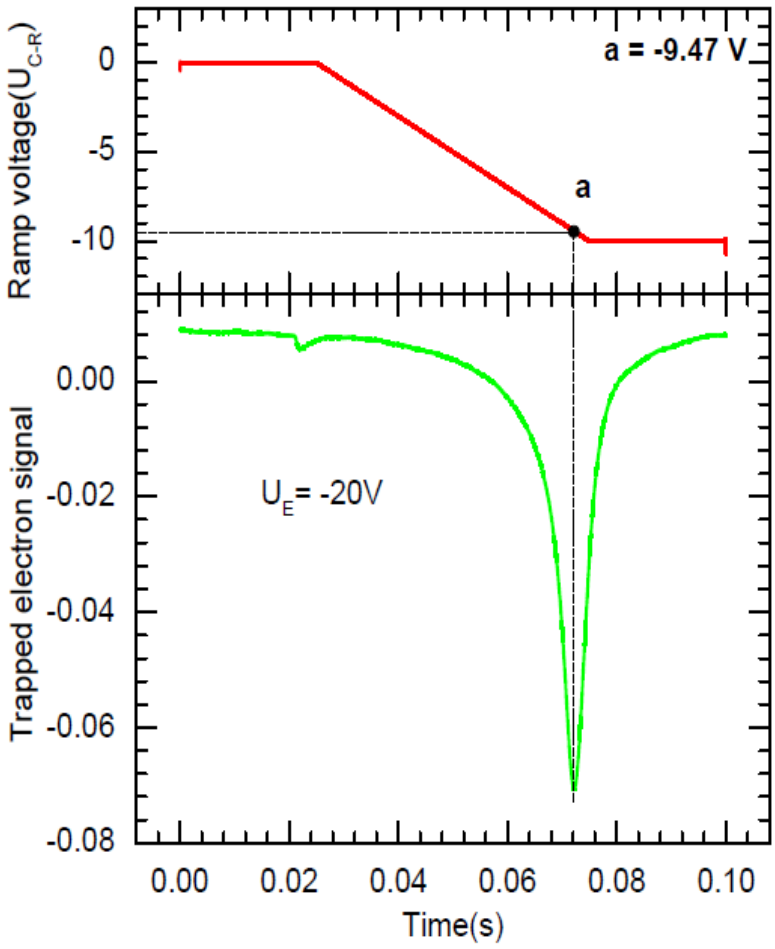

Fig. 6.20: *Representative dip signal for trapped cloud of electrons in 7x10^{-9} mbar at 100 K is shown in the lower panel and the upper panel shows the corresponding ramp voltage applied to the ring and compensation electrodes for a fixed voltage applied to end-cap electrodes(U_E= -20 V).*

The trapping potential was created by applying voltage to the ring and the compensation electrodes (U_{C-R}) and the applied voltage was varied from 0 to -10 V at a ramp frequency of 100 Hz. A fixed DC voltage (U_E) was applied to the end-cap electrodes. The trapped electrons saw the potential difference given by

$$U_{dc} = U_E - U_{C-R} \qquad (6.32)$$

As the trapping voltage U_{dc} between ring and endcap was varied, the axial electron frequency varied according to eqn. 6.1. As the applied voltage matched with the resonance frequency of the tank circuit, the trapped electrons absorbed maximum energy from the RF signal which was applied to the tank circuit and the lower end-cap at the resonance frequency of the tank circuit. Consequently, a resonant damping in the response of the tank circuit was observed. The signal from the tank circuit was sent through a low noise amplifier and mixed with resonance frequency (ν_R) signal and then passed through a low pass filter as shown in Fig. 6.19. This produced a signal whose strength was proportional to the number of the trapped electrons. The resulting beat frequency spectrum showed prominent dips and a sample of such a dip is shown in the lower panel of Fig. 6.20 and the corresponding variation of ramp voltage (U_{dc}) versus time is shown in the upper panel. The signal was produced by a cloud of trapped electrons at $7x10^{-9}$ mbar pressure and at 100 K. The voltage (U_E) applied to end-cap electrodes was -20 V. The tank circuit was excited at its resonance frequency with RF drive power of -30 dBm. It was observed that the magnitude of the dip signal along with position of the ramp voltage where the dip occurred, varied from time to time in the experiment. This variation could be because of the variation in space-charge effect produced by different numbers of trapped electrons in different cycles. It has been observed that the ramp voltage position where the dip signal occurred, shifted with the change in the applied voltage to the end-cap electrodes. Moreover, as the RF excitation power applied to lower end-cap was varied for a fixed end-cap voltage, the magnitude of the absorption signal changed accordingly. In Fig. 6.21, we show the variation of the magnitude of dip signal for different RF drive power in the range of -15 dBm to -60 dBm. We also show the observation of dip signal when no RF drive was applied to the end-cap electrodes.

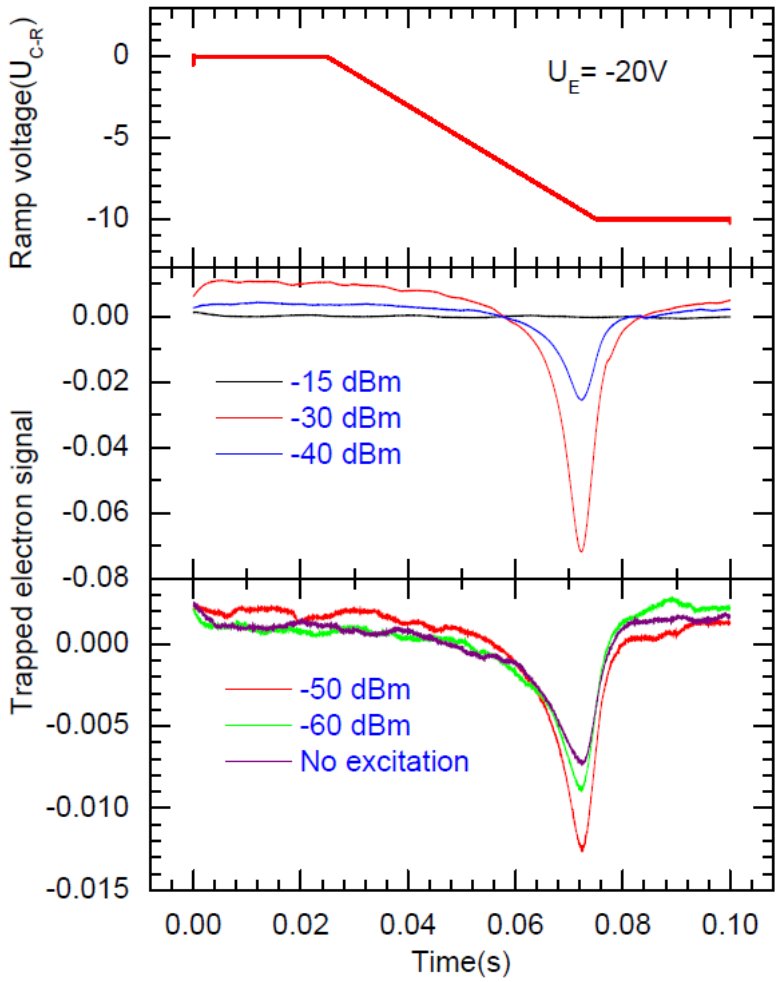

Fig. 6.21: *Variation of dip signal with different RF excitation for fixed end-cap voltage (U_E=-20 V). The top panel shows the corresponding ramp voltage applied to the ring and compensation electrodes.*

It is clear from Fig. 6.21 that the magnitude of dip signal increased with the increase in RF power drive from -60 dBm to -30 dBm, because the trapped electrons oscillated more coherently and absorbed more power with increase in applied RF power. When large power (-15 dBm) was applied, the electrons escaped from the trapping well leading to the disappearance of dip signal at

high power drive. One of the interesting observations is the occurrence of dip signal when no RF drive was applied. This is the attributed to the excellent performance of our low noise amplifier which could pick up tiny signal of trapped cloud of electrons which are oscillating coherently inside the trap without any RF excitation. This observation could also be termed as a different way to observe noise dip signal and it is a unique observation in its own sense.

Thus, in conclusion, a multitude of operational tests have been performed for the realization of Cryogenic Penning trap at VECC. It includes commissioning of superconducting magnet, design and fabrication of Penning trap electrodes, fabrication and testing at 77 K of entire mechanical assembly, indigenous development of cryogenic coaxial vacuum feedthrough and its successful testing at 77 K, development of detection electronics capable of working at cryogenic temperature and finally the initial commissioning of the Penning trap setup at a low magnetic field and liquid nitrogen temperature. In future, this setup would be commissioned by putting it in the liquid helium filled bore of our superconducting magnet. However, due to the non-availability of liquid helium, it could not be performed under this thesis work. However, we have obtained the first signal of trapped electrons in flat ended cylindrical Penning trap where the electrons had been generated from a field emission tip held in a low magnetic field and liquid nitrogen temperature.

Chapter 7

Conclusion and future work

7.1 Summary

In this thesis work, we have measured fission time for the first time from the intrinsic width of K x-ray lines of the ion containing the fissioning nucleus. The intrinsic width of the K x-ray line is directly related to the fission time of the fissioning nucleus by the quantum mechanical energy-time uncertainty principle [Anh85] and so the method does not require any other input parameter. The experimental challenge was to see the narrow K x-ray line of plutonium produced in the $^{4}He+^{238}U$ fusion reaction. In our experiment, highly excited plutonium nucleus ($E_X \approx 55$ MeV) has been formed by the bombardment of a 60 MeV ^{4}He on ^{238}U by the complete fusion reaction. Incomplete fusion process and the electronic configuration mixing should be negligible for this reaction. Hence, one expects to see sharp $K_{\alpha 1}$ and $K_{\alpha 2}$ lines of plutonium atom containing the fissioning plutonium nucleus in coincidence with the fission fragments, if the fission time of highly excited plutonium nucleus is comparable to the lifetime of atomic K vacancy of plutonium (6×10^{-18} sec). In earlier experiments [Fre12, Mol93, Wil04] involving heavy ion collisions, incomplete fusion and large electronic configuration mixing were expected resulting in large widths of the K x-ray lines of the fused element. Hence, it was not possible to extract any information of the fission time from the width of the K x-ray lines and they determined fission time from the K x-ray fluorescence yield and the probability of creation of K orbital vacancies. Of course, heavy ion collisions have a high probability of producing vacancies in the K orbital of the target atom that are converted to the K orbital vacancies of the fused

element, thus making it easier to see the K x-ray lines of the fused element. In the case of heavy ion collisions, it is generally sufficient to consider the probability of formation of K orbital vacancies in the target atom by the direct ionization process and the shake-off ionization of the element produced by the fusion process is comparatively small. In $^{4}He+^{238}U$ fusion reaction, the probability of producing K orbital vacancies in the target atom by ^{4}He is very small and the shake-off ionization of plutonium ion due to the fusion process becomes significant compared to the direct ionization produced by ^{4}He in ^{238}U, thus somewhat increasing the total probability of creating K orbital vacancies in plutonium. We estimated the contribution of this shake-off ionization process to determine the percentage of long fission time component, but no such estimation is required to obtain the fission time from the intrinsic width of the K x-ray lines. We have found that most of the fission events for the highly excited plutonium nuclei are slow with a mean fission time > 1×10^{-18} sec, in agreement with the long fission time seen earlier in uraniumlike and transuranium nuclei by atomic techniques. The long survival time of the plutonium atom containing the highly excited nucleus appears to be inconsistent with the short fission delays obtained from the nuclear experiments and calculations.

To probe this inconsistency problem further, we have investigated [Sik16] the fission timescale of highly excited Z=120 nucleus where a lot of measurements by atomic and nuclear techniques are available in the literature. In the analysis, we have found that the long fission lifetime (~10^{-18} sec) measured by atomic techniques cannot be reconciled with the short fission lifetime (~10^{-20} sec) measured by nuclear techniques using the standard sensitivity argument of different techniques in different time domains. These interesting results found for the superheavy Z=120 nuclei holds true for many different fissioning and/or quasifissioning nuclei far away from the

island of the predicted superheavy nuclei [Sik16]. So, this fission time measurement anomaly appears to be a general problem and cannot be understood by fission dynamics.

We have discussed a probable solution of the fission time anomaly using a quantum decoherence model [Ray15]. According to this quantum decoherence model, in early time decay should be non-exponential and much slower [Fon78, Hom97]. The classical exponential decay would start when the decay could be defined due to the interaction with the environment resulting in complete loss of quantum coherence between the initial undecayed state and decayed state. Nuclear techniques relying on the measurement of nuclear decay products to obtain fission time cannot probe the non-exponential decay time due to the insignificant emission of fission observables in such early time. So, nuclear techniques essentially measure the exponential decay time of the fission process and measure short fission time ~10^{-20} sec for all fission events. On the other hand, the atomic techniques measure the survival time of the ion containing the fissioning nucleus and thus effectively measure the sum of non-exponential and exponential decay times. Using our decoherence model [Ray15], we have estimated the quantum decoherence time of the fission process which is the time taken by the fission fragments to cross over the radius of the compound ion when the parent atomic structure gets completely destroyed to generate orthogonal pointer states needed for monitoring the decay and it is on the order of 10^{-18} sec. Since the decay could be defined only after the interaction of the fissioning system with the environment, the atomic techniques measure fission time ~10^{-18} sec for most of the detected events. In this model, fission could not occur as long as the atom containing the fission nucleus could emit characteristic photons corresponding the compound element and the atom is surviving for that long. So in this model, atomic techniques could measure a longer fission time for almost

all recorded events for which the nuclear techniques would measure short fission time and provide a probable explanation of the fission time measurement anomaly.

The high precision mass measurement of very heavy nuclei by Penning trap would provide significantly more information on this important topic. In this context, we have discussed the developmental work related to a Cryogenic Penning Trap facility at Variable Energy Cyclotron Centre, Kolkata, India. The development of a cryogenic Penning trap facility is a technically challenging project and a lot of progress has been made in this area as a part of this thesis work. The system has been designed, fabricated, assembled and tested at 77 K. High precision Penning trap electrodes were fabricated at VECC workshop. Cryogenic coaxial vacuum feedthroughs, cryo-electronics (tank circuit and low noise cryogenic amplifier) as well as the entire mechanical holding assembly that would be required to place the setup inside the bore of superconducting magnet have been fabricated. The superconducting magnet has been commissioned. An improved design of seven electrodes cylindrical Penning trap has been obtained which could generate better quadrupolar electric potential at the trap centre with higher degree of harmonicity [Sik13]. Since liquid helium was not available for further testing, the Penning trap setup has been tested at a low magnetic field and at liquid nitrogen temperature.

7.2 Future perspective

The measurement of fission time from the intrinsic width of K x-ray lines of the ion containing a fissioning nucleus at a high excitation energy opens up a new way of looking at the characteristics of a fissioning nucleus. We propose a few probable experiments that could further test the fission time anomaly and the application of quantum decoherence model to the nuclear systems.

1) New fission time data of highly excited fissile nuclei produced by the bombardment of high energy proton/alpha on ^{232}Th or ^{252}Cf target could be obtained from the intrinsic width of K x-ray lines of the fused element in fission fragment K x-ray coincidence experiments. The experiments should be done with high energy $^{4}He^{2+}$ or proton beams to produce compound nucleus with a very high excitation energy (up to 250 MeV) and observe narrow characteristic K x-ray lines, if the fission time is on the order of 10^{-18} sec. Such experiments would provide data regarding the variation of the survival time of the ion containing the fissioning nucleus with different excitation energies. The experiments could be performed with larger arrays of detectors to obtain better statistical accuracy. Using the crystal blocking technique, Goldenbaum *et al.* [Gol99] obtained the fission times of highly excited uraniumlike nucleus (Z=92±5) as a function of excitation energy. They could probe fission time upto 3×10^{-19} sec and obtained that fission gradually becomes faster with the increasing excitation energy. Since the intrinsic width of the characteristic K x-ray of the compound element is a direct measure of the fission time [Anh85] and alpha induced reaction would produce a unique compound nucleus, it would be interesting to study the evolution of peak shape of the characteristic K x-ray of uranium atom with the excitation energy.

2) The quantum decoherence model should be applicable to all types of radioactive decays. In the case of α or β decays, the dramatic change of the valence orbitals of the parent could be considered as orthogonal pointer states [Fon78, Zur03] and the decoherence time could be on the order of 10^{-16} sec [Ray16]. Pre-scission alpha multiplicity measurement [Les91] for fusion of ^{164,167,170}Er with ^{28}Si (E_X>20 MeV) gives fission timescale ~ 6 x 10^{-20} sec. This suggest that the emitted alpha particles from the compound nucleus have lifetime ~ 10^{-20} sec. So, if one performs alpha particle x-ray coincidence measurement and could obtain characteristic K x-ray of compound element (Pb), then this would indicate long lifetime of the compound element supporting our conjecture. For the beta decay processes, considering repeated measurement of the nuclear charge by the orbiting valence electron inhibiting the time evolution of the decaying nuclear state, Fonda *et al.* [Fon78] obtained that the measured nuclear lifetime would be slightly longer (~1%) than the theoretical lifetime. Since the theoretical lifetime is generally not known very accurately, it is difficult to do this comparison. However, if the atom containing the beta unstable nucleus is subjected to a high pressure, it would take longer time to distinguish between outer orbital valence states of parent and daughter atom resulting in shorter nuclear lifetime under compression. So, applying high pressure (~100 GPa) on the atom containing the beta unstable nucleus, one might study the effect of quantum decoherence time on the beta decay process [Ray16].

Bibliography

[Ahm83] I. Ahmad, J. Hines, and J. E. Gindler, "*Electron capture decay of ^{237}Pu, ^{235}Np, and ^{236}Np*", Phys. Rev. C 27 (1983) 2239.

[Aji91] N. N. Ajitanand, R. P. Anand, S. R. S. Murthy and K. N. Iyengar, "*The photovoltaic cell - an eminent fission fragment detector*", Nuclear Instruments and Methods in Physics Research A 300 (1991) 354.

[And08] J. U. Andersen, J. Chevallier, J. S. Forster, S. A. Karamian, C. R. Vane, J. R. Beene, A. Galindo-Uribarri, J. Gomez del Campo, C. J. Gross, H. F. Krause, E. Padilla-Rodal, D. Radford, D. Shapira, C. Broude, F. Malaguti and A. Uguzzoni, "*Attosecond time delays in heavy-ion induced fission measured by crystal blocking*", Phys. Rev C 78 (2008) 064609.

[Anh85] R. Anholt, "*X rays from quasimolecules*", Rev. Mod. Phys. 57 (1985) 995.

[Art05] A. N. Artemyev, V. M. Shabaev, V. A. Yerokhin, G. Plunien, and G. Soff, "*QED calculation of the n=1 and n=2 energy levels in He-like ions*", Phys. Rev. A 71 (2005) 062104.

[Bar02] F. Barrué, S. Basnary, A. Chbihi, M. Chevallier, C. Cohen, D. Dauvergne, H. Ellmer, J. Frankland, D. Jacquet, R. Kirsch, P. Lautesse, A. L'Hoir, M. Morjean, J.-C. Poizat, C. Ray and M. Toulemonde, "*Nuclear fission time measurements as a function of excitation energy: A crystal blocking experiment*", Nuclear Instruments and Methods in Physics Research B 193 (2002) 852.

[Bas08] C. D. Bass, "*A demountable nonmagnetic multiconductor feedthrough suitable for use in liquid helium applications*", Rev. Sci. Instrum. 79 (2008) 055101.

[Ben90] M. Bender, K. Rutz, P. G. Reinhard, J. A. Maruhn, and W. Greiner, "*Shell structure of superheavy nuclei in self-consistent mean-field models*", Phys. Rev. C 60 (1990) 034304.

[Ber08] J. Bernu, S. Deléglise, C. Sayrin, S. Kuhr, I. Dotsenko, M. Brune, J. M. Raimond, and S. Haroche, "*Freezing Coherent Field Growth in a Cavity by the Quantum Zeno Effect*", Phys. Rev. Lett. 101 (2008) 180402.

[Bla06] K. Blaum, "*High-accuracy mass spectrometry with stored ions*", Phys. Rep. 425 (2006) 1.

[Blo10] M. Block, D. Ackermann, K. Blaum, C. Droese, M. Dworschak, S. Eliseev, T. Fleckenstein, E. Haettner, F. Herfurth, F. P. Heßberger, S. Hofmann, J. Ketelaer, J. Ketter, H. J. Kluge, G. Marx, M. Mazzocco, Yu. N. Novikov, W. R. Plaß, A. Popeko, S. Rahaman, D. Rodrı´guez, C. Scheidenberger, L. Schweikhard, P. G. Thirolf, G. K. Vorobyev and C. Weber, "*Direct mass measurements above uranium bridge the gap to the island of stability*", Nature 463 (2010) 785.

[Bol03] J. J. Bollinger, J. M. Kriesel, T. B. Mitchell, L. B. King, M. J. Jensen, W. M. Itano and D. H. E. Dubin, "*Laser-cooled ion plasmas in Penning traps*", J. Phys. B 36 (2003) 499.

[Bro82] L. Brown and G. Gabrielse, "*Precision spectroscopy of a charged particle in an imperfect Penning Trap*", Phys. Rev. A 25 (1982) 2423.

[Bro86] L. Brown and G. Gabrielse, "*Geonium theory: Physics of a single electron or ion in a Penning Trap*", Rev. Mod. Phys. 58 (1986) 233.

[Bru86] R. Brun et al., GEANT3, CERN/DD/EE/84-1, (1986).

[Bul16] Aurel Bulgac, Piotr Magierski, Kenneth J. Roche and Ionel Stetcu, "*Induced Fission of ^{240}Pu within a Real-Time Microscopic Framework*", Phys. Rev. Lett. 116 (2016) 122504.

[But72] D. K. Butt and A. R. Wilson, "*A study of the radioactive decay law*", J. Phys. A 5 (1972) 1248.

[Cab03] J. Cabrera, Th. Keutgen, Y. El Masri, Ch. Dufauquez, V. Roberfroid, I. Tilquin, J. Van Mol, R. Régimbart, R. J. Charity, J. B. Natowitz, K. Hagel, R. Wada, and D. J. Hinde, "*Fusion-fission and fusion-evaporation processes in $^{20}Ne+^{159}Tb$ and $^{20}Ne+^{169}Tm$ interactions between E/A=8 and 16 MeV*", Phys. Rev C 68 (2003) 034613.

[Cam98] D. Camin, G. Pessina and E. Previtali, "*Cryogenic Semiconductor Electronics*", Jpn. J. App. Phys. 37 (1998) 2.

[Car94] N. Carjan, O. Serot and D. Strottman, "*Time-Dependent Schrodinger Approach to Sub-Barrier Fission*", Z. Phys. A 349 (1994) 353.

[Chi77] C. B. Chiu, B. Misra and E. C. G. Sudarshan, "*Time Evolution of Unstable Quantum States and a Resolution of Zeno's Paradox*", Phys. Rev. D 16 (1977) 520.

[Dec73] G. Deconninck and N. Longequeue, "*X-Ray Emission Following Nuclear Reactions*", Phys. Rev. Lett. 30 (1973) 863.

[Deh68] H. G. Dehmelt and F. L. Walls, "*Bolometric technique for the rf spectroscopy of stored ions*", Phys. Rev. Lett. 21 (1968) 127.

[Dua02] A. Dicus Duane, W. Repko Wayne, F. Schwitters Roy and M. Tinsley Todd, "*Time development of a quasistationary state*", Phys. Rev. A 65 (2002) 032116.

[Fac98] P. Facchi and S. Pascazio, "*Temporal behavior and quantum Zeno time of an excited state of the hydrogen atom*", Phys. Lett. A 241 (1998) 139.

[Far02] K. A. Farrar, "*Calculation of the electrostatic potential field for an open-endcap cylindrical penning trap*", Nuclear Instruments and Methods in Physics Research A 485 (2002) 780.

[Fei99] Xiang Fei and W.M. Snow, "*Cylindrical Penning traps with dynamic orthogonalized anharmonicity compensation for precision experiments*", Nuclear Instruments and Methods in Physics Research A 425 (1999) 431.

[Fis01] M. C. Fischer, B. Gutiérrez-Medina and M. G. Raizen, "*Observation of the Quantum Zeno and Anti-Zeno Effects in an Unstable System*", Phys. Rev. Lett. 87 (2001) 040402.

[Fon78] L. Fonda, G. C. Ghirardi and A. Rimini, "*Decay theory of unstable quantum systems*", Rep. Prog. Phys. 41 (1978) 587.

[Fra09] G. Franz, "*Low Pressure Plasmas and Microstructuring Technology*", Springer-Verlag Berlin, Heidelberg 2009.

[Fre12] M. O. Frégeau, D. Jacquet, M. Morjean, E. Bonnet, A. Chbihi, J. D. Frankland, M. F. Rivet, L. Tassan-Got, F. Dechery, A. Drouart, L. Nalpas, X. Ledoux, M. Parlog, C. Ciortea, D. Dumitriu, D. Fluerasu, M. Gugiu, F. Gramegna, V. L. Kravchuk, T. Marchi, D. Fabris, A. Corsi and S. Barlini, "*X-Ray Fluorescence from the Element with Atomic Number Z=120*", Phys. Rev. Lett. 108 (2012) 122701.

[Gab09] G. Gabrielse, "*Why is Sideband Mass Spectrometry Possible with Ions in a Penning Trap?* ", Phys. Rev. Lett. 102 (2009) 172501.

[Gab83] G. Gabrielse, "*A Relaxation Calculation of the Electrostatic Properties of Compensated Penning Traps with Hyperbolic Electrodes*", Phys. Rev. A 27 (1983) 2277.

[Gab84] G. Gabrielse and F. Colin MacKintosh, "*Cylindrical Penning Traps with Orthogonalized Anharmonicity Compensation*", Int. J. Mass Spectroscopy and Ion Processes 57 (1984) 1.

[Gab89] G. Gabrielse, X. Fei, L. A. Orozco, S.L. Rolston, R. L. Tjoekler, T. A. Trainor, J. Haas, H. Kalinowsky and W. Kells, "*Barkas Effect With Antiprotons and Protons*", Phys. Rev. A 40 (1989) 481.

[Gab90] G. Gabrielse, X. Fei, L. A. Orozco, R. L. Tjoelker, J. Haas, H. Kalinowsky, T. A. Trainor and W. Kells, "*Thousand-fold Improvement in the Measured Antiproton Mass*", Phys. Rev. Lett. 65 (1990) 1317.

[Ger78] Gerhard Soff, Volker Oberacker and Walter Greiner, "*Inner-Shell Ionization Induced by Nuclear Coulomb Excitation in Collisions of Very Heavy Ions*", Phys. Rev. Lett. 41 (1978) 1167.

[Gol99] F. Goldenbaum, M. Morjean, J. Galin, E. Liénard, B. Lott, Y. Périer, M. Chevallier, D. Dauvergne, R. Kirsch, J. C. Poizat, J. Remillieux, C. Cohen, A. L'Hoir, G. Prévot, D. Schmaus, J. Dural, M. Toulemonde and D. Jacquet, "*Fission Time Evolution with Excitation Energy from a Crystal Blocking Experiment*", Phys. Rev. Lett. 82 (1999) 5012.

[Gon02] I. Gontchar, M. Morjean and S. Basnary, "*Nuclear dissipation from fission time*", Europhys. Lett. 57 (2002) 355.

[Gop84] P. M. Gopych, I. I. Zalyubovskii, V. V. Sotnikov , A. F. Shchus', I. F. Barchuk, V.S. Bulkin, V.I. Golyshkin and A.F. Ogorodnik, "*Study of the exponential nature of the decay law in the case of* ^{116m}*In*" , Yad. Fiz. 39 (1984) 257 [Sov. J. Nucl. Phys. 39 (1984) 159].

[Gri99] David J. Griffiths, "*Introduction to Electrodynamics*", Pearson Education, Inc., New Jersey, USA, 3rd edition, 1999.

[Hin15] D. J. Hinde, E. Williams, R. du Rietz, M. Dasgupta, A. Wakhle, C. Simenel, D. H. Luong and K. J. Cook, "*Mapping quasifission characteristics in heavy element formation reactions*", EPJ web of conferences 86 (2015) 00015.

[Hin92] D. J. Hinde, D. Hilscher, H. Rossner, B. Gebauer, M. Lehmann and M. Wilpert, "*Neutron emission as a probe of fusion-fission and quasifission dynamics*", Phys. Rev. C 45 (1992) 1229.

[Hin96] D. J. Hinde, M. Dasgupta, J. R. Leigh, J. C. Mein, C. R. Morton, J. O. Newton, and H. Timmers, "*Conclusive evidence for the influence of nuclear orientation on quasifission*", Phys. Rev. C 53 (1996) 1290.

[Hof08] S. Hofmann, "*Overview and Perspectives of SHE Research at GSI SHIP*", GSI Scientific Report, 131 (2008).

[Hom97] D. Home, "*Conceptual Foundation of Quantum Physics*" (Plenum, New York, 1997).

[Hub94] J. H. Hubbell, P. N. Trehan, Nirmal Singh, B. Chand, D. Mehta, M. L. Garg, R. R. Garg, Surinder Singh and S. Puri, "*A Review, Bibliography, and Tabulation of K, L, and Higher Atomic Shell X-Ray Fluorescence Yields*", J. Phys. Chem. Ref. Data 23 (1994) 339.

[Ita90] W. M. Itano, D. J. Heinzen, J. J. Bollinger and D. J. Wineland, "*Quantum Zeno effect*", Phys. Rev. A 41 (1990) 2295.

[Jac09] D. Jacquet and M. Morjean, "*Fission times of excited nuclei: An experimental overview*", Prog. Partcl. Nucl. Phys. 63 (2009) 155.

[Jac75] J. D. Jackson, "*Classical Electrodynamics*", 2nd Edition, Wiley, New York, 1975.

[Jai95] R. K. Jain, S. K. Bose and J. Rama Rao, "*Fission fragment angular distribution in alpha-particle-induced fission of actinide elements*", Pramana - J. Phys. 45 (1995) 519.

[Joh75] Noah R. Johnson, R. J. Sturm, E. Eichler, M. W. Guidry, G. D. O'Kelley, R. O. Sayer and D. C. Hensley, "*Lifetimes of rotational states in ^{232}Th*", Phys. Rev. C 12 (1975) 1927.

[Kha58] L. A. Khalfin, "*Contribution to the Decay Theory of a Quasi-Stationary State*", Zh. Eksp. Teor. Fiz. 33 (1957) 1371 [Sov. Phys. JETP 6 (1958) 1053].

[Kim15] Kyung Hwan Kim, Jong Goo Kim, Shunsuke Nozawa, Tokushi Sato, Key Young Oang, Tae Wu Kim, Hosung Ki, Junbeom Jo, Sungjun Park, Changyong Song, Takahiro Sato, Kanade Ogawa, Tadashi Togashi, Kensuke Tono, Makina Yabashi, Tetsuya Ishikawa, Joonghan Kim, Ryong Ryoo, Jeongho Kim, Hyotcherl Ihee and Shin-ichi Adachi, "*Direct observation of bond formation in solution with femtosecond X-ray scattering*", Nature 518 (2015) 385.

[Kof01] A. G. Kofmann and G. Kurizki, "*Frequent Observations Accelerate Decay: The anti-Zeno Effect*", Phys. Rev. Lett. 87 (2001) 270405.

[Kos05] Kazuki Koshino and Akira Shimizu, "*Quantum Zeno effect by general measurements*" , Physics Reports 412 (2005) 191.

[Koz10] E. M. Kozulina, G. N. Knyazheva, I. M. Itkis, M. G. Itkis , A. A. Bogachev , L. Krupa, T. A. Loktev, S. V. Smirnov, V. I. Zagrebaev, J. Äystö, W. H. Trzaska, V. A. Rubchenya, E. Vardaci, A. M. Stefanini, M. Cinausero, L. Corradi, E. Fioretto, P. Mason, G. F. Prete, R. Silvestri, S. Beghini, G. Montagnoli, F. Scarlassara, F. Hanappe, S. V. Khlebnikov , J. Kliman, A. Brondi, A. Di Nitto, R. Moro, N. Gelli and S. Szilner, "*Investigation of the reaction $^{64}Ni + ^{238}U$ being an option of synthesizing element 120*", Phys. Lett. B 686 (2010) 227.

[Kra01] V.L. Kravchuk, A. M. van den Berg, F. Fleurot, M. A. de Huu, H. Löhner, H. W. Wilschut, M. Polasik, M. Lewandowska-Robak and K. Slabkowska, "K- *and L-shell ionization of heavy targets by various 20- and 80-MeV/u projectiles*", Phys. Rev. A 64 (2001) 062710.

[Kra04] V. L. Kravchuk, "*Development of an Atomic Clock for Fission Lifetime Measurements*", Ph.D Thesis, Kernfysisch Versneller Instituut, Netherlands (2004).

[Kra79] M. O. Krause and J. H. Oliver, "*Natural Widths of Atomic K and L Levels, Kα X-Ray Lines and Several KLL Auger Lines*", J. Phys. Chem. Ref. Data 8 (1979) 329.

[Kre09] Susanne Waltraud Kreim, "*Direct Observation of a Single Proton in a Penning Trap*", Ph.D. thesis, Johannes Gutenberg-Universität, Mainz (2009).

[Lap98] Lisa J. Lapidus, "*Synchronization and Stochastic Behavior of Electrons in a Penning Trap*", Ph.D. Thesis, Harvard University (1998).

[Led78] C. M. Lederer and V. S. Shirley, "Table of Isotopes", (John Wiley & Sons, Inc., New York, 1978).

[Les91] J. P. Lestone, J. R. Leigh, J. O. Newton, D. J. Hinde, J. X. Wei, J. X. Chen, S. Elfstrom, and D. G. Popescu, "*Fission time scales from prescisson charged-particle multiplicities*", Phys. Rev. Lett. 67 (1991) 1078.

[Les93] J. P. Lestone, J. R. Leigh, J. O. Newton, D. J. Hinde, J. X. Wei, J. X. Chen, S. E. Elfstrom, and M. Zielinska-Pfabé, "*Pre-scission charged-particle multiplicities following the reactions* $^{164,167,170}Er + {}^{28}Si$", Nucl. Phys. A 559 (1993) 277.

[Lev88] Jacob Levitan, "*Small time Behaviour of an Unstable Quantum System*", Phys. Lett. A 129 (1988) 267.

[Mac59] W. W. Macalpine and R. O. Schildknecht, "*Coaxial resonators with helical inner conductor*" Proc. IRE 47 (1959) 2099.

[Mei39] L. Meitner and O. R. Frisch, "*Disintegration of uranium by neutrons: a new type of nuclear reaction*", Nature 143 (1939) 239.

[Mis77] B. Misra and E. C. G. Sudarshan, "*The Zeno's paradox in quantum theory*", J. Math. Phys. 18 (1977) 756.

[Moe94] P. Moeller and J. R. Nix, "*Stability of heavy and superheavy elements*", J. Phys. G 20 (1994) 1681.

[Mol09] Peter Möller, Arnold J. Sierk, Takatoshi Ichikawa, Akira Iwamoto, Ragnar Bengtsson, Henrik Uhrenholt and Sven Åberg, "*Heavy-element fission barriers*", Phys. Rev. C 79 (2009) 064304.

[Mol93] J. D. Molitoris, W. E. Meyerhof, Ch. Stoller, R. Anholt, D. W. Spooner, L. G. Moretto, L. G. Sobotka, R. J. McDonald, G. J. Wozniak, M. A. McMahan, L. Blumenfeld, N. Colonna, M. Nessi and E. Morenzoni, "*Molecular-orbital study of late-fission times in deep-inelastic U238+238U collisions*", Phys. Rev. Lett. 70 (1993) 537.

[Mor08] M. Morjean, D. Jacquet, J. L. Charvet, A. L'Hoir, M. Laget, M. Parlog, A. Chbihi, M. Chevallier, C. Cohen, D. Dauvergne, R. Dayras, A. Drouart, C. Escano-Rodriguez, J. D. Frankland, R. Kirsch, P. Lautesse, L. Nalpas, C. Ray, C. Schmitt, C. Stodel, L. Tassan-Got, E. Testa and C. Volant, "*Fission Time Measurements: A New Probe into Superheavy Element Stability*", Phys. Rev. Lett. 101 (2008) 07270.

[Mou15] M. Roy Basu, S. Ray, A. Bisoi and M. SahaSarkar, "*Characterisation of a composite LEPS*"**,** Journal of Instrumentation 10 (2015) 1748-0221.

[Nor88] B. E. Norman, Stuart B. Gazes, Stephanie G. Crane and Dianne A. Bennett, "*Tests of the Exponential Decay Law at Short and Long Times*", Phys. Rev. Lett. 60 (1988) 2246.

[Nor95] Eric B. Norman, Bhaskar Sur, K. T. Lesko, Ruth-Mary Larimer, Donald J. De Paolo and Thomas L. Owens, "*An improved test of the exponential decay law*", Phys. Lett. B 357 (1995) 521.

[Nov06] D. Novkovic´, L. Nadderd, A. Kandic´, I. Vukanac, M. Duraˇsevic´ and D. Jordanov, "*Testing the exponential decay law of gold* ^{198}*Au*", Nuclear Instruments and Methods in Physics Research A 566 (2006) 477.

[NuDat] NuDat 2.6, September 2016 http://www.nndc.bnl.gov/nudat2/.

[Pag11] G. Pagliara and F. Giacosa, "Non exponential decays of hadrons" , Acta Phys. Polon. Supp. 4 (2011) 753.

[Pal08] Santanu Pal, Gargi Chaudhuri and Jhilam Sadhukhan, "*The role of neck degree of freedom in nuclear fission*", Nuclear Physics A 808 (2008) 1.

[Ram12] E. Minaya Ramirez, D. Ackermann, K. Blaum, M. Block, C. Droese, Ch. E. Düllmann, M. Dworschak, M. Eibach, S. Eliseev, E. Haettner, F. Herfurth, F. P. Heßberger, S. Hofmann, J. Ketelaer, G. Marx, M. Mazzocco, D. Nesterenko, Yu. N. Novikov, W. R. Plaß, D. Rodríguez, C. Scheidenberger, L. Schweikhard, P. G. Thirolf and C. Weber, "*Direct Mapping of Nuclear Shell Effects in the Heaviest Elements*", Science 337 (6099) (2012) 1207.

[Ray15] A. Ray, A. K. Sikdar and A. De, "*Quasifision timescale: Zeptosecond versus attosecond*", EPJ Web of Conferences 86 (2015) 38.

[Ray16] A. Ray and A. K. Sikdar, "*Timescale of non-exponential decay for the nuclear* β*-decay process in a decoherence model",* Phys. Rev. C. 94 (2016) 055503.

[Rei84] J. Reinhardt and W. Greiner, "*Heavy-ion atomic physics- theoretical. edited by D. A. Bromley*" , "*Treatise on Heavy-Ion Science Vol. 2* " , Plenum, New York, 1984.

[Rez15] Ashif Reza, Anuraag Misra, Saikat Sarkar, Arindam Kumar Sikdar and Parnika Das, "*Development of a helical resonator for ion trap application*", 2015 IEEE Applied Electromagnetics Conference (AEMC) (2015) 1 ; DOI: 10.1109/AEMC.2015.7509206.

[Rez16] Ashi Reza, Anuraag Misra and Parnika Das, "*An improved model to predict bandwidth enhancement in inductively tuned common source amplifier*", Rev. Sci. Instrum. 87 (2016) 054710.

[Rie11] R. du Rietz, D. J. Hinde, M. Dasgupta, R. G. Thomas, L. R. Gasques, M. Evers, N. Lobanov and A. Wakhle, "*Predominant Time Scales in Fission Processes in Reactions of S, Ti and Ni with W: Zeptosecond versus Attosecond*", Phys. Rev. Lett. 106 (2011) 05271.

[Ros89] H. Rossner, D. Hilscher, D. J. Hinde, B. Gebauer, M. Lehmann, M. Wilpert and E. Mordhorst, "*Analysis of pre- and post-scission neutrons emitted in the reaction* $^{169}Tm(^{36}$ *Ar,f) at* $_{Elab}$*=205 MeV*", Phys. Rev. C 40 (1989) 2629.

[Rot06] C. Rothe, S. I. Hintschich and A. P. Monkman, "*Violation of the Exponential-Decay Law at Long Times*", Phys. Rev. Lett. 96 (2006) 163601.

[Rus46] B. Russell, "*A History of Western Philosophy*", (George Allen & Unwin, London, 1946).

[Rut11] E. Rutherford and Stizungsber. Akad. Wiss. Wien, Math-Naturwiss. K1. Abt. 2A 120 (1911) 303.

[Sat10] K. T. Satyajith, "*Spectroscopy of Electrons and Ions in Electromagnetic Traps*", Ph.D. thesis, Bangalore University (2010).

[Sax94] A. Saxena, A. Chatterjee, R. K. Choudhury, S. S. Kapoor and D. M. Nadkarni, "*Entrance channel effects in the fusion-fission time scales from studies of prescission neutron multiplicities*", Phys. Rev. C 49 (1994) 932.

[Sch14] F. Schäfer, I. Herrera, S. Cherukattil, C. Lovecchio, F. S. Cataloitti, F. Caruso and A. Smerzi, "*Experimental realization of quantum zeno dynamics*", Nat. Commun. 5 (2014) 3194.

[Sch84] W. U. Schroder and J. R. Huizenga, "*Treatise on Heavy-Ion Science*", (Plenum Press, New York, 1984), Vol. 2.

[Sek13] K. Sekizawa and K. Yabana, "*Time-dependent Hartree-Fock calculations for multinucleon transfer processes in* $^{40,48}Ca+^{124}Sn$, $^{40}Ca+^{208}Pb$, *and* $^{58}Ni+^{208}Pb$ *reactions*", Phys. Rev. C 88 (2013) 014614.

[Sik13] A. K. Sikdar, A. Ray, P. Das and A. Reza, "*Design of a dynamically orthogonalized Penning trap with higher order anharmonicity compensation*", Nuclear Instruments and Methods in Physics Research A 712 (2013) 174.

[Sik16] A. K. Sikdar, A. Ray and A. Chatterjee, "Examination *of the fission time of the Z = 120 nucleus*", Phys. Rev. C 93 (2016) 041604.

[Sim8.0] SIMION 8.0 user manual.

[Str06] Erik W. Streed, Jongchul Mun, Micah Boyd, Gretchen K. Campbell, Patrick Medley, Wolfgang Ketterle and David E. Pritchard, "*Continuous and Pulsed Quantum Zeno Effect*", Phys. Rev. Lett. 97 (2006) 260402.

[Stu11] Sven Sturm, "*The g-factor of the electron bound in* $^{28}Si^{13+}$", Ph.D. thesis, Johannes Gutenberg-Universität, Mainz (2011).

[Tan89] J. Tan and G. Gabrielse, "*One electron in an orthogonalized cylindrical Penning Trap*", Appl. Phys. Lett. 55 (1989) 2144.

[Tho08] R. G. Thomas, D. J. Hinde, D. Duniec, F. Zenke, M. Dasgupta, M. L. Brown, M. Evers, L. R. Gasques, M. D. Rodriguez and A. Diaz-Torres, "*Entrance channel dependence of quasifission in reactions forming* ^{220}Th", Phys. Rev. C 77 (2008) 034610.

[Tho68] Thomas A. Carlson, C. W. Nestor, Jr. and Thomas C. Tucker and F. B. Malik, "*Calculation of Electron Shake-Off for Elements from Z=2 to 92 with the Use of Self-Consistent-Field Wave Functions*", Phys. Rev 169 (1968) 27.

[Tok85] J. Toke, R. Bock, G.X. Dai, A. Gobbi, S. Gralla, K.D. Hildenbrand, I. Kuzminski, W.F.J. Muller, A. Olmi and H. Stelzer, "*Quasi-Fission- The mass drift mode in Heavy Ion Reactions*", Nucl. Phys. A 440 (1985) 327.

[Tra80] D. Trautmann and F. Rösel, "On the semiclassical description of Coulomb ionization of inner shells", Nucl. Instrum. Methods 169 (1980) 259.

[Uni] en.wikipedia.org/wiki/Unbinilium.

[Van73] R. Vandenbosch and J. R. Huizenga, "*Nuclear fission*", Academic Press, New York, 1973.

[Vin98] Bryan A. Vining, Guo-Zhong Li and Alan G. Marshall, "*Laser-induced fluorescence for ion tomography in a Penning trap*", Journal of the American Society for Mass Spectrometry 9 (1998) 925.

[Wak14] A. Wakhle, C. Simenel, D. J. Hinde, M. Dasgupta, M. Evers, D. H. Luong, R. du Rietz and E. Williams, "*Interplay between Quantum Shells and Orientation in Quasifission*", Phys. Rev. Lett. 113 (2014) 182502.

[War96] D. Ward, H. R. Andrews, G. C. Ball, A. Galindo-Uribarri, V. P. Janzen , T. Nakatsukasa, D. C. Radford, T. E. Drake, J. DeGraaf, S. Pilotte and Y. R. Shimizu, "*Rotational bands in* ^{238}U", Nucl. Phys. A 600 (1996) 88.

[Wil04] H. W. Wilschut and V. L. Kravchuk, "*Developing an "atomic clock" for fission lifetime measurements*", Nucl. Phys. A 734 (2004) 156.

[Wil97] S. R. Wilkinson, Cyrus F. Bharucha, Martin C. Fischer, Kirk W. Madison, Patrick R. Morrow, Qian Niu, Bala Sundaram and Mark G. Raizen, "*Experimental evidence for non-exponential decay in quantum tunnelling*", Nature 387 (1997) 575.

[Win61] R. G. Winter, "*Evolution of a Quasi-Stationary State* ", Phys. Rev. 123 (1961) 1503.

[Win62] R. G. Winter, "*Large-Time Exponential Decay and "Hidden Variables"*", Phys. Rev. 126 (1962) 1152.

[Win73] D. Wineland, P. Ekstrom and H. Dehmelt, "*Monoelectron Oscillator*", Phys. Rev. Lett. 31 (1973) 1279.

[Win93] D. Wineland, C. Weimer and J. Bollinger, "*Laser-cooled positron source*", Hyperfine Interactions 76 (1993) 115.

[Xia06] Li Xiao and Jonathan A. Jones, "*NMR analogues of the quantum Zeno effect*", Phys. Lett. A 359 (2006) 424.

[Zur02] W. H. Zurek, "*Decoherence and the Transition from Quantum to Classical—Revisited*" Los Alamos Science 27 (2002) 2.

[Zur03] W. H. Zurek, "*Decoherence, einselection, and the quantum origins of the classical*", Rev. Mod. Phys. 75 (2003) 715.